Characterization of High Grafting Density Polymer Brushes Using Molecular Dynamics Simulations and Experimental Methods

By

IAN GOULD ELLIOTT
B.S. Chemical Engineering (Oregon State University) 2007
B.S. Chemistry (Oregon State University) 2007

DISSERTATION

Submitted in partial satisfaction of the requirements for the degree of

DOCTOR OF PHILOSOPHY

in

Chemical Engineering

in the

OFFICE OF GRADUATE STUDIES

of the

UNIVERSITY OF CALIFORNIA

DAVIS

Approved:

_____

Tonya Kuhl, Chair

_____

Roland Faller

_____

Ronald Phillips

Committee in Charge

2012

ProQuest LLC.
789 East Eisenhower Parkway
P.O. Box 1346
Ann Arbor, MI 48106 - 1346

TABLE OF CONTENTS

Ian Gould Elliott
December 2012
Chemical Engineering

Abstract

Polymer brushes have the ability to modify surface properties for numerous applications. To better understand how they can be used, thorough characterization is necessary. Polymer brushes were studied from both a computational and experimental standpoint. The structure and interactions between two layers were examined, providing an understanding of how the systems respond to situations encountered in their applications.

A coarse-grained model for molecular dynamics simulations was used to allow larger system sizes and longer simulation times. The simulations first characterized the structure of a single brush in good solvent, examining polymer and solvent density profiles, radial distribution functions, chain orientation, and brush height.

Next, a method was developed to simulate confined polymer brushes using molecular dynamics with an explicit solvent. Density profiles and normal forces were measured for several levels of compression, and features in the force-distance profile were justified by looking at the corresponding density profiles. A significant correlation was observed between the degree of interpenetration of the brushes to the measured normal force.

Experimentally, polystyrene polymer brushes were synthesized using atomic transfer radical polymerization to create durable, very high grafting density layers. They were studied using a surface force apparatus to determine both normal force and frictional properties. The shear force experiments indicate that even at a very high grafting density, the polymer brushes provide a good lubricant for the surface.

Chapter 1

Introduction

1.1 Polymer Brush Introduction

A polymer brush is formed when polymer chains are attached to a surface at a high enough density to laterally interact with each other. Crowding between the grafted polymers causes the chains to behave much differently than they would in solution or a melt, stretching from the surface into the solvent.[1] The chains can either be physically adsorbed, such as with two unlike blocks of a copolymer where one block has a favorable interaction with the surface, or chemically bonded to the substrate. The principle variables that will affect polymer brushes are grafting density, molecular weight, temperature, and solvent quality. By understanding how these variables will change the polymer brush structure and interactions, a system can be designed that targets a specific response.

Generally, the primary application of polymer brushes is to alter surface properties to yield numerous desired effects. One simple application is to use a grafted polymer layer to provide a protective coating to a fragile surface. More complicated applications arise when the brush is brought into contact with another surface or polymer brush layer. In a colloidal system containing particles which would aggregate over time, coating the particles in brushes can cause the particles to remain dispersed.[2] So long as the polymers have a more favorable interaction with the solvent than with each other, once the particles are close enough to interact the brush layers will repel one another, thus preventing flocculation. Surface properties can be modified by using diblock copolymers with two

dissimilar ends. For instance, a hydrophobic surface could be made hydrophilic using a diblock copolymer which has one hydrophilic end and one hydrophobic end. The hydrophobic end of the polymer would adsorb to the hydrophobic surface, and the block of the polymer at the interface in air or solution now is hydrophillic.[3] Such a transformation is an example of altering the wettibility of a surface, which could be useful for waterproofing materials. Similarly, polymer brushes can be used to make materials biocompatible.[4] If an artificial device is added to a biological system, the surfaces need to be able to interact with the surroundings. Polymer brushes can be added to a metal or plastic device to make the surface interactions compatible with other tissue or fluids. When properly designed, a polymer brush system can also act as a lubricant.[5-9] Under good solvent conditions they have shown a significant reduction in the friction coefficient.[5, 9] This evidence has given rise to the idea of using high density polymer brushes as lubricants for artificial joints.[4] If these polymer brush layers can be designed to be both lubricating and durable, using them as an improved lubricant in artificial joints could extend the lifetime of the device, reducing the need for multiple surgeries.

To be able to effectively design a system for any of the applications listed above, polymer brush structures and interactions first must be understood. In this work, examining brushes under confinement was conducted using two complimentary methods. The first approach employed molecular dynamics simulations. Simulations have the advantage that they are not confined to systems that can be created in the lab, so conditions can be examined which may be very difficult to measure experimentally.

The second approach to study polymer brush systems was to synthesize and examine polymer brushes experimentally. Interactions of opposing brushes brought into contact

can be measured with the surface force apparatus, while neutron reflectivity can provide structural information with density profiles.

1.2 Simulation Details

Molecular simulation is an excellent tool for analyzing polymer brush systems. Structure can be measured as density profiles very easily as all particle locations are known throughout the trajectory. Likewise, forces can be extracted with relatively little effort. An advantage of using simulations is that multiple experiments are not required to gain different types of information about the same system. If both structure and force information are desired, they can be extracted from one simulation. This allows for direct comparison of both types of data to determine the effect that the structure of each polymer brush layer has on the interactions measured.

For polymer systems that are anywhere close to experimental molecular weights, atomistic simulations become impractical due to both the system size and the times required to reach equilibration. Thus, coarse-graining can greatly increase the efficiency. Generally, coarse-graining replaces groups of individual atoms with a larger particle or interaction site, therefore reducing the total number of particles in the system. For all simulations conducted in this work, the MARTINI model was used.[10] The MARTINI coarse-grained model has all particles the same size and weight. The particles do not have a specific chemical identity, but instead are assigned Lennard-Jones parameters making them polar, non-polar, or charged. A polymer can thus be simulated in a good solvent by the proper choice of particle type. This model had been successfully used previously to model polymer systems,[11] and was able to accurately model polymer brushes as well.[12, 13]

For this work it was desired to simulate opposing brushes in confinement, using an explicit solvent. Frequently, confined systems are simulated with an implicit solvent.[6, 14-16] This simplifies the procedure, as the question of the amount of solvent between the surfaces can be omitted. Doing so also sacrifices details concerning the solvent, so effects such as depletion layers or solvent layering would not be seen. Some previous work which did use explicit solvent maintained a constant solvent density throughout the compression,[17, 18] therefore not reproducing experimental conditions. The confinement procedure for the simulations in this work involved setting up the systems at the correct solvent density prior to the simulation. This led to a much more physically realistic compression that still allowed for explicit solvent.

1.3 Experimental Work

Experimental studies of the interaction forces between polymer brushes have often examined physically adsorbed systems,[19-23] as opposed to chemically grafted ones. In these cases, polymer chains are self assembled on the surface after already being fully synthesized. This method leads to a relatively low grafting density as once some chains are adsorbed to the surface, steric hindrance makes it increasingly difficult to attach more chains. To attain higher grafting densities, a "grafted from" technique needs to be employed. In this method, initiator sites are first chemically bonded to the surface. A polymerization reaction grows the chains up piece by piece from the surface. This creates much less steric hindrance as diffusing monomers can reach the reacting site much easier than a full polymer chain can to the surface. Atomic transfer radical polymerization (ATRP) is a relatively new polymerization technique in which polymers are grown in a controlled manner from the surface one monomer at a time.[24, 25] The

technique employs both an activating and deactivating catalyst. This means the reaction sites are often inactive, which reduces the likelihood of termination by two chain ends reacting. The slow growth also leads to more uniform chains across the brush which propagate at a relatively consistent rate, providing a low polydispersity.[26]

Force-distance profiles can be obtained using the surface force apparatus (SFA) with a resolution of 1 Å in separation distance and 10 μN in normal force.[27] An SFA brings two curved surfaces into contact, one of which is attached to a spring with a known spring constant to determine the force. Mica is used as a substrate on top of the curved discs as it is molecularly smooth and can be cleaved thin enough to allow for good optics for interferometry. Mica is also inert, which presents a problem for chemically bonding polymers to it. The first challenge for experimentally studying high grafting density ATRP grown brushes was finding a suitable surface for both the reaction and the force spectroscopy measurements. The requirements for this surface were to be smooth, have a uniform thickness of 3-5 μm, and to be chemically reactive. The reaction could take place on an SiO_2 surface, so all efforts at finding a reactive surface for use in the SFA involved thin glass layers.

The first attempt at creating the glass substrates involved etching 280 μm silicon wafers with a 3 μm SiO_2 layer on either side. The idea was to etch away one side of the SiO_2 completely, and then etch through the silicon layer until only the 3 μm SiO_2 layer remained on one side. The wafers were etched from one side in KOH at 75°C for several hours, until only a thin layer of SiO_2 remained. A protective coating was applied to the wafer to create a frame that would not be etched so the substrates could be handled. The layer produced was extremely brittle and uneven, clearly not suitable for use in the SFA.

The second method to create thin glass substrates was using blown glass bubbles. This method had been used previously[28] for similar purposes, and was far more effective than using the etched wafers. One glass bubble could be broken to create several thin substrates. These pieces were glued to SFA discs and a polymer brush was grown on them. Once they were examined with the SFA, however, it was apparent that the glass substrates were not uniform in thickness, making thickness measurements very difficult. Additionally, the glass pieces were very fragile and difficult to glue on the SFA discs without cracking or breaking them. This method was used for multiple reactions, but eventually was disregarded for a better surface.

The final surface type used was mica with a layer of SiO_2 evaporated on it. These surfaces were much more durable than the previous attempts, and could be handled similarly to bare mica sheets when gluing them on the SFA discs. The SiO_2 layer was also very uniform, making the thickness measurements more straightforward. These substrates were used for all subsequent reactions and all published work.

Synthesis reactions largely followed previous work,[29, 30] but had the added challenge of performing the polymerizations on surfaces rather than in bulk. When surface reactions had taken place previously, the reaction was typically on silicon surfaces which require minimal preparation compared to the SFA discs used in these experiments. Reactions took place in a custom flask which could be taken apart to add or remove surfaces. Both silicon surfaces and SFA discs with the modifications described above were used to get structure data from neutron reflectivity and force profiles from the SFA.

Before the polymerization reaction could take place, other organic compounds first had to be synthesized. This process is provided in Chapter 5, but will be discussed here with some chemical structures, explanations, and additional detail not provided later.

The surface active initiator used for all reactions was (11-(2-Bromo-2-methyl)propionyloxy)undecyl trichlorosilane. This initiator was not commercially available, so had to be synthesized from 10-undecenyl 2-bromoisobutyrate, trichlorosilane, and the Karstedt catalyst. 10-undecenyl 2-bromoisobutyrate was commercially available, but was fairly expensive for the amount needed. Also, the initiator reaction is not always successful, and as such may have needed to be repeated several times. Due to the cost associated with using this reagent for potentially multiple reactions, 10-undecenyl 2-bromoisobutyrate was instead synthesized. It required 10-undecen-1-ol, and 2-bromoisobutyryl bromide, both of which were commercially available and inexpensive. The Karstedt catalyst can now be purchased cheaply from different vendors. Many publications will recommend synthesizing it, as its availability used to be limited. At this point it is highly recommended to purchase the Karstedt catalyst, as it is inexpensive and small quantities are used. A reaction scheme is provided in Figure 1-1 showing first the 10-undecenyl 2-bromoisobutyrate and then the surface active initiator synthesis.

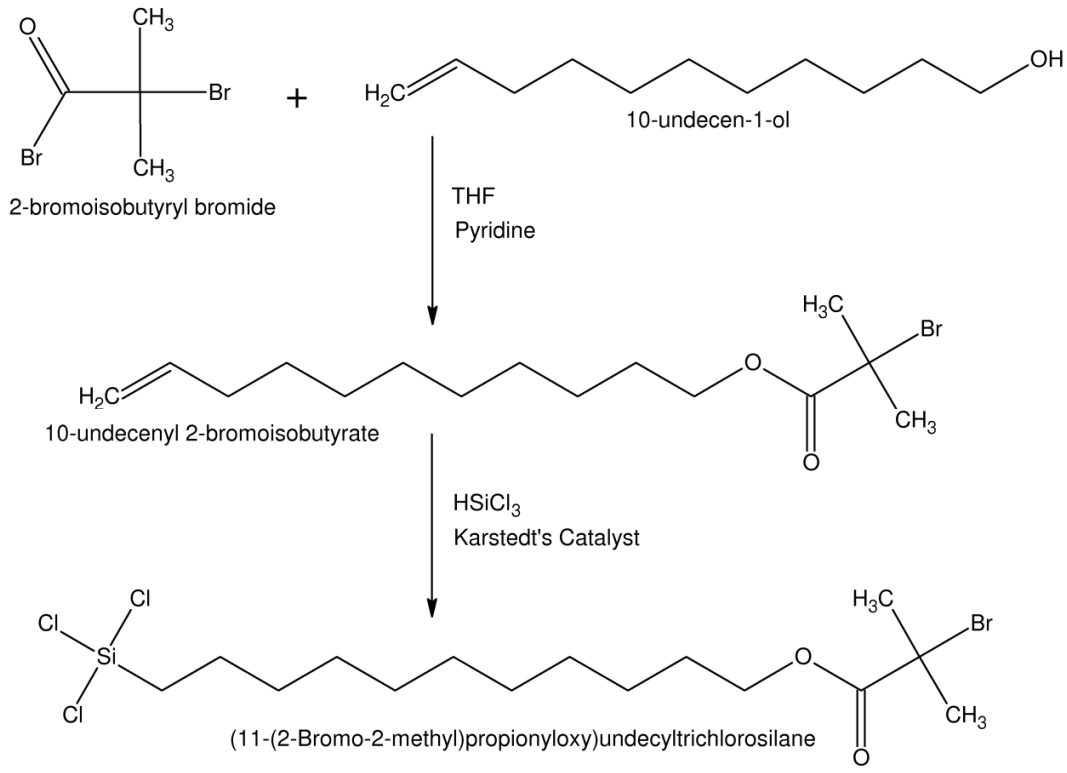

Figure 1-1. Synthesis of the surface active polymerization initiator used for ATRP reactions and its precursor. The silane group, shown as the left end of the initiator in Figure 1- 1, is the surface active portion of the molecule, and can bond to SiO_2 surfaces. The bromide at the opposite end of the molecule is the polymerization initiation site.

1.4 Strategy and Overview

The overall goal for the simulation study was to thoroughly characterize the high grafting density polymer brush system. The starting point for this was to first fully understand an equilibrium brush. Understanding the brush system with this model in the absence of confinement was important so once the system was confined later, the effects of perturbing it could be fully recognized. These first simulation studies also served to confirm that this coarse-grained model was suitable for polymer brush systems. The results for the single brush under different conditions are reported in Chapter 2. Once the

single brush was characterized with respect to variables such as grafting density and molecular weight, a second, opposing brush was added. Adding a second brush layer was a more complicated problem than anticipated, and thus Chapter 3 is dedicated to the development of a method for confining soft matter. Following this work, the method was implemented to study and characterize a polymer brush system under different levels of confinement. Forces and structure were analyzed simultaneously to create an understanding of the structure-response relationships. These results are presented in Chapter 4.

Similar systems were synthesized and studied experimentally. Very high grafting density polystyrene brushes were synthesized using ATRP. These were subsequently characterized for both normal force and shear force responses using the SFA. The goal of the experiments was to create a lubricating layer that was highly durable. By substantially increasing the surface coverage from many previous polymer brush studies, the polymer layer should be more robust. However, it was unknown if at such high grafting densities the polymer brushes would still act as good lubricants. The Shear force data from the SFA can provide insight into this problem. Chapter 5 gives the results of the experiments, answering the question of whether the more durable, high grafting density layer will also reduce friction.

Chapter 6 gives a brief conclusion and summary of both the simulation and experimental work. It also provides a path forward for future work in both of these areas, as well as explaining some ongoing work which will be completed soon.

An appendix is provided in Chapter 7 which details the simulation confinement method. Many details of this process were not included in Chapter 3 for brevity, and are

given here instead. The procedure involved using Gromacs tools which are not very common, as well as altering source code to allow for fixed surfaces. If future researchers need to do similar studies, this appendix will be a useful how-to guide for calculating chemical potential in a system with fixed particles.

1.5 References

1. Halperin, A.; Tirrell, M.; Lodge, T., Tethered chains in polymer microstructures Macromolecules: Synthesis, Order and Advanced Properties. In Springer Berlin / Heidelberg: 1992; Vol. 100, pp 31-71.

2. Napper, D. H., *Polymeric Stabilization of Colloidal Dispersions*. Academic Press: London, 1983.

3. Yokoyama, H.; Miyamae, T.; Han, S.; Ishizone, T.; Tanaka, K.; Takahara, A.; Torikai, N. Spontaneously Formed Hydrophilic Surfaces by Segregation of Block Copolymers with Water-Soluble Blocks. *Macromolecules* **2005,** 38, (12), 5180-5189.

4. Moro, T.; Takatori, Y.; Ishihara, K.; Konno, T.; Takigawa, Y.; Matsushita, T.; Chung, U.-i.; Nakamura, K.; Kawaguchi, H. Surface grafting of artificial joints with a biocompatible polymer for preventing periprosthetic osteolysis. *Nat Mater* **2004,** 3, (11), 829-836.

5. Klein, J.; Kumacheva, E.; Mahalu, D.; Perahia, D.; Fetters, L. J. Reduction of frictional forces between solid surfaces bearing polymer brushes. *Nature* **1994,** 370, (6491), 634-636.

6. Grest, G. S. Interfacial Sliding of Polymer Brushes: A Molecular Dynamics Simulation. *Phys. Rev. Lett.* **1996,** 76, 4979.

7. Pelletier, E.; Belder, G.; Hadziioannou, G.; Subbotin, A., Nanorheology of Adsorbed Diblock Copolymer Layers. In HAL - CCSD: 1997.

8. Grest, G. Normal and Shear Forces Between Polymer Brushes. *Adv. Polym. Sci.* **1999,** 138, 149-183.

9. Klein, J.; Kumacheva, E.; Perahia, D.; Mahalu, D.; Warburg, S. Interfacial sliding of polymer-bearing surfaces. *Faraday Discussions* **1994,** 98, 173-188.

10. Marrink, S. J.; de Vries, A. H.; Mark, A. E. Coarse Grained Model for Semiquantitative Lipid Simulations. *J. Phys. Chem. B* **2004,** 108, (2), 750-760.

11. Hatakeyama, M.; Faller, R. Coarse-grained simulations of ABA amphiphilic triblock copolymer solutions in thin films. *Phys. Chem. Chem. Phys.* **2007,** 9, (33), 4662-4672.

12. Elliott, I. G.; Mulder, D. E.; Traskelin, P. T.; Ell, J. R.; Patten, T. E.; Kuhl, T. L.; Faller, R. Confined polymer systems: synergies between simulations and neutron scattering experiments. *Soft Matter* **2009,** 5, (23), 4612-4622.

13. Elliott, I. G.; Kuhl, T. L.; Faller, R. Molecular Simulation Study of the Structure of High Density Polymer Brushes in Good Solvent. *Macromolecules* **2010,** 43, (21), 9131-9138.

14. Neelov, I. M.; Binder, K. Brownian dynamics simulation of grafted polymer brushes. *Macromolecular Theory and Simulations* **1995,** 4, (1), 119-136.

15. Neelov, I. M.; Borisov, O. V.; Binder, K. Shear deformation of two interpenetrating polymer brushes: Stochastic dynamics simulation. *J. Chem. Phys.* **1998,** 108, (16), 6973-6988.

16. Grest, G. S. Grafted polymer brushes in polymeric matrices. *J. Chem. Phys.* **1996,** 105, (13), 5532-5541.

17. Galuschko, A.; Spirin, L.; Kreer, T.; Johner, A.; Pastorino, C.; Wittmer, J.; Baschnagel, J. Frictional Forces between Strongly Compressed, Nonentangled Polymer Brushes: Molecular Dynamics Simulations and Scaling Theory. *Langmuir* **2010,** 26, (9), 6418-6429.

18. Spirin, L.; Galuschko, A.; Kreer, T.; Johner, A.; Baschnagel, J.; Binder, K. Polymer-brush lubrication in the limit of strong compression. *Eur. Phys. J. E* **2010,** 33, (4), 307-311.

19. Liao, W.-P.; Kuhl, T. L. Steric Forces of Tethered Polymer Chains as a Function of Grafting Density: Studies with a Single Diblock Molecular Weight. *Macromolecules* **2012,** 45, (14), 5766-5772.

20. Kilbey, S. M.; Watanabe, H.; Tirrell, M. Structure and Scaling of Polymer Brushes near the ϑ Condition. *Macromolecules* **2001,** 34, (15), 5249-5259.

21. Watanabe, H.; Tirrell, M. Measurement of forces in symmetric and asymmetric interactions between diblock copolymer layers adsorbed on mica. *Macromolecules* **1993,** 26, (24), 6455-6466.

22. Schorr, P. A.; Kwan, T. C. B.; Kilbey, S. M.; Shaqfeh, E. S. G.; Tirrell, M. Shear Forces between Tethered Polymer Chains as a Function of Compression, Sliding Velocity, and Solvent Quality. *Macromolecules* **2002,** 36, (2), 389-398.

23. Tian, P.; Uhrig, D.; Mays, J. W.; Watanabe, H.; Kilbey, S. M. Role of Branching on the Structure of Polymer Brushes Formed from Comb Copolymers. *Macromolecules* **2005,** 38, (6), 2524-2529.

24. Patten, T. E.; Matyjaszewski, K. Atom Transfer Radical Polymerization and the Synthesis of Polymeric Materials. *Advanced Materials* **1998,** 10, (12), 901-915.

25. Wang, J.-S.; Matyjaszewski, K. Controlled/"living" radical polymerization. atom transfer radical polymerization in the presence of transition-metal complexes. *Journal of the American Chemical Society* **1995,** 117, (20), 5614-5615.

26. Matyjaszewski, K.; Xia, J., Fundamentals of Atom Transfer Radical Polymerization. In *Handbook of Radical Polymerization*, John Wiley & Sons, Inc.: 2003; pp 523-628.

27. Israelachvili, J. N.; Adams, G. E. Measurement of forces between two mica surfaces in aqueous electrolyte solutions in the range 0-100 nm. *J. Chem. Soc., Faraday Trans.* **1978,** 74, 975-1001.

28. Ruths, M.; Johannsmann, D.; Ruhe, J.; Knoll, W. Repulsive Forces and Relaxation on Compression of Entangled, Polydisperse Polystyrene Brushes. *Macromolecules* **2000,** 33, (10), 3860-3870.

29. Ell, J. R.; Mulder, D. E.; Faller, R.; Patten, T. E.; Kuhl, T. L. Structural Determination of High Density, ATRP Grown Polystyrene Brushes by Neutron Reflectivity. *Macromolecules* **2009,** 42, (24), 9523-9527.

30. Matyjaszewski, K.; Miller, P. J.; Shukla, N.; Immaraporn, B.; Gelman, A.; Luokala, B. B.; Siclovan, T. M.; Kickelbick, G.; Vallant, T.; Hoffmann, H.; Pakula, T. Polymers at Interfaces: Using Atom Transfer Radical Polymerization in the Controlled Growth of Homopolymers and Block Copolymers from Silicon Surfaces in the Absence of Untethered Sacrificial Initiator. *Macromolecules* **1999,** 32, (26), 8716-8724.

Chapter 2

Molecular Simulation Study of the Structure of High Density Polymer Brushes in Good Solvent

Reproduced with permission from Elliott, I. G.; Kuhl, T. L.; Faller, R. Molecular Simulation Study of the Structure of High Density Polymer Brushes in Good Solvent. Macromolecules ***2010,*** *43, (21), 9131-9138,*

2.1 Chapter Abstract

Molecular dynamics simulations are presented of coarse-grained polar polymer brushes in a good polar solvent at high grafting densities. Chain extension is heavily influenced by temperature, stretching far from the surface at high temperature (350 K) while adsorbing to a weakly polar surface at low temperature (300 K). Resulting from adsorption and loop formation, average chain extension is low at 300 K. Simulations of isolated free polymers of different chain lengths in solution demonstrate the polymers are in good solvent conditions at both temperatures. Consistent with previous findings, increasing grafting density leads to larger chain extension under all conditions. A saturation limit is found at 350 K for high chain length and grafting density at about half the bulk polymer density. Even at very high grafting densities a polymer depletion region near the surface is observed at 350 K due to an orthogonal orientation of the chain at the grafting surface. Radial distribution functions reveal that the grafting pattern does not affect the overall brush configuration beyond the first five monomers of each chain as long as the surface is homogeneously covered.

2.2 Introduction

A polymer brush is formed when solvated polymer chains are grafted to a surface at a density high enough that they laterally interact with each other. Excluded volume

effects and the affinity of the polymer to the solvent cause the chains to stretch away from the surface.[1] Polymer brushes have been studied extensively due to their ability to modify surface properties to prevent colloid aggregation and enhance lubrication or adhesion.[2-5] When properly designed, polymer brushes in good solvent conditions have been shown to remarkably reduce friction.[6] The brush structure and its properties can be controlled by tuning grafting density, polymer molecular weight, temperature, and solvent quality.[7] In order to design polymer brushes effectively for specific applications it is necessary to understand how the system is affected by these variables. Numerous theoretical,[8-15] experimental,[16-20] and simulation[21-34] studies have examined polymer brush structure and properties, yet most of these have not investigated brushes at very high grafting densities.

Molecular simulations are excellent tools for studying polymer brush systems under varying conditions. Many conditions are difficult or impossible to examine with physical experiments, thus, simulations can provide insight to features of the system that cannot otherwise be accessed and understood. Simulation data corresponding to specific experimental conditions can be compared to validate or modify the simulation model. For this work, a polar polymer brush system in a good, polar solvent was simulated using a coarse-grained approach. All non-bonded interactions are based on a Lennard-Jones potential. The surface has an attractive interaction with both the polymer and solvent although not as strong as polymers and solvents among each other. The simulations represent roughly 3,000 to 10,000 g/mol chains (40 to 150 coarse-grained monomers) over a range of grafting densities. Coarse-graining is necessary to enable reasonable polymer lengths to be reached, while still allowing for high grafting densities. The high

grafting densities examined in this study are achievable experimentally by "grafting from" techniques such as atomic transfer radical polymerization (ATRP).[35, 36] For such systems, atomistic simulations are not feasible due to both the large number of particles and the ensuing long equilibration times.

2.3 Model

Coarse-grained molecular dynamics simulations were performed based on the MARTINI lipid model (V 1.4) developed by Marrink.[37] This model has been successfully used to study amphiphilic co-polymer systems interacting with surfaces[38] and polymer brush systems.[39] To increase polymer chain length and the efficiency of the simulation, every interaction site represents 4-5 heavy atoms as one "superatom". Each superatom is set to a mass of 72 amu, corresponding for example, to the mass of four water molecules. This mass is not intended to reproduce a specific polymer, but instead is representative of a generic polar polymer. One example of a coarse-grained mapping is shown in Figure 2-1 where water and polyethylene-oxide (PEO) are used to exemplify the model. Using such a representation, the effect of variables such as grafting density, chain length, and temperature on the brush structure can be qualitatively determined for systems that are too large for atomistic simulations. It should be noted, however, that specifics of the water – polyethylene-oxide system cannot be deduced from these coarse grained simulations. Rather, the properties of a generic polar solvent-polar polymer brush system are examined.

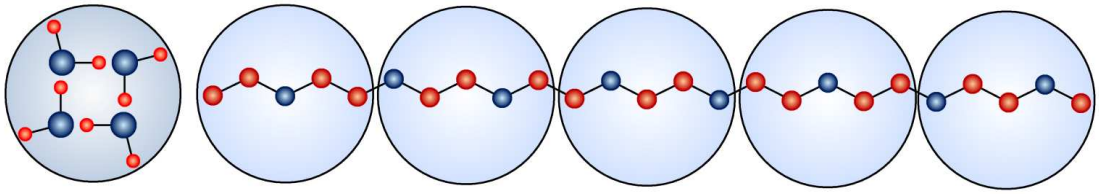

Figure 2-1. Coarse-grained representations for superatoms of solvent, e.g. water (left), and polymer, e.g. PEO (right). Each coarse-grained superatom has a mass of 72 amu, representing 4-5 heavy atoms.

In the model, superatoms along the polymer backbone interact by a weak harmonic potential based on an equilibrium bond length (R_{bond}) of 0.47 nm and a force constant (K_{bond}) of 1250 kJ mol^{-1} nm^{-2}.

$$V_{bond}(R) = \frac{1}{2} K_{bond} (R - R_{bond})^2 \tag{2-1}$$

R is the distance between a bonded pair. Similarly, angle bending is described with a weak cosine based angle potential with an equilibrium bond angle (θ_0) of 180° and a force constant (K_{angle}) of 25 kJ mol^{-1} rad^{-2}.

$$V_{angle}(\theta) = \frac{1}{2} K_{angle} [\cos(\theta) - \cos(\theta_0)]^2 \tag{2-2}$$

θ is the angle between three consecutive superatoms. The weak bonding potentials yield a flexible polymer chain. Non-bonded interactions are represented by a Lennard-Jones potential.

$$V_{LJ}(r) = 4\varepsilon \left[\left(\frac{\sigma}{r} \right)^{12} - \left(\frac{\sigma}{r} \right)^{6} \right] \tag{2-3}$$

r is the particle separation distance, σ represents the range of the interaction and ε the interaction strength. Lennard-Jones interactions, which are not considered for directly bonded particles, account for interactions of particles that are generically polar, non-

polar, or charged in the MARTINI model. Therefore, this model does not describe a specific polymer-solvent system. It instead can be used to represent a polar or non-polar brush system in good, theta, or poor solvents. For these studies, a polar polymer in a good, polar solvent was simulated. When using this coarse-grained model there is an inherent speed up of the dynamics by a factor of four and simulation times are often multiplied by four to reflect this.[37] All times reported in this paper are the actual simulation times, not the effective times accounting for the increase in dynamics.

Particles that compose the surface remained completely fixed throughout the simulation and only interacted with moving particles. The surface was infinitely extended through periodic boundary conditions in the *x*-*y* plane, and prevented particles from passing through. Polymer chains were grafted to the surface in a regular pattern. When possible a square grid was used (e.g. 25 chains grafted as 5 rows with 5 equally spaced chains each). If a square grid was not possible, the closest square was used with additional chains inserted and the in-plane distances within the augmented rows and columns were adapted to distribute chains evenly. One end monomer of each polymer chain was fixed 0.3 nm above the surface, creating an end-grafted system as shown in Figure 2-2. As with the polymer and solvent, the surface was polar. The surface interaction with the solvent and polymer chains was reduced to about one-third the interaction between all other polar particles to mitigate polymer adsorption to the surface. The Lennard-Jones values for each particle interaction are provided in Table 2-1.

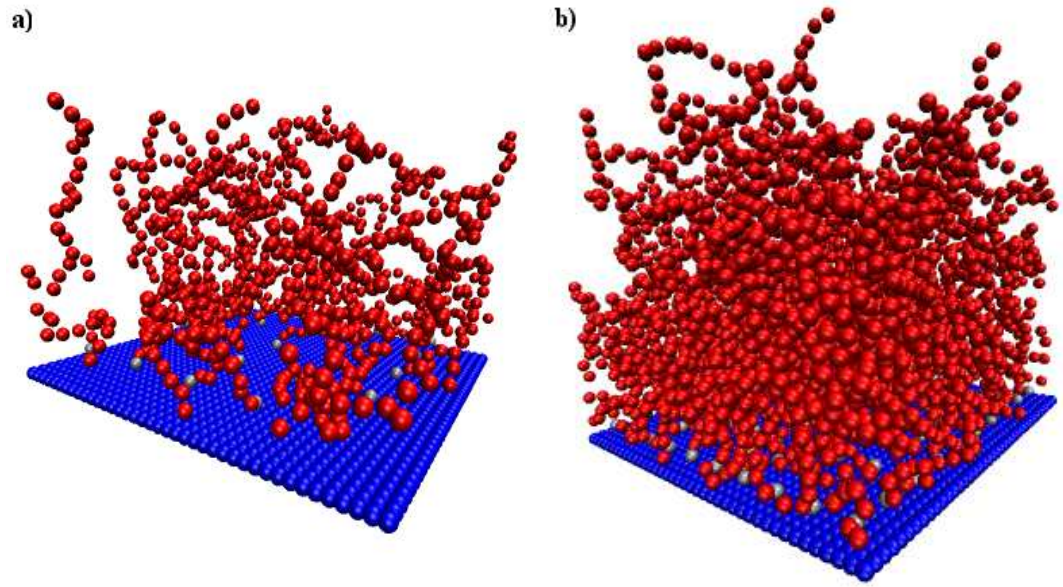

Figure 2-2. Snapshots using the VMD package[40] of the lowest (a) and highest (b) grafting density brush systems of 40 monomer chains at 350 K. Polymer atoms are red, surface atoms are blue, and chain grafting sites are silver. Solvent particles are omitted for clarity.

Interaction	σ (nm)	ε (kJ/mol)
Solvent-Solvent	0.47	5.00
Polymer-Polymer	0.47	5.00
Polymer-Solvent	0.47	5.00
Wall-Polymer	0.47	1.68
Wall-Solvent	0.47	1.68

Table 2-1. Lennard-Jones interaction parameters for each coarse-grained particle type.

Gromacs versions 3.3.3[41] or 4.0.4[42] were used for the simulations. Orthorhombic periodic boundary conditions were applied in all three dimensions. The box was 12 nm long in the *x* and *y* directions. The *z* direction length was selected to be larger than the length of a fully stretched chain plus the interaction cutoff radius. The *z* length was thus

different for each chain length, and ranged from about 20 to 80 nm. Semi-isotropic pressure coupling was invoked, fixing the box length in the *x* and *y* direction and allowing the *z* direction to vary, maintaining the normal pressure at one atmosphere. The *z* direction length typically changed less than 2 nm throughout the course of the simulation due to pressure coupling. A Berendsen barostat[43] was used for pressure coupling with a correlation time τ_P = 1 ps when using Gromacs 3.3.3 and τ_P = 2 ps when using Gromacs 4.0.4. Temperature was controlled using a Berendsen thermostat[43] with a correlation time of τ_T = 1 ps.

A steepest decent energy minimization algorithm was used to remove initial bad contacts created by placing atoms in the box. To stabilize the system further, the first nanosecond of each simulation used a small time step of 0.001 ps. Following this stabilization the simulation proceeded with a time step of 0.02 ps. A Verlet-type neighbor list was used and updated every 10 steps with a 1.2 nm cutoff with the twin-range cutoff method.[44] The Lennard-Jones cutoff distance was r_{cut} = 1.2 nm.

2.4 Systems

A polar polymer brush system in good solvent was examined under equilibrium conditions. Polymer brush properties were characterized at different grafting densities, temperatures, and chain lengths. The grafting densities studied were 0.174, 0.347, 0.486, and 0.694 chains/nm^2, the highest of which corresponds to the upper limit experimentally attainable with "grafting from" approaches such as ATRP.[32] Simulations at all grafting densities were performed for chains of 40 coarse-grained monomers at 300 and 350 K. All grafting densities were additionally studied using longer chains of 100 coarse-grained monomers at 350 K. The highest grafting density was further investigated with chains of

150 monomers at 350 K. Often grafting density is expressed as an overlap grafting density[36, 45, 46] defined by,

$$\sigma^* = \pi R_g^2 \Sigma \tag{2-4}$$

where Σ is the grafting density expressed as chains/area and R_g is the radius of gyration obtained from simulations of free polymer solutions under the same conditions as the brush. The overlap grafting density represents the ratio of the cross sectional area the chains would adopt in a free solution to the area the chains are restricted to per grafted site in the brush. When $\sigma^* < 1$, the system is considered to be in the mushroom regime where the chains do not have significant lateral interaction. For $\sigma^* > 1$ the chains are restricted to less area than they would occupy in solution, and therefore interact with neighboring chains forming a brush. σ^* in this study ranged from modest ($\sigma^* = 3.48$) to very high ($\sigma^* = 71.4$). The specifics of all systems are given in Table 2-2.

Grafting Density, Σ (chains/nm^2)	σ*	Monomers per Chain	Temperature (K)	Total Simulation Time (ns)	Production Time (ns)
0.174	3.85	40	300	5000	3000
	3.48	40	350	1100	1000
	9.87	100	350	2000	1500
0.347	7.71	40	300	800	500
	6.97	40	350	1300	1100
	19.7	100	350	8700	3700
0.486	10.8	40	300	5100	3100
	9.75	40	350	1300	1000
	27.6	100	350	6002	5002
0.694	15.4	40	300	6200	3000
	13.9	40	350	1400	1200
	39.5	100	350	6192	3192
	71.4	150	350	4292	1792

Table 2-2. Details for all simulations. Production time is the amount of time that reported properties were averaged over after equilibration.

2.5 Results

For a polymer system, the longest relaxation time is the chain reorientation time. Therefore, this property was monitored to confirm equilibration. Rotational autocorrelation functions accounted for the reorientation of a vector defined between the first and last monomers of a polymer chain. For a polymer melt or solution where the chains are able to freely move, the system would be considered equilibrated once the rotational autocorrelation function reached zero. A polymer brush system, however, has chains attached at the surface, which imposes an orientation on the chains throughout the simulation and thus the autocorrelation function never reaches zero. Therefore, for the

brush systems examined, equilibrium was defined as the point when the autocorrelation function reaches a steady long time limit. Depending heavily on chain length, equilibration took anywhere from 100 ns to several microseconds to achieve (See Table 2-2). The rotational autocorrelation functions for the lower temperature and longer chain systems showed greater variability compared to the 40 monomer chains at 350 K. Equilibrium was additionally confirmed for the low temperature and long chain systems by observing negligible change in the polymer density profile and the radius of gyration over several hundred nanoseconds. In the following, all reported property averages were taken after the system had equilibrated.

At the low temperature of 300 K, surface adsorption dominated over excluded volume stretching for all grafting densities. The chains adsorbed to the surface until roughly a monolayer was formed, and extended only weakly into the solvent as indicated in Figure 2-3. Density profiles for 350 K simulations at the same grafting densities are also shown in the plot in Figure 2-3 a) to clearly illustrate the influence of temperature. In addition, Figure 2-4 shows the increase in extension from the surface at 350 K with increasing grafting density for chain lengths of 40, 100, and 150 monomers. The 300 K simulations were initialized with the output configuration from the 350 K runs, and thus began stretched. As each low temperature simulation adsorbed from a stretched state, the final structures should be viewed as the equilibrium structure and not as the conformation of a brush in a kinetic trap.

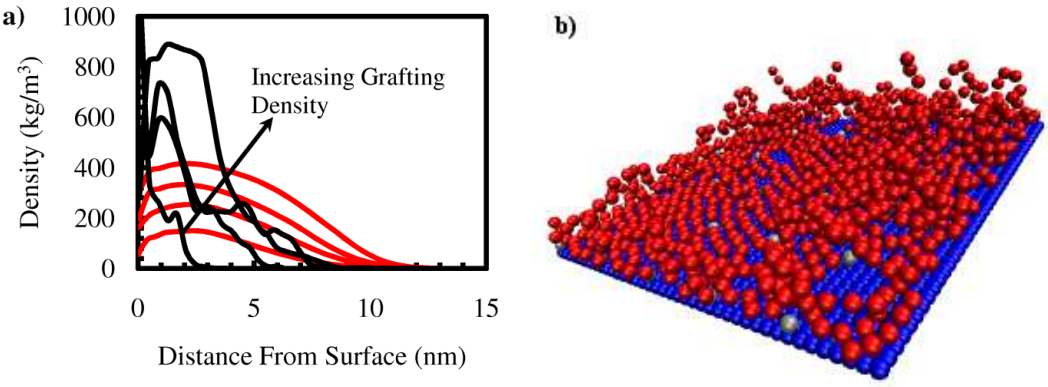

Figure 2-3. a) Polymer density profiles of a brush consisting of 40 monomer chains at four grafting densities (Σ = 0.174, 0.347, 0.486, and 0.694 chain/nm^2) at 300 K (black) and 350 K (red). Grafting density increases from bottom to top for both black and red curves. b) A VMD[40] image corresponding to the lowest grafting density system of Σ = 0.174 chains/nm^2 of 40 monomer chains at 300 K.

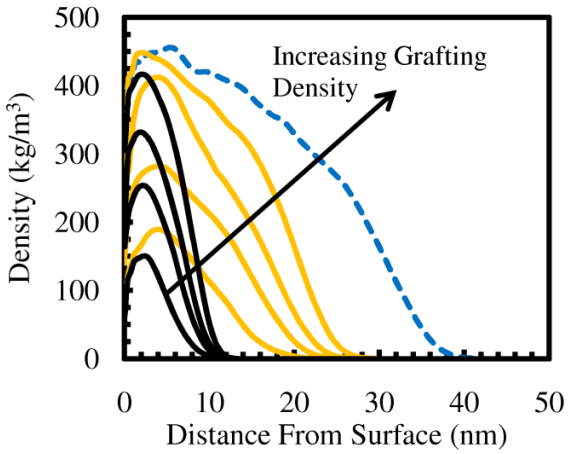

Figure 2-4. Polymer density profiles of polymer brushes at different grafting densities at 350 K. Data is presented for chains of 40 (solid black), 100 (solid orange) and 150 (dashed blue) monomers.

The difference between the brush structure at 300 and 350 K raises the question of solvent quality. Simulations of isolated ungrafted polymers in solution were conducted at several chain lengths ranging from 20 to 150 monomers at both 300 and 350 K to ascertain how the solvent quality depended on temperature. The radius of gyration data is

shown in Figure 2-5 a) for 300 K and b) for 350 K. A power law is fit to each set of data to determine the dependence of radius of gyration on chain length. This dependence is compared to the theoretical prediction of $R_g \sim N^{\nu}$ where $\nu = 0.5$ and 0.6 for theta and good solvents, respectively. As ν in each case is close to 0.6, all simulations at 300 and 350 K were conducted in good solvent conditions although at 300K a slight tendency towards theta conditions was observed ($\nu = 0.55$). The polymer adsorption observed at 300 K was therefore not due to poor solvent quality, but instead resulted from adsorption to the surface which often created chain loops. In the case of low grafting densities, most of the polymer is adsorbed in the monolayer above the surface. At higher grafting densities, a monolayer is still adsorbed to the surface, but many of the chains adsorb at segments in the middle or end of the chain, forming loops as shown in Figure 2-6. Loops of this sort were observed for $\Sigma = 0.347$, 0.486, and 0.694 chains/nm^2, and were not present for the lowest grafting density as too much of the chains were adsorbed to allow for loops as in Figure 2-3 b). This restriction accounts for the double peaks observed in the 300 K density profiles in Figure 2-3. Essentially there are two populations of chains with very different dimensions. One group forms loops or adsorbed chains, yielding a shorter brush height than expected for good solvent conditions. The second does not adsorb, as no adsorption sites are vacant, and stretches out into the solvent from excluded volume interactions as shown in Figure 2-6. The effect is the density profile exhibits one peak close to the surface from the loops, and a smaller peak farther away from the surface corresponding to the stretched chains. There are of course situations in between the two extremes shown in Figure 2-6, where the chains partially adsorb or form a loop near the

bottom of the chain, and then extend outward from the surface. This simply broadens the peaks in the density profiles and makes the second peak less noticeable.

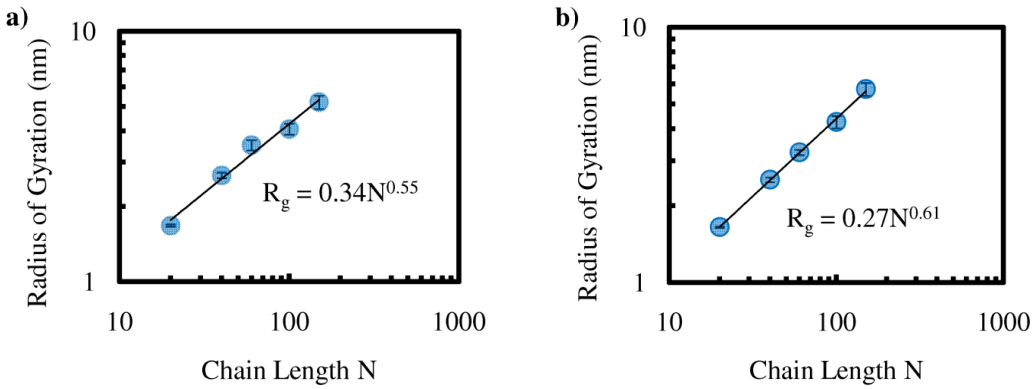

Figure 2-5. Radius of gyration versus chain length data for simulations of isolated, free chains in solution at a) 300 K and b) 350 K.

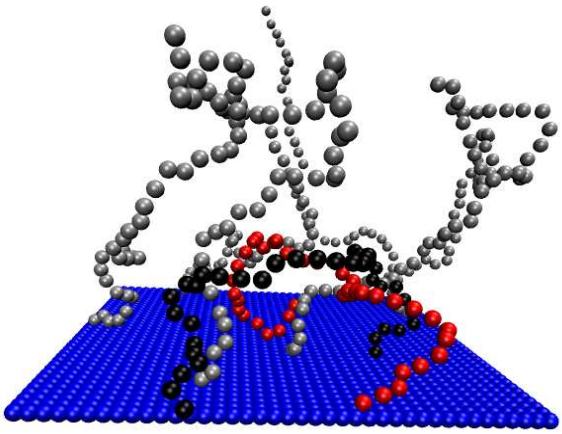

Figure 2-6. Snapshot of selected chains from a brush system at 300 K with grafting density $\Sigma = 0.694$ chains/nm^2 and $N = 40$. Two chains that form loops (red and black) by having monomers near their ungrafted ends adsorb to the surface are shown. Several stretched chains are present (silver) to illustrate the different conformations occurring at the lower temperature.

Another interesting difference of the profiles with respect to temperature is observed very close to the surface. As the temperature increases from 300 to 350 K (Figure 2-3), the absorbed layer of polymer vanishes completely and a solvent rich polymer depletion layer forms. This effect is even more obvious in the solvent density profiles for varying

polymer grafting densities presented in Figure 2-7. For all grafting densities at 350 K, a peak occurs in each solvent density profile near the surface. There is more solvent (and correspondingly less polymer) directly above the surface than throughout the bulk of the brush, indicating a polymer depletion layer. The depletion region is due to the surface limiting the chain orientations that can be adopted close to the surface, reducing their entropy. This has been observed for low grafting densities previously[47-49] but was not expected for high grafting densities as the entropic penalty for chain extension decreases with increasing grafting density or chain length. A depletion layer for high grafting densities has rarely been reported.[29, 30]

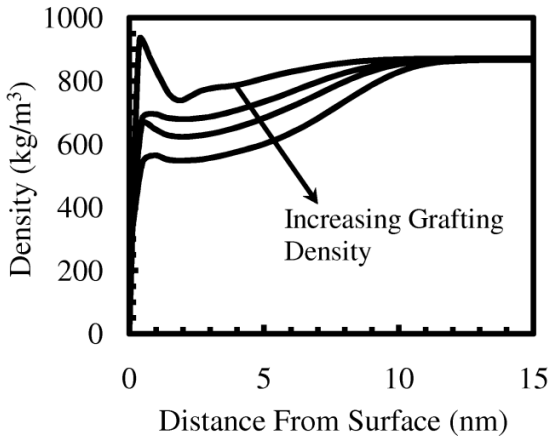

Figure 2-7. Solvent density profiles corresponding to polymer brush systems comprised of 40 monomer chains at 350 K for different grafting densities.

The structural dependence of the brush with respect to chain length was also examined. Focusing on the highest grafting density curves of Figure 2-4 at chain lengths of 40, 100 and 150 monomers, the influence of chain length at high grafting density can be deduced. A plateau in the density profile occurred at around 450 kg/m^3. Increasing the chain length by 50% from 100 to 150 monomers did not significantly increase the maximum polymer density, but rather broadened the curve through greater chain extension. Therefore, once

the peak polymer density reached about half the bulk density, increasing the chain length caused further chain extension away from the surface as opposed to increasing the amount of polymer near the surface. At the plateau density the brush reaches its maximum density where the numerical value is assumed to be model dependent. However, the concept of a maximum density is not expected to be model dependent as the only alternative would be a continuous decay in density from the surface outwards. At low grafting densities such a continuous decay is expected and observed but at a critical grafting density the brush eventually reaches a maximal density. A plateau was reached in the simulations with a grafting density of 0.694 chains/nm^2 but not for any of the lower grafting densities. Thus, the critical grafting density for saturation is between 0.486 and 0.694 chains/nm^2. A flattening out of the density profile has been reported for large σ^* values in other simulation studies.[30, 31]

The polymer chain end distribution was calculated for the 350 K systems by using the density profile of each chain's end monomer and normalizing it to a total probability of unity (Figure 2-8). In all cases the chain end has finite probability of being at the surface. The peak in the end distribution profile is shifted away from the surface when either grafting density or chain length is increased. Self consistent field theory[1, 9] predicts the peak to occur at $z = 0.7\ h_0$. The simulated density profiles are close to this peak value for all but the lowest grafting density.

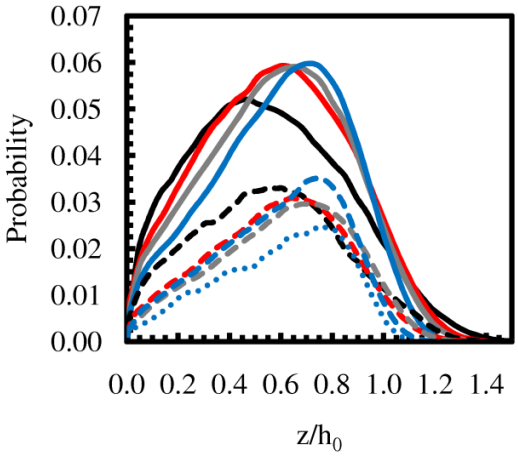

Figure 2-8. Chain end distributions of polymer brushes at 350 K in good solvent. Grafting densities are Σ = 0.174, 0.347, 0.486, and 0.694 chains/nm^2 represented by black, red, gray, and blue lines respectively. Chain lengths are N = 40, 100, and 150 monomers represented with solid, dashed, and dotted lines respectively.

The average chain tilt was calculated to quantify the brush orientation with respect to the surface. A vector was defined for each polymer chain from the grafting site to the free end monomer and the angle between this vector and the surface normal defined the tilt. Smaller tilt angles indicate a chain orientation more normal to the surface. Tilt as a function of overlap grafting density is provided in 2-9 a) and yields an almost linearly decreasing tilt with overlap grafting density. To explicitly show the effect of chain length, tilt is also plotted against grafting density for different chain lengths in Figure 2-9 b). The average chain tilt substantially decreased with either grafting density or chain length. The lowest average angle was observed for the highest grafting density and chain length, indicating an increased orientation normal to the surface (i.e. greater extension from the surface).

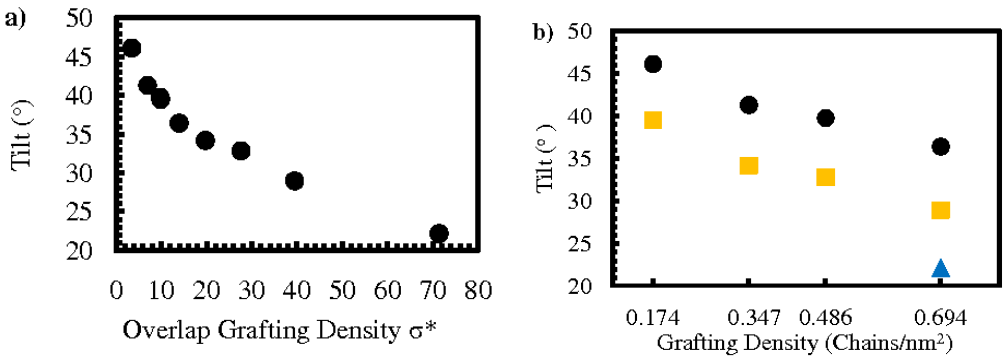

Figure 2-9. Average tilt angle of polymer chains at 350 K as a function of overlap grafting density (a) and grafting density (b). In figure b), data is given for three different chain lengths of 40 (black circles), 100 (orange squares), and 150 (blue triangles) monomers. Tilt is defined as the angle between the surface normal and a vector from the grafting site to the end monomer of each chain.

The uncompressed brush height is another useful quantity from simulation results that can be compared to theoretical models. Following the work of Binder's group[32, 33] brush height was defined as,

$$h_0 = \frac{8}{3}\langle z \rangle = \frac{8}{3}\frac{\int_0^\infty z\phi(z)dz}{\int_0^\infty \phi(z)dz} \qquad (2\text{-}5)$$

where $\phi(z)$ is the polymer density profile and z is the distance from the surface.

This value was normalized by chain length and compared to theoretical models predicting the dependence of brush height on grafting density. Theoretically, for a single brush in good solvent the brush height is expected to scale as $h_0/N \sim \sigma^{*1/3}$ where h_0 is the uncompressed brush height, N the number of monomers per chain, and σ^* the overlap grafting density.[14, 45] Figure 2-10 depicts the simulated brush height values as a function of overlap grafting density with a power law fit to compare to theory.

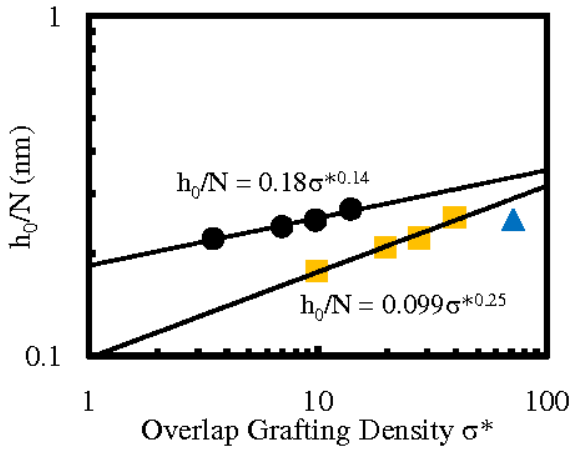

Figure 2-10. Values of uncompressed brush height normalized by chain length versus overlap grafting density. Three different chain lengths of 40 monomers (black circles), 100 monomers (orange squares), and 150 monomers (blue triangles) are shown.

While Figure 2-10 was expected to yield a universal curve, two distinct trends were observed depending on chain length. The 40 and 100 monomer chain data scale as $\sigma^{*0.14}$ and $\sigma^{*0.25}$ respectively. Increasing chain length pushes the trend towards the theoretically predicted $\sigma^{*0.33}$. As self-consistent mean field theory becomes more reliable with increasing chain length, it is expected that data for the 150 monomer chains would follow the theoretical trend more closely. Experimentally, however, deviations from the theoretical trend have been reported. Kent[50] found brush height varying as $\sigma^{*0.22}$ for good solvent, which is quite close to the trend for the longer chains in Figure 2-10.

Similar to Equation 2-5, the root-mean-squared (rms) brush height is defined as,[45, 51]

$$h_{rms}^2 = \frac{\int_0^\infty z^2 \phi(z) dz}{\int_0^\infty \phi(z) dz} \quad (2\text{-}6)$$

For good solvent, analytical self consistent field theory (ASCF)[45, 51] predicts parabolic density profiles where the root mean squared brush height values relate to the brush height as $h_{rms}^0 = h_0/\sqrt{5}$. The brush heights in this study follow this relation nearly

perfectly (see Table 2-3), with the good solvent ASCF predicted h^0_{rms} values deviating by less that 0.5% of the calculated h^0_{rms} for all systems at 350 K. A similar relationship exists for theta solvents, predicting $h^0_{rms} = h_0/2$. The ASCF theta solvent prediction deviates significantly from the calculated h^0_{rms} values in this work. Along with the free chain radius of gyration data, this additionally confirms that the simulations conducted at 350 K were in good solvent conditions. Table 2-3 indicates that although the chains are short in comparison to the long chains of self consistent field theory, the ratios predicted are nonetheless applicable as they depend very weakly on chain length.

Monomers per Chain	Grafting Density, Σ (chains/nm^2)	h_0 (nm)	h^0_{rms} (nm)		
			Simulated Good Solvent	ASCF Good Solvent	ASCF θ Solvent
40	0.174	8.852	3.957	3.959	4.426
	0.347	9.603	4.305	4.295	4.802
	0.486	10.032	4.496	4.486	5.016
	0.694	10.812	4.835	4.835	5.406
100	0.174	17.77	7.905	7.947	8.885
	0.347	20.889	9.333	9.342	10.445
	0.486	22.182	9.962	9.920	11.091
	0.694	25.591	11.407	11.445	12.796
150	0.694	37.696	16.810	16.858	18.848

Table 2-3. Comparison of the simulated h^0_{rms} values to theoretical predictions for good and theta solvents based on h_0.

To further compare the simulated results with theoretical predictions, calculations were performed using the numerical self consistent field (NSCF) theory model developed by Whitmore et al.[45] using the same conditions as in the simulations. Figure 2-11 presents

simulated density profiles for 40 monomer chains at 350 K for the four grafting densities studied and compares them to profiles produced using NSCF theory with parameters N = 40, b = 0.47 nm, l = 0.157 nm, χ = -1.25, $\rho_{0A} = 0.85b^{-3}$ and $\rho_{0S} = 0.75b^{-3}$. NSCF profiles were also examined for χ = 0 and 0.4, but both of these yielded results that significantly deviated from the simulations.

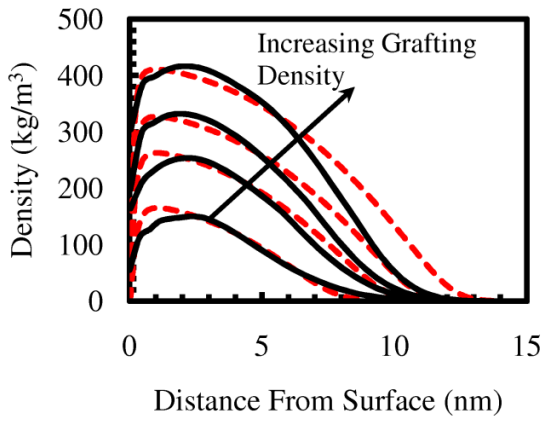

Figure 2-11. Polymer density profiles from simulations (solid black) and numerical self consistent field theory (dashed red) at grafting densities of (from bottom to top) Σ = 0.174, 0.347, 0.486, and 0.694 chains/nm^2.

The predictions from NSCF theory match the simulation results relatively well considering the short chain lengths. The primary difference is that NSCF theory predicts a smaller polymer depletion region as the peak occurs closer to the surface. NSCF theory also predicts larger chain extension than was observed for the higher grafting densities.

Radial distribution functions g(r) were calculated to investigate lateral order within the brush and to determine how grafting patterns influence the structure. Reflecting the two dimensional nature of the system, the radial distribution functions were calculated within the *x-y* plane for a given set of atoms in the polymer chains. A specific monomer in each chain was considered, and its correlation with respect to the same monomer in all other chains determined. For low grafting density, peaks were observed in the radial

distribution function that directly corresponded to the applied grafting pattern. These peaks are most pronounced for the monomers close to the grafting point, and dissipate by about the fifth monomer as shown in Figure 2-12 a). Radial distribution functions for the highest grafting density in Figure 2-12 b) indicate correlations at intervals corresponding to the bead size (0.47 nm) up to two layers away. For monomers at the base of the chain, there are also peaks corresponding to the grafting pattern, but this quickly vanishes except for the nearest neighboring chain. Therefore, at low grafting density the grafting pattern only influenced the chain segments closest to the surface. For high grafting density systems, correlations were observed between nearest neighboring chains throughout most of the brush. These correlations are due to the fact that it is a densely packed brush, and as such correlations with neighboring particles are inevitable. Therefore, the grafting pattern used (regular or random) does not affect the overall structure of the brush provided the grafting density heterogeneity is not significant.

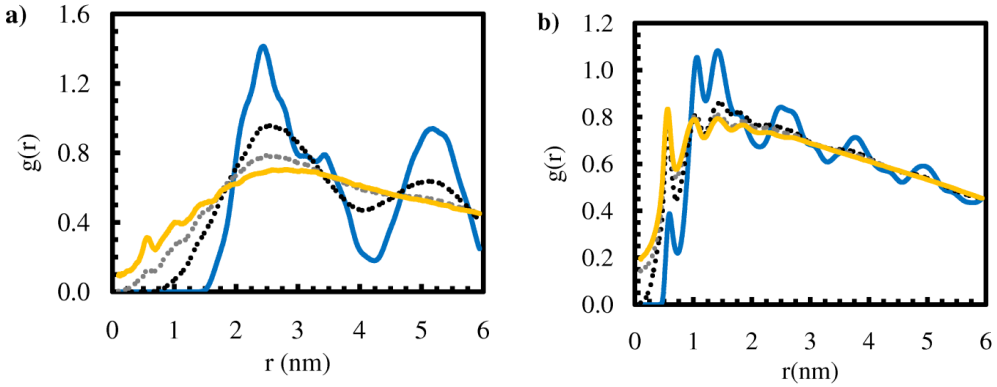

Figure 2-12. Lateral radial distribution functions of specific monomers in a polymer brush. The brush consists of chains of 40 monomers at 350 K grafted at the lowest grafting density of 0.174 chains/nm^2 (a) and the highest grafting density of 0.694 chains/nm^2 (b). Data is given for the correlation between the 2nd (solid blue), 3rd (dotted black), 4th (dotted gray), and 5th (solid orange) monomers from the grafting site. A running average was taken over the data such that each data point is averaged over about 0.1 nm.

2.6 Conclusion

Polymer brushes were characterized with respect to grafting density, temperature, and molecular weight. A coarse-grained representation of a polar polymer in polar solvent was used to obtain qualitative structure information on the system. Static properties such as density profiles, radial distribution functions, chain tilt, and brush height were used to quantify brush structure. High grafting densities up to $\Sigma = 0.694$ chains/nm^2 or $\sigma^* = 71.4$ were examined.

Temperature substantially affected brush structure, dictating whether adsorption to the surface or chain extension dominates. Lower temperature favored surface adsorption, while higher temperature led to greater chain extension. Determination of the single chain radius of gyration at various chain lengths demonstrated that both the 300 and 350 K simulations were conducted under good solvent conditions. Brush height relations between h_0 and h^0_{rms} were also found to be consistent with good solvent predictions. The structure of the 300 K brushes as determined by density profiles resembled a collapsed brush in poor solvent conditions. This was not the case, however. Upon closer inspection of the trajectories, the collapsed structure was attributed to the formation of absorbed loops. The loops restrict the maximum height that any polymers adsorbed in this way could attain. Chains which did not form loops extended from the surface normally for a good solvent.

Grafting density strongly affected the structure of the brush. Higher grafting densities had more excluded volume interactions causing greater chain extension from the surface at all temperatures and chain lengths. This was additionally confirmed by the average chain tilt relative to the surface which demonstrated that chains oriented more normal to

the surface with increasing grafting density or chain length. In addition, the presence of the surface and resulting configurational entropy loss of chain ends close to the surface also contributed to the normal orientation of the chains. As a result, in all 350 K simulations a polymer depletion region was observed near the grafting surface even at the very high grafting densities studied. Increasing chain length led to an increase in the maximum polymer density and chain extension for the three lower grafting densities studied. The highest grafting density system eventually reached a saturation limit, and therefore only chain extension was affected by polymer size after this limit was reached. This should be a general feature for all polymer – solvent systems and provide a limit on the maximum density of polymer near the surface.

Lateral radial distribution functions indicate that the grafting pattern only substantially affected the first five monomers from the surface on each chain. Beyond that, there was little order between chain segments corresponding to the grafting site separation, and thus the grafting pattern was essentially lost. Similar results may therefore be expected for systems formed with a regular or random grafting pattern, provided the grafting points are reasonably distributed on the surface.

With static properties understood, similar studies will be conducted to examine the system's dynamic response to perturbation such as shear and compression. Polydispersity, which has been shown to greatly affect brush structure particularly at high grafting densities,[52] will also be investigated.

The structure of the adsorbed polymers at the surface may be influenced by kinetic traps whereas the simulations overall are definitely in equilibrium. So in order to address the structure of the adsorbed layer advanced Monte Carlo moves may be helpful.

2.7 Acknowledgements

This work was supported by the United States Department of Energy, Office of Basic Energy Science under grant DE-FG02-06ER46340. IGE additionally thanks the Graduate Assistance in Areas of National Need (GAANN) program of the US Department of Education. Computer time at the National Energy Research Supercomputer Center which is supported by the Office of Science of the U.S. Department of Energy under Contract No. DE-AC03-76SF00098 has been used for parts of the simulations.

2.8 References

1. Milner, S. T. Polymer Brushes. *Science* **1991,** 251, (4996), 905-914.

2. Advincula, R. C.; Brittain, W. J.; Caster, K. C.; Ruhe, J., *Polymer Brushes*. Wiley-VCH: Weinheim, 2004.

3. Napper, D. H., *Polymeric Stabilization of Colloidal Dispersions*. Academic Press: London, 1983.

4. Hamilton, W. A.; Smith, G. S.; Alcantar, N. A.; Majewski, J.; Toomey, R. G.; T. L. Kuhl. Determining the density profile of confined polymer brushes with neutron reflectivity. *Journal of Polymer Science Part B: Polymer Physics* **2004,** 42, (17), 3290-3301.

5. Pastorino, C.; Binder, K.; Kreer, T.; Muller, M. Static and dynamic properties of the interface between a polymer brush and a melt of identical chains. *J. Chem. Phys.* **2006,** 124, (6), 064902.

6. Klein, J.; Kumacheva, E.; Mahalu, D.; Perahia, D.; Fetters, L. J. Reduction of frictional forces between solid surfaces bearing polymer brushes. *Nature* **1994,** 370, (6491), 634-636.

7. Auroy, P.; Auvray, L.; Léger, L. Characterization of the brush regime for grafted polymer layers at the solid-liquid interface. *Phys. Rev. Lett.* **1991,** 66, (6), 719.

8. Alexander, S. Adsorption of chain molecules with a polar head: a scaling description. *Journal de physique.* **1977,** 38, 983-987.

9. Milner, S. T.; Witten, T. A.; Cates, M. E. Theory of the grafted polymer brush. *Macromolecules* **1988,** 21, (8), 2610-2619.

10. Milner, S. T.; Witten, T. A.; Cates, M. E. A Parabolic Density Profile for Grafted Polymers. *EPL (Europhysics Letters)* **1988,** 5, (5), 413-418.

11. Halperin, A.; Zhulina, E. B. Stretching polymer brushes in poor solvents. *Macromolecules* **1991,** 24, (19), 5393-5397.

12. Biesheuvel, P. M. Ionizable polyelectrolyte brushes: brush height and electrosteric interaction. *Journal of Colloid and Interface Science* **2004,** 275, (1), 97-106.

13. Biesheuvel, P. M.; de Vos, W. M.; Amoskov, V. M. Semianalytical Continuum Model for Nondilute Neutral and Charged Brushes Including Finite Stretching. *Macromolecules* **2008,** 41, (16), 6254-6259.

14. de Gennes, P. G. Conformations of Polymers Attached to an Interface. *Macromolecules* **1980,** 13, (5), 1069-1075.

15. Wijmans, C. M.; Scheutjens, J. M. H. M.; Zhulina, E. B. Self-consistent field theories for polymer brushes: lattice calculations and an asymptotic analytical description. *Macromolecules* **1992,** 25, (10), 2657-2665.

16. Auroy, P.; Mir, Y.; Auvray, L. Local structure and density profile of polymer brushes. *Phys. Rev. Lett.* **1992,** 69, (1), 93.

17. Cho, J.-H. J.; Smith, G. S.; Hamilton, W. A.; Mulder, D. J.; Kuhl, T. L.; Mays, J. Surface force confinement cell for neutron reflectometry studies of complex fluids under nanoconfinement. *Review of Scientific Instruments* **2008,** 79, (10), 103908.

18. Smith, G. S.; Kuhl, T. L.; Hamilton, W. A.; Mulder, D. J.; Satija, S. Structure of confined polymer thin films subject to shear. *Physica B: Condensed Matter* **2006,** 385-386, (Part 1), 700-702.

19. de Vos, W. M.; Biesheuvel, P. M.; de Keizer, A.; Kleijn, J. M.; Cohen Stuart, M. A. Adsorption of the Protein Bovine Serum Albumin in a Planar Poly(acrylic acid) Brush Layer As Measured by Optical Reflectometry. *Langmuir* **2008,** 24, (13), 6575-6584.

20. de Vos, W. M.; Biesheuvel, P. M.; de Keizer, A.; Kleijn, J. M.; Cohen Stuart, M. A. Adsorption of Anionic Surfactants in a Nonionic Polymer Brush: Experiments, Comparison with Mean-Field Theory, and Implications for Brush−Particle Interaction. *Langmuir* **2009,** 25, (16), 9252-9261.

21. Grest, G. S. Grafted polymer brushes in polymeric matrices. *J. Chem. Phys.* **1996,** 105, (13), 5532-5541.

22. Murat, M.; Grest, G. S. Structure of a grafted polymer brush: a molecular dynamics simulation. *Macromolecules* **1989,** 22, (10), 4054-4059.

23. Lai, P. Y.; Zhulina, E. B. Structure of a bidisperse polymer brush: Monte Carlo simulation and self-consistent field results. *Macromolecules* **1992,** 25, (20), 5201-5207.

24. Lai, P.-Y.; Binder, K. Structure and dynamics of polymer brushes near the Theta point: A Monte Carlo simulation. *J. Chem. Phys.* **1992,** 97, (1), 586-595.

25. Lai, P.-Y.; Binder, K. Grafted polymer layers under shear: A Monte Carlo simulation. *J. Chem. Phys.* **1993,** 98, (3), 2366-2375.

26. Neelov, I. M.; Binder, K. Brownian dynamics simulation of grafted polymer brushes. *Macromolecular Theory and Simulations* **1995,** 4, (1), 119-136.

27. Neelov, I. M.; Borisov, O. V.; Binder, K. Stochastic dynamics simulation of grafted polymer brushes under shear deformation. *Macromolecular Theory and Simulations* **1998,** 7, (1), 141-156.

28. Neelov, I. M.; Borisov, O. V.; Binder, K. Shear deformation of two interpenetrating polymer brushes: Stochastic dynamics simulation. *J. Chem. Phys.* **1998,** 108, (16), 6973-6988.

29. He, G.-L.; Merlitz, H.; Sommer, J.-U.; Wu, C.-X. Static and Dynamic Properties of Polymer Brushes at Moderate and High Grafting Densities: A Molecular Dynamics Study. *Macromolecules* **2007,** 40, (18), 6721-6730.

30. Coluzza, I.; Hansen, J.-P. Transition from Highly to Fully Stretched Polymer Brushes in Good Solvent. *Phys. Rev. Lett.* **2008,** 100, 016104.

31. Seidel, C.; Netz, R. R. Individual Polymer Paths and End-Point Stretching in Polymer Brushes. *Macromolecules* **2000,** 33, (2), 634-640.

32. Kreer, T.; Metzger, S.; Muller, M.; Binder, K.; Baschnagel, J. Static properties of end-tethered polymers in good solution: A comparison between different models. *J. Chem. Phys.* **2004,** 120, (8), 4012-4023.

33. Dimitrov, D. I.; Milchev, A.; Binder, K. Polymer brushes in cylindrical pores: Simulation versus scaling theory. *J. Chem. Phys.* **2006,** 125, (3), 034905.

34. Dimitrov, D. I.; Milchev, A.; Binder, K. Polymer brushes in solvents of variable quality: Molecular dynamics simulations using explicit solvent. *J. Chem. Phys.* **2007,** 127, (8), 084905.

35. von Werne, T.; Patten, T. E. Atom Transfer Radical Polymerization from Nanoparticles: A Tool for the Preparation of Well-Defined Hybrid Nanostructures and for Understanding the Chemistry of Controlled/"Living" Radical Polymerizations from Surfaces. *Journal of the American Chemical Society* **2001,** 123, (31), 7497-7505.

36. Ell, J. R.; Mulder, D. E.; Faller, R.; Patten, T. E.; Kuhl, T. L. Structural Determination of High Density, ATRP Grown Polystyrene Brushes by Neutron Reflectivity. *Macromolecules* **2009,** 42, (24), 9523-9527.

37. Marrink, S. J.; de Vries, A. H.; Mark, A. E. Coarse Grained Model for Semiquantitative Lipid Simulations. *J. Phys. Chem. B* **2004,** 108, (2), 750-760.

38. Hatakeyama, M.; Faller, R. Coarse-grained simulations of ABA amphiphilic triblock copolymer solutions in thin films. *Phys. Chem. Chem. Phys.* **2007,** 9, (33), 4662-4672.

39. Elliott, I. G.; Mulder, D. E.; Traskelin, P. T.; Ell, J. R.; Patten, T. E.; Kuhl, T. L.; Faller, R. Confined polymer systems: synergies between simulations and neutron scattering experiments. *Soft Matter* **2009,** 5, (23), 4612-4622.

40. Humphrey, W.; Dalke, A.; Schulten, K. VMD: Visual molecular dynamics. *J. Mol. Graphics* **1996,** 14, (1), 33-38.

41. Lindahl, E.; Hess, B.; van der Spoel, D. GROMACS 3.0: a package for molecular simulation and trajectory analysis. *Journal of Molecular Modeling* **2001,** 7, (8), 306-317.

42. Hess, B.; Kutzner, C.; van der Spoel, D.; Lindahl, E. GROMACS 4: Algorithms for Highly Efficient, Load-Balanced, and Scalable Molecular Simulation. *J. Chem. Theory Comput.* **2008,** 4, (3), 435-447.

43. Berendsen, H. J. C.; Postma, J. P. M.; van Gunsteren, W. F.; DiNola, A.; Haak, J. R. Molecular dynamics with coupling to an external bath. *The Journal of Chemical Physics* **1984,** 81, (8), 3684-3690.

44. de Vlieg, J.; Berendsen, H. J. C.; van Gunsteren, W. F. An NMR-based molecular dynamics simulation of the interaction of the *lac* repressor headpiece and its operator in aqueous solution. *Proteins: Structure, Function, and Genetics* **1989,** 6, (2), 104-127.

45. Whitmore, M. D.; Baranowski, R. End-Anchored Polymers: Compression by Different Mechanisms and Interpenetration of Apposing Layers. *Macromolecular Theory and Simulations* **2005,** 14, (2), 75-95.

46. Baranowski, R.; Whitmore, M. D. Numerical self-consistent field study of tethered chains in Theta solvent. *J. Chem. Phys.* **1998,** 108, (23), 9885-9892.

47. Chen, C. M.; Fwu, Y. A. Monte Carlo simulations of polymer brushes. *Physical Review E* **2000,** 63, 011506.

48. Chakrabarti, A.; Toral, R. Density profile of terminally anchored polymer chains: a Monte Carlo study. *Macromolecules* **1990,** 23, (7), 2016-2021.

49. Grest, G. S.; Murat, M. Structure of grafted polymeric brushes in solvents of varying quality: a molecular dynamics study. *Macromolecules* **1993,** 26, (12), 3108-3117.

50. Kent, M. S. A quantitative study of tethered chains in various solution conditions using Langmuir diblock copolymer monolayers. *Macromolecular Rapid Communications* **2000,** 21, (6), 243-270.

51. Baranowski, R.; Whitmore, M. D. Theory of the structure of adsorbed block copolymers: Detailed comparison with experiment. *J. Chem. Phys.* **1995,** 103, (6), 2343-2353.

52. Merlitz, H.; He, G.-L.; Wu, C.-X.; Sommer, J.-U. Surface Instabilities of Monodisperse and Densely Grafted Polymer Brushes. *Macromolecules* **2008,** 41, (13), 5070-5072.

Chapter 3

A Molecular Dynamics Technique to Extract Forces in Soft Matter Systems Under Compression With Constant Solvent Chemical Potential

Reproduced with permission from Elliott, I. G.; Kuhl, T. L.; Faller, R. A Molecular Dynamics Technique to Extract Forces in Soft Matter Systems Under Compression With Constant Solvent Chemical Potential. J. Chem. Theory Comput. 2012, 8, (3), 1072-1077.

3.1 Chapter Abstract

Molecular dynamics simulations of opposing polymer brushes at varying surface separation distances were performed to develop a method for conducting a static compression of soft matter. As all separation distances were represented by independent simulations, the proper solvent density for every level of compression needed to be determined to acquire realistic data. This was accomplished by maintaining a constant solvent chemical potential for each separation distance. In doing so, each independent simulation is equilibrated with all others, reproducing conditions encountered experimentally in force spectroscopy measurements. Chemical potential was determined using the Widom test particle insertion method. Force information was extracted from pressure profiles, such that unphysical forces occurring within the surface layers were not accounted for in the calculation. Each individual simulation was a canonical ensemble molecular dynamics simulation, but taken together they approximate a grand canonical ensemble for the solvent particles by holding their chemical potential constant.

3.2 Introduction

Confined soft matter systems are encountered in biological science,[1, 2] tribology,[3, 4] and polymer science,[5, 6] and have numerous applications. The focus of this work is polymer brushes, which, for instance, have applications as lubricants[7] and colloidal stabilizers.[8, 9] For any system where two layers are brought into contact, forces and structure should be examined in concert to understand their joint response. Molecular dynamics simulations are an effective means to study these systems. Structure, in the form of a density profiles, is readily available in simulations as the location of all particles is tracked throughout the span of the simulation. Likewise, forces are directly accessible by examining the particle trajectories.

When conducting a simulation of a confined material, it may be desirable to imitate conditions experienced in force spectroscopy measurements such as the surface force apparatus (SFA)[10] or atomic force microscope (AFM) so that meaningful comparisons can be made. In a typical force experiment, two surfaces are brought into contact and forces are measured statically for different separation distances. There is normally a large reservoir of solvent, allowing solvent to flow out of the space between the surfaces throughout the compression.

A number of simulation studies of confined polymer brush systems have been performed with implicit solvent models.[11-15] While these studies are useful in examining the polymer brush characteristics, details concerning the solvent are mostly lost. When using an explicit solvent, a question arises as to what solvent density should be used. Often the solvent density between the surfaces is kept constant throughout the compression.[16, 17] Again, these methods can extract valuable information about structure-

force relationships, but do not exactly reproduce experimental conditions as there is no restriction on solvent density between the surfaces during an experiment. Naturally, the solvent density within a large reservoir in an experimental apparatus will be constant, but the density between two surfaces under strong confinement will vary with separation distance. When keeping solvent density between the surfaces constant throughout the compression, it is assumed that the solvent will interact with the brush equally whether highly compressed or fully separated, and therefore configurational entropy changes within the system caused by confinement are ignored. Some recent studies have instead opted to hold the chemical potential constant during the compression, thereby imitating a system which is in equilibrium with its different levels of compression.[18-20] These studies were conducted in the grand canonical ensemble to maintain constant chemical potential in dissipative particle dynamics simulations, where the solvent is represented by large fluid elements rather than individual particles.

This paper details a procedure to conduct molecular dynamics simulations of confined soft matter with explicit solvent at a constant solvent chemical potential. Discrete simulations at different surface separations were performed allowing static compression of a polymer brush system. This is the same situation encountered in an experiment where the solvent between the surfaces at all separation distances has the same chemical potential as the solvent reservoir, as shown in Figure 3-1. For the simulation technique no solvent reservoir is used. Instead, similar conditions are met by requiring the solvent chemical potential to be equal within a certain tolerance at each separation distance.

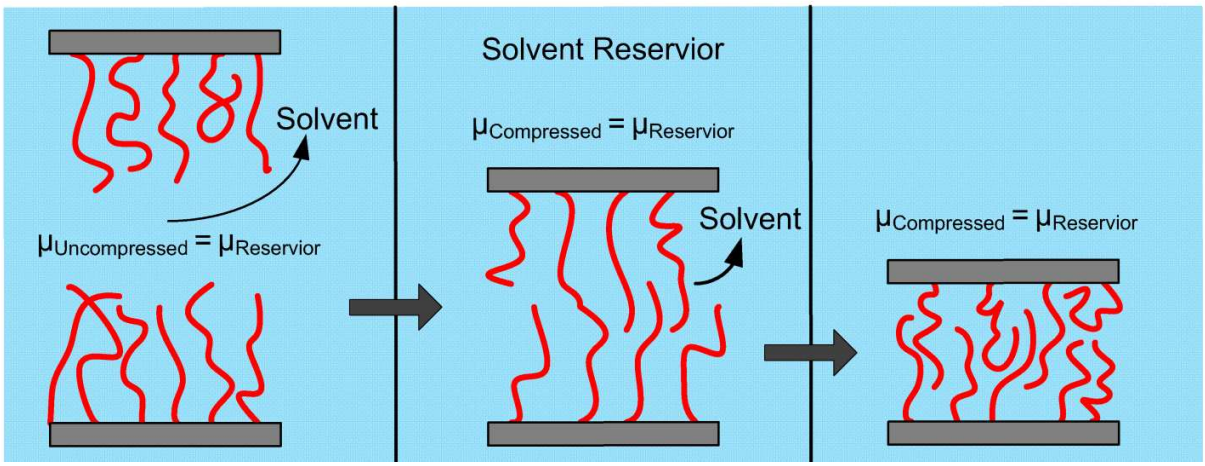

Figure 3-1. Schematic of experimental conditions encountered when compressing soft matter. μ is the chemical potential of the solvent. The solvent between the surfaces at all separation distances has the same chemical potential as the solvent reservoir. As an example, an opposing polymer brush system is shown, which was the system used to develop the technique.

The method described was used specifically for opposing polymer brushes for development, but can be straight forwardly extended to other confined soft matter systems. The process is distinct from previous constant chemical potential simulations[18-20] in that all individual simulations are performed in the canonical ensemble rather than the grand canonical ensemble. There is no solvent addition or removal during individual simulations. While the principle of holding chemical potential is the same, the method is entirely different. In this work, simulations are conducted, prior to a production run, which determine the solvent density required to provide a solvent chemical potential equal to that of the reference system. Essentially, work is put in ahead of time to set up the systems properly and from there can be simulated normally, without the need for additional calculations or changing the amount of solvent. The individual simulations hold number of particles, volume, and temperature constant (NVT), but as a whole approximate the grand canonical ensemble with respect to the solvent by holding its chemical potential constant. For the purposes of this work, exactly reproducing the grand

canonical ensemble is not important. What is desired is to most accurately simulate the experimental ensemble, which can be achieved by holding solvent chemical potential constant. When the simulations at different separations are viewed together, the number of solvent particles decreases with compression. This is comparable to solvent being expelled from between the surfaces as they come together in an experiment, and the polymer amount remains unchanged. An additional difference from the previous works in this area is that an explicit solvent is used to preserve detailed information concerning solvent interactions and configurations. This level of detail can be important when investigating solvent behavior or shear flow.[21]

As individual simulations conducted for each separation are conventional canonical ensemble molecular dynamics simulations, this method can be easily implemented in common molecular dynamics packages. Some programs, such as Gromacs,[22] have features which can implement the chemical potential calculations quite easily. In this paper, the methodology is presented. A second, application paper will detail findings of force and structure information of confined polymer brushes.

3.3 Model

The simulation model used in these studies has been validated and thoroughly described previously,[23] so it will only be briefly explained here. The coarse-grained MARTINI model[24] (version 1.4) was used due to the long simulation times and large number of simulations required. This is a generic coarse-grained model where each particle is set to a mass of 72 g/mol and is assigned Van der Waals parameters that make it polar, non-polar, or charged. Polar particles were used for all components, but the interaction strength of the surface particles was reduced by a factor of three to prevent

surface adsorption. This model has been used successfully to characterize single unconfined polymer brushes.[23, 25] A similar version of the MARTINI model has also been applied to diblock polymer systems.[26] All non-bonded interactions are represented by a 6-12 Lennard-Jones potential. Bonded interactions use a harmonic bonding potential and a cosine angle potential. The specific equations and constants used can be found in reference 23, which studied the same system with only a single surface of grafted polymer brushes.

The surfaces define the *x*-*y* plane and were comprised of overlapping particles that remained fixed throughout all simulations and prevented any solvent or polymer particles from passing through. The first monomer of each polymer chain was fixed during the simulation 0.3 nm above the surface in a regular grafting pattern, yielding an end-grafted polymer brush. Non-bonded interactions were not considered between fixed particles. A grafting density of 0.347 chains/nm^2 and linear chains of 40 monomers were used to develop and test the method. Previous work[23] has shown that under these conditions, the polymer is in good solvent and in the brush regime. Periodic boundary conditions were employed in all three directions. The *x* and *y* box dimensions were 12 nm each and the *z* dimension was determined by the surface separation examined in the individual simulation. The Lennard-Jones cutoff was 1.2 nm, and the surfaces were 1.41 nm thick so that the two brushes do not affect one another through periodic boundaries. A Berendsen thermostat[27] was used to maintain the temperature at 350 K with a correlation time of τ_T = 1 ps. The time step for all production runs was 0.02 ps. The neighbor list was updated every 10 steps with a cutoff of 1.4 nm.

3.4 Theory

The solvent chemical potential was kept constant between simulations at different fixed separations, imitating the conditions of a dynamic compression. Chemical potential, μ, can be separated into an ideal portion and an excess component as shown in Equation 3-1.

$$\mu = \mu_{id} + \mu_{ex} \tag{3-1}$$

Equation 3-2 gives the ideal chemical potential.

$$\mu_{id} = kT\ln(x_i) + \mu_0 \tag{3-2}$$

where k is the Boltzmann constant, T is temperature, x_i is the mole fraction of solvent, and μ_0 is a reference chemical potential.

In this case it is not appropriate to consider the mole fraction as the systems contain chemically grafted brushes. All polymers of each brush are chemically connected to each other through the surface, essentially yielding one very large molecule for each brush. Experimentally brushes are often generated by adsorbing an insoluble part on the surface, but in the simulations, the polymers are permanently affixed to the surface. As desorption is not possible, each polymer chain will always be chemically linked to all others on the surface, and therefore cannot be considered as a separate molecule. Thus, in this case, mole fraction is not an easily defined or meaningful quantity. Instead, the volume fraction of the solvent was used here technically assuming the monomers and not the polymers as second species for simplicity.

The excess component of the chemical potential was determined using the Widom test particle insertion method.[28] In this method, a ghost particle is inserted randomly into the system, and its interaction energy, ΔU_{tpi}, with all other particles is calculated. The particle

does not remain in the system, but is theoretically inserted solely for the purpose of the calculation. This process is then repeated many times to obtain an ensemble average $\langle \exp(-\Delta U_{tpi}/kT) \rangle$ for the system. The excess chemical potential can then be calculated from Equation 3-3.

$$\mu_{ex} = -kT \ln \left\langle \exp \frac{-\Delta U_{tpi}}{kT} \right\rangle \tag{3-3}$$

As the chemical potential is to be kept constant relative to a non-interacting system, the chemical potential of the fully separated system (non-interacting brushes), μ_{sep}, was subtracted from each compressed system's chemical potential, μ_{comp}. In doing so, the reference chemical potential μ_0 cancels out and after simplification yields

$$\mu_{comp} - \mu_{sep} = kT \ln \left(\frac{x_{i,comp}}{x_{i,sep}} \right) + kT \ln \left[\frac{\left\langle \exp\left(\frac{-\Delta U_{tpi}}{kT} \right) \right\rangle_{sep}}{\left\langle \exp\left(\frac{-\Delta U_{tpi}}{kT} \right) \right\rangle_{comp}} \right] \tag{3-4}$$

By definition, the difference on the left hand side of Equation 3-4 is zero when the two systems are in equilibrium.

To exactly reproduce the grand canonical ensemble, particle fluctuations would also need to be negligibly small. The data supports that they are indeed small, as relatively small particle additions or removals will significantly affect the chemical potential value.

3.5 Computational Details

Gromacs 4.0.4[22] was used for all simulations. All systems were initially solvated to an arbitrary density and energy minimized using a steepest decent algorithm to remove particle overlaps. A brief molecular dynamics simulation of 10,000 steps with a time step of 0.001 ps followed to further remove bad contacts.

A zero point system which served as reference throughout this study was simulated first. The reference system was uncompressed with the two opposing brushes separated sufficiently that they were non-interacting. From previous simulations using this model,[23] the brush extension is known to be about 10 nm. Therefore, a separation distance of 30 nm between the surfaces was selected for the initial set up of the reference system. The reference system was equilibrated semi-isotropically under constant normal pressure and constant lateral area to obtain the correct density. As the brushes were fully separated, no normal forces were found. The pressure coupled simulation ran for 100 ns using a Berendsen barostat[27] with a correlation time of τ_P = 2 ps and a reference pressure of 1 bar. The total change to the box size was less than 1.5 nm, and it occurred within the first 5 ns. The average z dimension obtained after equilibration was used for a subsequent 2 μs NVT simulation. This fully separated system was then used as a reference system, where all other compressed systems were required to have the same solvent chemical potential.

Each compressed system was initially set up with the desired surface separation distance and a total particle density close to the reference system. NVT simulations for each separation distance were run for 2 to 4 μs. The highly compressed systems needed to run longer to equilibrate. Equilibrium was defined as when the radius of gyration of the compressed polymer brush stabilized as structural evolution is one of the slowest equilibration modes. All systems had at least 1.5 μs of data after equilibration for analysis. Separation distances of 20, 17.5, 15, 12.5, 10, 7.5, 6, and 5 nm were examined for the compressed systems. Snapshots of the compression are shown in Figure 3-2.

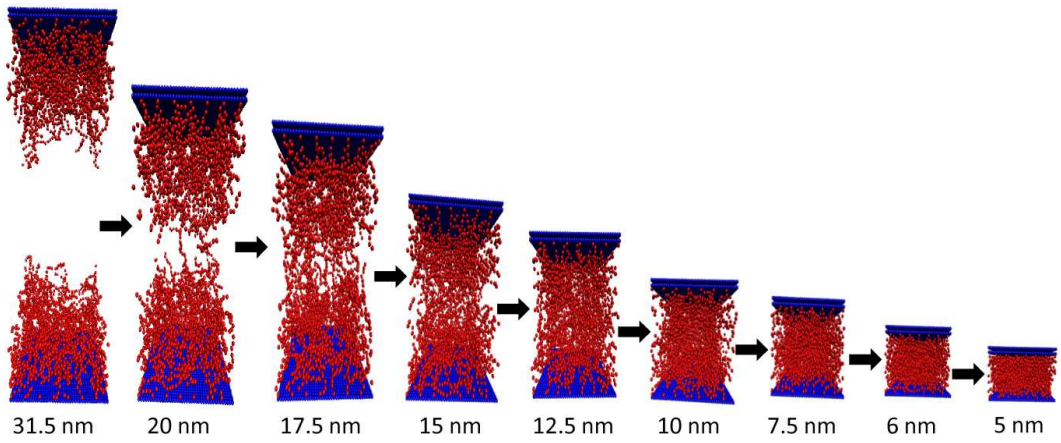

Figure 3-2. VMD[29] images of the brush system for each simulated separation distance examined. The series illustrates the static compression of the polymer brush system.

As discussed in the theory section, the solvent chemical potential was calculated using the Widom test particle insertion method,[28] which can be implemented in Gromacs 4.5.2.[22] We caution that earlier versions of Gromacs gave incorrect results when using this feature. If using a molecular dynamics package without this capability, a code can be written to perform random test particle insertions and to calculate the interaction energy. A crucial aspect of the particle insertion method is to eliminate contributions from insertions into the surface layers. Any insertion into the surface will result in very large, positive contributions to ΔU_{tpi}. These values will not simply cancel out between systems as the surface occupies a larger volume fraction of the box in the compressed systems than in the uncompressed. As the system is compressed, surface layer sampling becomes more pronounced, and if not accounted for, will result in a systematic reduction of the excess chemical potential (or lower density at equilibrium with the reference state) with greater compression. This problem can be avoided by disallowing random particle insertions within the surface which is physically sound as in a real chemically grafted brush no solvent can penetrate the surface. In this work, the test particle insertion

function in Gromacs was modified to bias the random *z* coordinate selected. The *z* coordinate was required to be at least one particle diameter away from the surface as even a small overlap would significantly impact the values obtained.

In each system for which the chemical potential was calculated, a solvent test particle was inserted at random positions in each frame examined. The number of insertions necessary was determined by finding when the value for μ_{ex} from Equation 3-3 converged. In general the number of insertions increased with system size, and ranged from 100 million to 600 million. Denser systems may require a larger number of particle insertions. The test particle calculations are computationally cheap compared to the simulation runs, so efficiency for the Widom method is not a major concern. For each insertion, a random position in the box was selected, and the test particle was inserted randomly ten times into a 0.05 nm radius sphere around that point to obtain better statistics at relatively little computational cost as the neighbor list had already been compiled. A depiction of the test particle insertion method is shown in Figure 3-3. As can be seen, the ghost particles are inserted in random locations between the surfaces. Higher levels of overlap with polymer or solvent particles lead to less favorable interaction energies. That energy, when put into Equations 3-3 and 3-4, gives a measure of how many solvent particles need to be added or removed from the system to be equilibrated with the reference system.

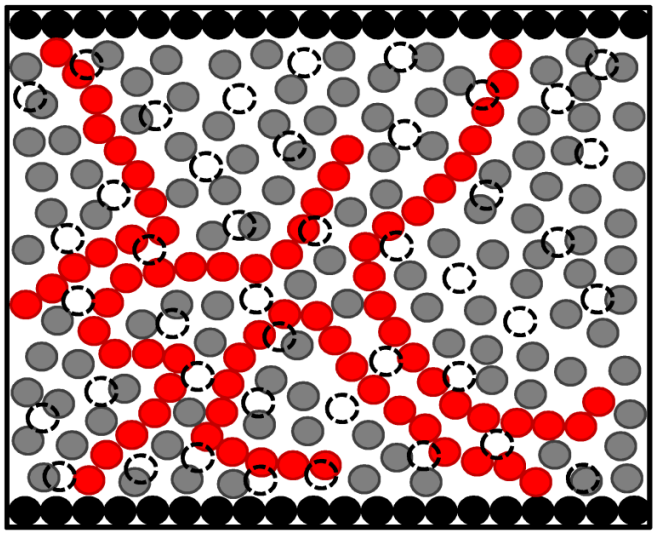

Figure 3-3. Illustration of the test particle insertion method. Surface particles are black, polymers are red, and solvent particles are gray. The dashed black circles indicate ghost particles which are randomly inserted for the purposes of the calculation, but do not remain in the system.

Frames from which the chemical potential was calculated were initially each 5 ns apart to ensure that independent configurations were examined. Once it was determined from these tests what the solvent density should be, the chemical potential for that system was recalculated based on frames 1 ns apart to decrease the error and to confirm the findings, but overall values generally changed very little. The resulting chemical potential was calculated from independent configurations over the last 1.5 μs of the simulation. The excess contribution to the chemical potential was found from these insertions, and combined with the ideal portion to find the total chemical potential for a given separation distance.

Once the chemical potential was calculated for the compressed and reference systems, the reference system's chemical potential was subtracted off as in Equation 3-4. To be considered in equilibrium the difference between the compressed and separated system's solvent chemical potential was required to be less than 0.05 kT for all but the most highly

compressed systems (5 and 6 nm separation). At these high compressions, the error due to increasing polymer density became much larger so they were required to be within 0.1 kT of the reference system. If the difference ($\mu_{comp} - \mu_{sep}$) was negative more particles were needed, while if it was positive the system was too dense and particles had to be removed from the compressed system. Solvent particles were added or removed accordingly. After any solvent particle number change, a new simulation with the new amount of solvent ran again for 2 to 4 μs, and the new chemical potential was calculated. Generally it took 2-4 iterations to settle on the right number of solvent particles. After two attempts, interpolation or extrapolation was used to give a reasonable next guess for the number of solvent particles. As there is error associated with the excess chemical potential obtained from the test particle insertions, it should be viewed as determining a range of solvent particle numbers which will provide a chemical potential in agreement close to the reference system. An example of the chemical potentials found for different amounts of solvent in a compressed system is shown in Figure 3-4. As stated earlier, final results for each separation distance were recalculated using more frames which brought down error bars to less than 0.1 kT, but were not done so for preliminary data. Figure 3-4 is shown for illustrative purposes as the system with the most iterations, but as stated earlier in most cases fewer iterations yielded good results.

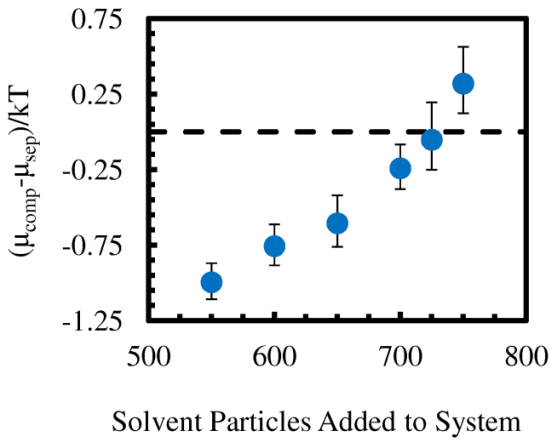

Figure 3-4. Chemical potential relative to the reference system versus particles added to the system starting at an arbitrary density. This data is from the system at 5 nm surface separation distance.

3.6 Pressure and Force Calculation

A primary interest of simulating confined soft matter is to obtain force information which can be compared to experimental results. A typical surface force apparatus experiment yields a profile of normal force versus separation distance.[30-32] The normal force data can be obtained by calculating profiles of the normal component of the pressure tensor (P_{zz}). Including the frozen surface layers will lead to incorrect pressure calculations by conventional methods, as the surface layers do not interact with one another. They do, however, interact with the material between the surfaces, which leads to highly attractive, unrealistic energies. For the normal pressure, this means that within the surface there are large, negative values, which artificially lower the pressure if it is averaged over the entire box. For this reason, pressures must be calculated from a pressure profile and not averaged over the system in the conventional way.

To find pressures which omit the data within the surface layer, pressure profiles were calculated[33-35] and averaged only between the surfaces. A typical normal pressure profile, along with its corresponding polymer density profile is given in Figure 3-5.

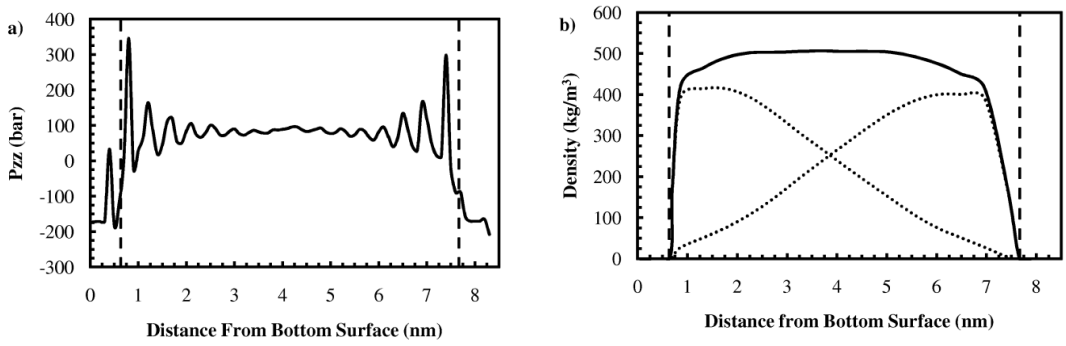

Figure 3-5. a) Profile of the normal pressure versus distance from the bottom surface for a surface separation distance of 7.5 nm. Dashed lines indicate the edges of the surface. b) Corresponding polymer density distribution for a separation of 7.5 nm. Dashed lines are the edges of the surfaces, dotted lines show the top and bottom density profiles of the brush independently, and the solid line gives the overall polymer density.

The details of the pressure profile in Figure 3-5 a) are not important for this discussion. What should be noted is that the normal pressure is positive in the fluid, but becomes strongly negative within the surface. This negative pressure will lower the average normal pressure obtained, and will contribute more to the average at higher compressions (smaller system sizes). For the pressure profile calculation, the system was binned into 0.1 nm segments, and the Coulomb cutoff was set to 2.0 nm. For comparison, the corresponding average density distribution is shown in Figure 3-5 b), which helps illustrate where in the brush system the pressures are being calculated. Detailed analysis of this data and comparisons to other experimental and simulation work will be made in a subsequent, application paper.

3.7 Conclusion

A method for conducting a static compression of soft matter with molecular dynamics was described. It allows for molecular dynamics simulations in the canonical (NVT) ensemble to be used in a way that approximates a grand canonical ensemble for the solvent. The chemical potential of each simulated separation distance was calculated using the Widom test particle insertion method. By fixing the solvent chemical potential at each separation distance, every simulation is in equilibrium with all others. This more realistically reproduces the conditions encountered experimentally by confined systems than simply using a constant solvent density. This approach resembles and can be compared to experimentally measured force profiles from the surface force apparatus or atomic force microscope. In the present case, the method was specifically used on confined polymer brush systems, but can easily be adapted for confining other soft materials such as polymer melts, proteins, etc.

As described, fixed surface layers can cause problems with both the chemical potential and pressure calculations, and their effects need to be excluded from both calculations. In the case of the chemical potential, sampling the surface with test particle insertions will lead to a lower solvent density, therefore not realistically simulating a compression. The test particle code needs to exclude the surfaces layers for all particle insertions to avoid this problem. Similarly, accurate pressure data was obtained by calculating pressure profiles and averaging over only the data in the fluid region, thereby omitting any non realistic pressure values within the frozen surface.

This method differentiates itself from previous work in that it allows for explicit solvent particles, which provides a greater level of detail on the solvent. While the initial

computational requirements are somewhat large, once the system is set up it can be simulated or analyzed efficiently without the need to adjust solvent particles or density. This could be especially useful if a very long simulation is desired, then the initial set up costs are miniscule compared to the length of the run.

Using this method will allow molecular dynamics simulations to be conducted which realistically confine or compress various soft matter systems. Further work will be specifically focused on applying this method to polymer brushes and direct comparison to experimentally measured force profiles. The influence of variables such as grafting density and chain length on the force and structure can be obtained and compared. Additionally, once the compression is accurately described, the system can be sheared at each separation distance to investigate lubrication properties.

3.8 Acknowledgments

The authors thank Giulia Rossi for many stimulating discussions and Juan Vanegas for assistance with code adaptation. This work was supported by the United States Department of Energy, Office of Basic Energy Science, under Grant DE-FG02-06ER46340. I.G.E. additionally thanks the Graduate Assistance in Areas of National Need (GAANN) program of the US Department of Education. Computer time at the National Energy Research Supercomputer Center, which is supported by the Office of Science of the U.S. Department of Energy under Contract No. DE-AC03-76SF00098, has been used for parts of the simulations.

3.9 References

1. Leckband, D. Measuring the Forces That Control Protein Interactions. *Annu. Rev. Biophys. Biomol. Struct.* 2000, 29, (1), 1-26.

2. Wong, J. Y.; Park, C. K.; Seitz, M.; Israelachvili, J. Polymer-Cushioned Bilayers. II. An Investigation of Interaction Forces and Fusion Using the Surface Forces Apparatus. *Biophys. J.* 1999, 77, (3), 1458-1468.

3. Luengo, G.; Schmitt, F.-J.; Hill, R.; Israelachvili, J. Thin Film Rheology and Tribology of Confined Polymer Melts: Contrasts with Bulk Properties. *Macromolecules* 1997, 30, (8), 2482-2494.

4. Alsten, J. V.; Granick, S. Shear rheology in a confined geometry: polysiloxane melts. *Macromolecules* 1990, 23, (22), 4856-4862.

5. Sun, G.; Kappl, M.; Butt, H.-J. Confined polymer melts studied by atomic force microscopy. *Colloids Surf., A* 2004, 250, (1-3), 203-209.

6. Shin, K.; Obukhov, S.; Chen, J.-T.; Huh, J.; Hwang, Y.; Mok, S.; Dobriyal, P.; Thiyagarajan, P.; Russell, T. P. Enhanced mobility of confined polymers. *Nat Mater* 2007, 6, (12), 961-965.

7. Klein, J.; Kumacheva, E.; Mahalu, D.; Perahia, D.; Fetters, L. J. Reduction of frictional forces between solid surfaces bearing polymer brushes. *Nature* 1994, 370, (6491), 634-636.

8. Advincula, R. C.; Brittain, W. J.; Caster, K. C.; Ruhe, J., *Polymer Brushes*. Wiley-VCH: Weinheim, 2004.

9. Napper, D. H., *Polymeric Stabilization of Colloidal Dispersions*. Academic Press: London, 1983.

10. Israelachvili, J. N.; Adams, G. E. Measurement of forces between two mica surfaces in aqueous electrolyte solutions in the range 0-100 nm. *J. Chem. Soc., Faraday Trans.* 1978, 74, 975-1001.

11. Murat, M.; Grest, G. S. Interaction between grafted polymeric brushes: A molecular-dynamics study. *Phys. Rev. Lett.* 1989, 63, (10), 1074.

12. Grest, G. S.; Murat, M. Structure of grafted polymeric brushes in solvents of varying quality: a molecular dynamics study. *Macromolecules* 1993, 26, (12), 3108-3117.

13. Kreer, T.; Müser, M. H.; Binder, K.; Klein, J. Frictional Drag Mechanisms between Polymer-Bearing Surfaces. *Langmuir* 2001, 17, (25), 7804-7813.

14. Kreer, T.; Binder, K.; Müser, M. H. Friction between Polymer Brushes in Good Solvent Conditions: Steady-State Sliding versus Transient Behavior. *Langmuir* 2003, 19, (18), 7551-7559.

15. Pastorino, C.; Binder, K.; Kreer, T.; Muller, M. Static and dynamic properties of the interface between a polymer brush and a melt of identical chains. *J. Chem. Phys.* 2006, 124, (6), 064902.

16. Spirin, L.; Galuschko, A.; Kreer, T.; Johner, A.; Baschnagel, J.; Binder, K. Polymer-brush lubrication in the limit of strong compression. *Eur. Phys. J. E* 2010, 33, (4), 307-311.

17. Galuschko, A.; Spirin, L.; Kreer, T.; Johner, A.; Pastorino, C.; Wittmer, J.; Baschnagel, J. Frictional Forces between Strongly Compressed, Nonentangled Polymer Brushes: Molecular Dynamics Simulations and Scaling Theory. *Langmuir* 2010, 26, (9), 6418-6429.

18. Goujon, F.; Malfreyt, P.; Tildesley, D. J. Dissipative Particle Dynamics Simulations in the Grand Canonical Ensemble: Applications to Polymer Brushes. *ChemPhysChem* 2004, 5, (4), 457-464.

19. Goujon, F.; Malfreyt, P.; Tildesley, D. J. Mesoscopic Simulation of Entangled Polymer Brushes under Shear: Compression and Rheological Properties. *Macromolecules* 2009, 42, (12), 4310-4318.

20. Goujon, F.; Malfreyt, P.; Tildesley, D. J. Interactions between polymer brushes and a polymer solution: mesoscale modelling of the structural and frictional properties. *Soft Matter* 2010, 6, (15), 3472-3481.

21. Grest, G. Normal and Shear Forces Between Polymer Brushes. *Adv. Polym. Sci.* 1999, 138, 149-183.

22. Hess, B.; Kutzner, C.; van der Spoel, D.; Lindahl, E. GROMACS 4: Algorithms for Highly Efficient, Load-Balanced, and Scalable Molecular Simulation. *J. Chem. Theory Comput.* 2008, 4, (3), 435-447.

23. Elliott, I. G.; Kuhl, T. L.; Faller, R. Molecular Simulation Study of the Structure of High Density Polymer Brushes in Good Solvent. *Macromolecules* 2010, 43, (21), 9131-9138.

24. Marrink, S. J.; de Vries, A. H.; Mark, A. E. Coarse Grained Model for Semiquantitative Lipid Simulations. *J. Phys. Chem. B* 2004, 108, (2), 750-760.

25. Elliott, I. G.; Mulder, D. E.; Traskelin, P. T.; Ell, J. R.; Patten, T. E.; Kuhl, T. L.; Faller, R. Confined polymer systems: synergies between simulations and neutron scattering experiments. *Soft Matter* 2009, 5, (23), 4612-4622.

26. Hatakeyama, M.; Faller, R. Coarse-grained simulations of ABA amphiphilic triblock copolymer solutions in thin films. *Phys. Chem. Chem. Phys.* 2007, 9, (33), 4662-4672.

27. Berendsen, H. J. C.; Postma, J. P. M.; Gunsteren, W. F. v.; DiNola, A.; Haak, J. R. Molecular dynamics with coupling to an external bath. *J. Chem. Phys.* 1984, 81, (8), 3684-3690.

28. Widom, B. Some Topics in the Theory of Fluids. *J. Chem. Phys.* 1963, 39, (11), 2808-2812.

29. Humphrey, W.; Dalke, A.; Schulten, K. VMD: Visual molecular dynamics. *J. Mol. Graphics* 1996, 14, (1), 33-38.

30. Taunton, H. J.; Toprakcioglu, C.; Fetters, L. J.; Klein, J. Interactions between surfaces bearing end-adsorbed chains in a good solvent. *Macromolecules* 1990, 23, (2), 571-580.

31. Moore, N. W.; Kuhl, T. L. The Role of Flexible Tethers in Multiple Ligand-Receptor Bond Formation between Curved Surfaces. *Biophys. J.* 2006, 91, (5), 1675-1687.

32. Tirrell, M.; Patel, S.; Hadziioannou, G. Polymeric amphiphiles at solid-fluid interfaces: Forces between layers of adsorbed block copolymers. *Proc. Natl. Acad. Sci. U. S. A.* 1987, 84, (14), 4725-4728.

33. Lindahl, E.; Edholm, O. Spatial and energetic-entropic decomposition of surface tension in lipid bilayers from molecular dynamics simulations. *J. Chem. Phys.* 2000, 113, (9), 3882-3893.

34. Ollila, O. H. S.; Risselada, H. J.; Louhivuori, M.; Lindahl, E.; Vattulainen, I.; Marrink, S. J. 3D Pressure Field in Lipid Membranes and Membrane-Protein Complexes. *Phys. Rev. Lett.* 2009, 102, (7), 078101.

35. Ollila, S.; Hyvönen, M. T.; Vattulainen, I. Polyunsaturation in Lipid Membranes: Dynamic Properties and Lateral Pressure Profiles. *J. Phys. Chem. B* 2007, 111, (12), 3139-3150.

Chapter 4

Compression of High Grafting Density Opposing Polymer Brushes Using Molecular Dynamics with an Explicit Solvent

4.1 Chapter Abstract

Opposing polymer brush layers at high grafting density were examined under confinement and characterized with respect to structure and interaction forces using molecular dynamics simulations with an explicit solvent. The brush system underwent a static compression, where the system is simulated at several discrete separation distances. These simulations are all designed to have an equivalent solvent chemical potential as a non-interacting reference state to produce a realistic compression. Normal pressure-distance profiles were generated and compared to density profiles at each separation distance to determine structure-property relationships. Significant interpenetration of brush layers occurred at the higher levels of compression, to the extent that each brush reached all the way to the opposing surface. Higher levels of interpenetration corresponded to a sharp increase in the pressure-distance curve, suggesting a correlation between interpenetration and interaction forces.

4.2 Introduction

A polymer brush is a group of polymer chains end grafted to a surface. Crowding from the molecules at the surface leads to chain extension away from the surface, and numerous useful properties.[1, 2] Polymer brushes can be used to modify surface properties and interactions to change the nature of the surface. Examples of applications which take advantage of surface modification by polymer brushes include, altering wetting

properties,[3] biocompatiblizing surfaces or devices,[4] and reducing friction between surfaces.[5-8] The latter application is gaining a large amount of attention as opposing polymer brushes have been shown to significantly lower friction, therefore acting as a viable lubricant for various applications.[9] The first step in understanding the lubricating properties of polymer brushes is to thoroughly understand how the brushes interact when brought into confinement opposed to one another. Polymer brushes are typically characterized by either examining structure or interaction forces. Experimentally this is achieved with neutron reflectivity to determine density profiles[10, 11] and using the surface force apparatus to determine forces.[12-16] In addition to the experiments mentioned, there has been significant theoretical[17-19] and simulation[20-23] work on characterizing and predicting the structure and interactions of polymer brushes.

Molecular simulations have the advantage of obtaining high resolution structure and force information simultaneously. As all particle locations are always known throughout the simulation, structure can be investigated at points of interest dictated by the force measurements. In this way, force data can be understood by linking it to structural features.

This paper details static compression of polymer brushes in an explicit solvent. Often simulations will investigate confined brushes without explicit solvent,[6, 24-26] as this both simplifies and speeds up the simulations. Doing so, however, sacrifices detail about how the solvent responds in these circumstances. Some recent simulations[27, 28] have included explicit solvent, but upon compression maintained a constant total number density, not exactly reproducing conditions found in an experiment. Constant chemical potential simulations have been conducted using dissipative particle dynamics,[29-31] but again, these

do not contain as much detail on the solvent as explicit solvent simulations. This work differs from previous studies in that it characterizes high grafting density opposing polymer brushes with explicit solvent, where the solvent density is determined based on maintaining constant solvent chemical potential at all levels of compression. The solvent chemical potential in all compressed cases is equal to that of a fully separated reference system, and thus all compressed systems are considered equilibrated with one another. This process approximates a compression in the grand canonical ensemble, but is conducted by a series of NVT simulations.

4.3 Simulation Details

All simulations were conducted with Gromacs 4.0.4.[32] The coarse-grained MARTINI[33] model (version 1.4) was used, which allowed for much longer simulation times and larger systems. While originally developed for lipids, this model has been effectively used previously for polymer systems.[34-37] In this model, all particles are set to a mass of 72 grams/mole and are assigned Lennard-Jones interactions which cause them to be generically polar, non-polar, or charged. For this study all particles were polar. The polymer and solvent particles had equivalent interactions, and the surface was made of particles which, while still polar, had one-third the non-bonded interactions of the solvent and polymer. The surface was composed of overlapping frozen particles spanning 12 nm by 12 nm in the *x* and *y* directions, which was the total area of the simulation box. It consisted of three surface layers to ensure there were no interactions through the *z* periodic boundary. To create a brush system, one end of each polymer was fixed 0.3 nm above either surface in a regular grafting pattern. Non-bonded interactions between frozen particles were omitted for all simulations.

Each simulation was initialized with a steepest descent energy minimization, followed by a brief simulation with a small time step of 0.001 ps. Simulations used for the production runs had a time step of 0.02 ps. Temperature was held constant at 350 K for all simulations using a Berendsen thermostat[38] with a correlation time of 1 ps. Previous work has shown that at these temperatures, the polymer brushes are in a good solvent condition.[36] In simulations that were pressure coupled, a Berendsen barostat[38] was used with a correlation time of 2 ps. The neighbor list was updated every 10 steps and had a 1.4 nm cutoff length. The cutoff distance for Lennard-Jones interactions was 1.2 nm. Further details concerning this system can be found in reference 36.

The polymer brush system studied consisted of 40 monomer long linear chains at a grafting density of 0.347 chains/nm^2. Images of the system at two different levels of compression are shown in Figure 4-1.

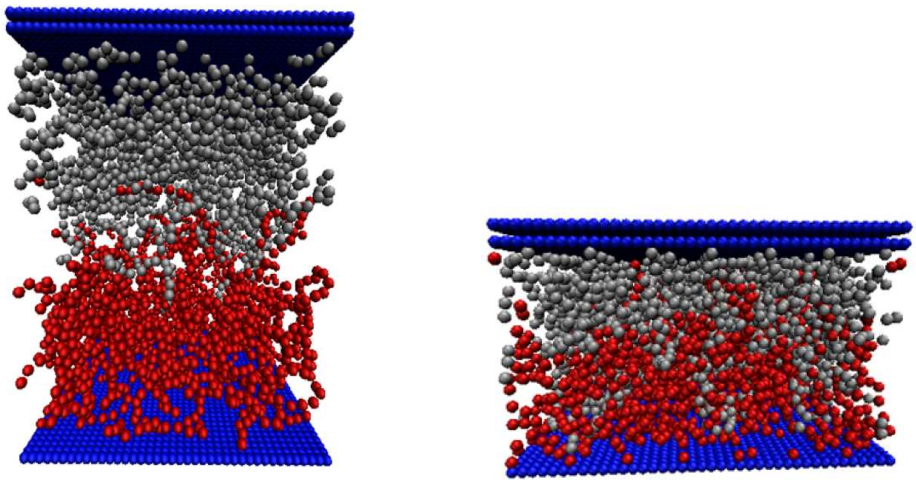

Figure 4-1. Images obtained with the VMD software[39] of the opposing polymer brush system at two stages in the compression. Solvent molecules have been removed for clarity.

A single equilibrium brush of the same grafting density and chain length was thoroughly characterized previously,[36] so the effects of confinement were very clear. A measure of the degree to which the chains interact laterally is the overlap grafting density. Overlap grafting density can be represented by Equation 4-1.

$$\sigma^* = \pi R_g^2 \Sigma \quad (4\text{-}1)$$

Σ is the grafting density in chains/area and R_g is the radius of gyration calculated from a simulation of a single free polymer chain in solution. For $\sigma^* > 1$ the system is said to be in the brush regime, where a high amount of lateral interaction will cause the chains to extend from the surface.[40] For this study, the specific chain length and grafting density led to an overlap grafting density of 6.97, which is well within the brush regime.

To generate a reference system, opposing brushes were set up with a large enough separation distance such that the two brushes did not interact. The surfaces and brushes were initially placed in the center of the box so pressure coupling in the *z* direction could be applied without interference from fixed surface particles. A simulation proceeded with the *z* pressure set to 1 bar for at least 100 ns. This was enough time for the *z* dimension of the box to stabilize, and the average box height after equilibration was used for further simulation with a fixed volume. An NVT simulation was conducted next for 2 μs, and data from the last 1.5 μs was used as the reference system.

All compressed systems were initially solvated to an arbitrary density and run for two microseconds. Chemical potential was calculated for each system to determine if more or less solvent particles were required to match the reference system's chemical potential. The details of this procedure have been thoroughly covered in a previous publication,[41] so will only be briefly presented here. Essentially, chemical potential has two components: ideal and excess. The ideal component is based on the concentration of solvent particles.

The excess chemical potential was determined using the test particle insertion method developed by Widom.[42] In this method, theoretical solvent particles are randomly added to the system and their interaction energy with all particles in the system is calculated. Enough insertions must occur in each frame of the trajectory evaluated such that the ensemble average is stable. The frequency of frames analyzed depends on the desired accuracy. For this work the frequency ranged from 0.1 to 1 ns, with more frames being required for highly compressed systems.

The values of solvent chemical potential obtained from the insertion calculations will indicate if solvent particles need to be added or removed for the confined system to be in equilibrium with the reference system. After the initial simulation, the solvent density was adjusted accordingly, the simulation was run again, and chemical potential was re-calculated by the test particle insertion method. Once the difference between the solvent chemical potential of the reference system and the compressed system was close to zero, the system was considered in equilibrium with the other states and was analyzed for all structural and force properties.

4.4 Results

The first step in simulating a static compression was to determine the correct solvent density of each compressed system. Solvent chemical potential was extremely sensitive to solvent density, to the point where even minor changes in the number of solvent particles could strongly affect both the chemical potential and normal pressure. To illustrate this sensitivity, the system with a surface separation of 6.75 nm is used as an example. The system had roughly 4000 solvent particles and 4000 polymer beads at this separation. When at equilibrium with the reference system, the normal pressure was 73 bar and the solvent chemical potential was -0.02kT. Two systems at nearly the same

density had also been set up. One had 23 solvent particles less than the correct system and one had 27 particles more. While it would seem that 20-30 particles would have minimal impact in a system with 8000 particles, it was enough to bring the system substantially out of equilibrium with the reference state, and completely change the pressure obtained. These two systems deviated significantly in normal pressure from the 73 bar observed in the correct system. The system with 23 fewer solvent particles dropped to 38 bar and -0.09kT, and the system with 27 more particles shot up to 118 bar and a chemical potential of 0.1kT. Clearly the solvent density strongly affected the normal pressure, so the systems had to be set up with very little error in the chemical potential to get a meaningful value for pressure.

Based on these data points, an uncertainty in pressure can be estimated based on the uncertainty in the chemical potential calculation. Not all systems at different separation distances had multiple runs, so the exact effect of adding or removing particles cannot be determined for each system individually. However, for all systems where there was data for different solvent densities, a pressure change of 4-5 bar was associated with a 0.01kT change in chemical potential. This was true for systems at both high and low confinement. A reasonable estimation for the error in pressure can be made by using the average value of 4.65 bar change in normal pressure per 0.01kT change in solvent chemical potential. It was decided therefore that the allowable error in chemical potential would be 0.02kT and that all systems had to be within 0.02kT of the reference system's solvent chemical potential, yielding an error in pressure less than 10 bar. The only exception to this was the most compressed system (5 nm separation distance), as it

finished within 0.03kT of equilibrium, and at such a high level of compression was much more sensitive to density changes.

Normal pressure versus distance profiles were created by calculating pressure profiles[43-45] at each separation distance to omit surface effects. An example of a normal pressure profile is shown in Figure 4-2. As can be seen, the pressure within the surface layers deviates dramatically from the average pressure in the rest of the system. To calculate the normal pressure for each system, the pressure profile was averaged between the surfaces, omitting any volume that the surface extended into. After averaging, the pressure of the reference system was subtracted from the normal pressure of all confined systems to yield pressure values relative to the non-interacting system.

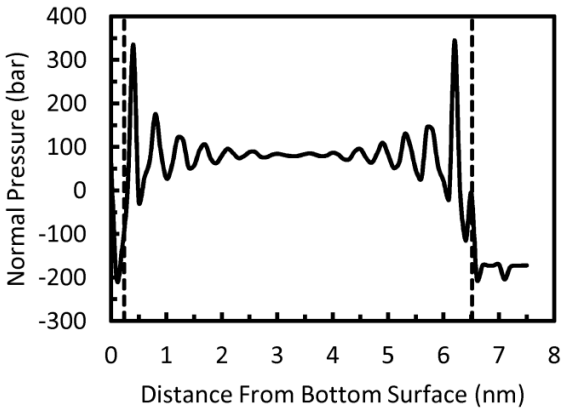

Figure 4-2. Normal pressure profile for a surface separation of 6.75 nm. Dashed lines indicate where the surfaces extend in the system

The average pressure itself for any given separation remained stable through the course of the simulation, but as stated before has an error associated with how accurately the system was set up. Each pressure-distance profile has error bars for each of the data points based on the uncertainty in the chemical potential.

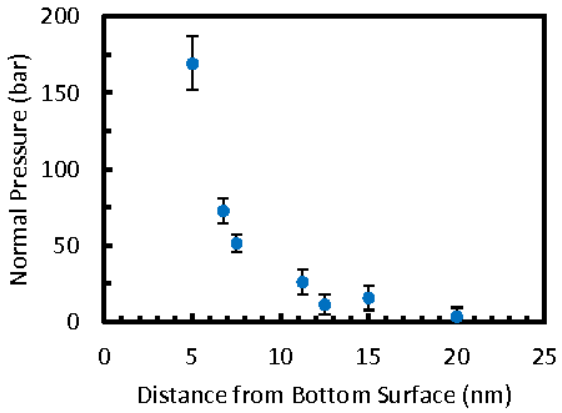

Figure 4-3. Normal pressure versus separation distance for the opposing brush system at 0.347 chains/nm^2 grafting density under different levels of confinement.

As much of the work associated with these simulations was setting up the systems at the correct density, it is informative to look at how the density changes with compression. All polymer beads and solvent particles were the same mass and size, so density is represented as a number density in particles/nm^3. The total particle density versus separation distance is shown in Figure 4-4. Clearly, the number density increases throughout the compression. This suggests that using the constant density approximation is inadequate to realistically represent the physics of the compression.

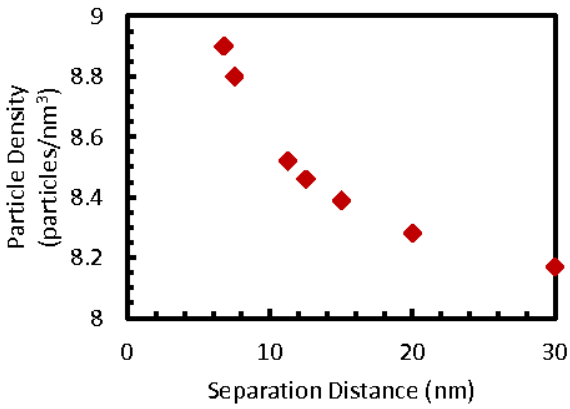

Figure 4-4. Total particle number density, including both polymer and solvent, for each separation distance in equilibrium with the reference system. Error bars are not shown as they were much smaller than the data points.

Interesting features concerning the structure of the opposing brush systems can be elucidated by examining the brush density profiles. Figure 4-5 shows the density profile of a single brush layer as it is compressed by the opposing brush.

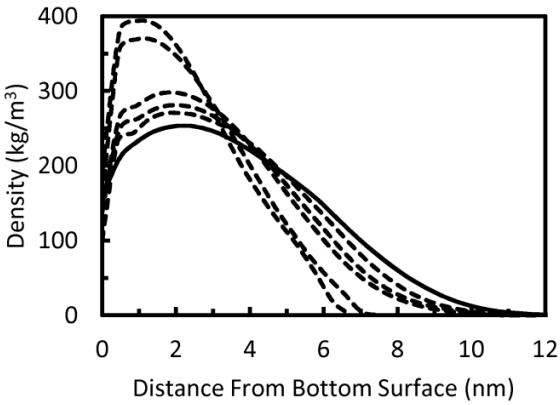

Figure 4-5. Density profile of a single brush layer at different stages in the compression. The solid line represents the equilibrium brush density profile for a surface separation of 30nm. All dashed lines are for the system as it compresses which correspond to surface separations of 6.75, 7.5, 11.25, 12.5,and 15 nm going from left to right.

The most noticeable change in structure from the equilibrium system is a shift from a long tail in the density profile of the less compressed systems to a profile which goes more sharply to zero when highly confined.

The compression progression represented by density profiles is shown in Figure 4-6. Both the overall density and the density of each individual layer are shown.

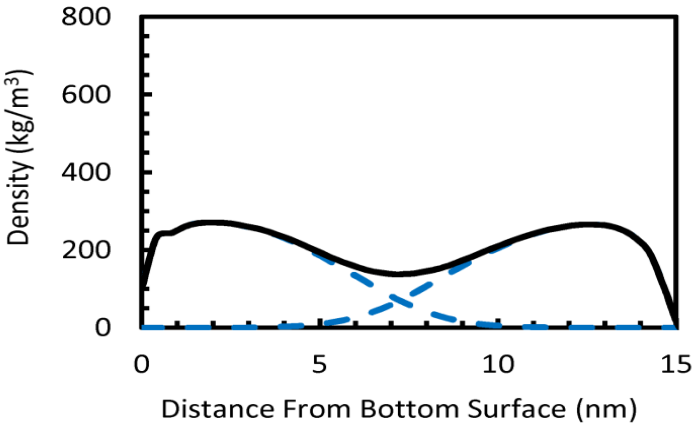

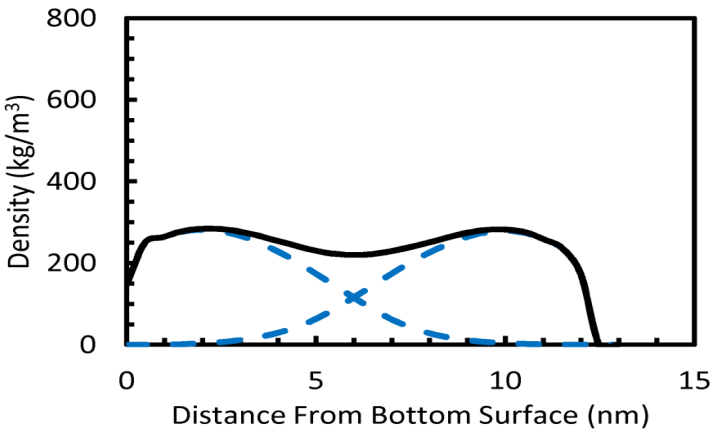

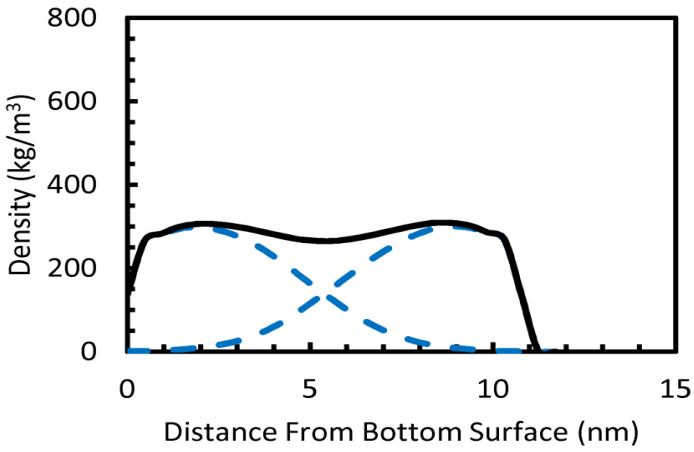
800
600
400
200
0
Density (kg/m³)
0
5
10
15
Distance From Bottom Surface (nm)

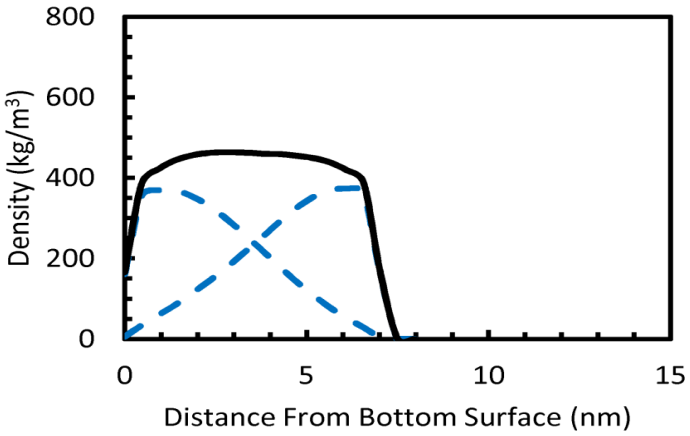
800
600
400
200
0
Density (kg/m³)
0
5
10
15
Distance From Bottom Surface (nm)

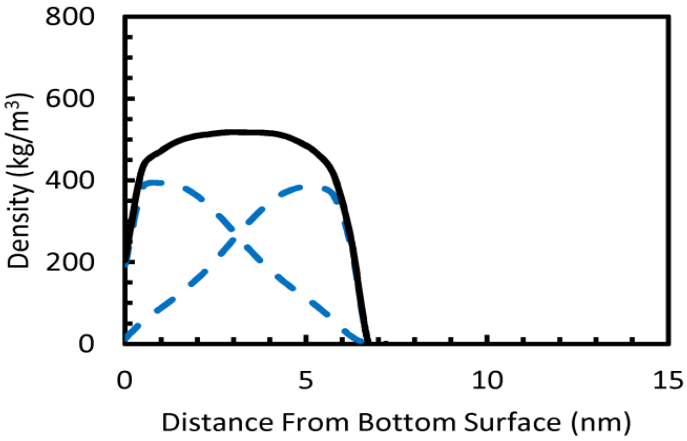
800
600
400
200
0
Density (kg/m³)
0
5
10
15
Distance From Bottom Surface (nm)

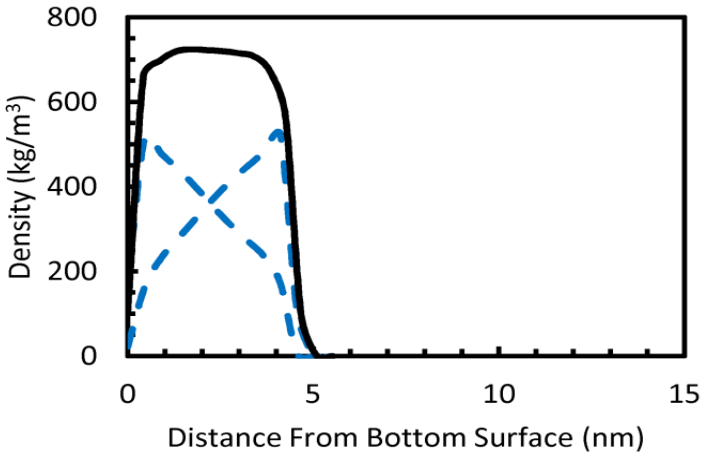

Figure 4-6. Density profiles at various stages in the compression. The solid black line represents the total polymer density, while the dashed blue lines represent each individual brush layer.

One characteristic that can be monitored throughout the compression is the interpenetration of the brushes. Interpenetration is the degree to which each brush extends into the opposing brush, and can be quantified by examining the amount that each individual density profile overlaps with the other. There are several ways to define interpenetration, and one method is to calculate the fraction of a brush layer that is past the mid-plane of the system. This is presented mathematically in Equation 4-2.[7, 46, 47]

$$I(D) = \frac{\int_{D/2}^{D} \phi(z)dz}{\int_{0}^{D} \phi(z)dz} \qquad (4\text{-}2)$$

In Equation 4-2, D is the separation distance between surfaces, ϕ is the volume fraction of polymer, and z is the distance from the bottom surface. Interpenetration data using Equation 4-2 is shown in Figure 4-7.

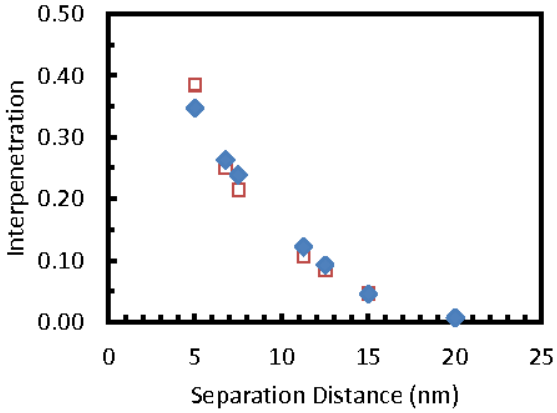

Figure 4-7. Interpenetration results as defined by Equation 4-2. Blue solid symbols represent interpenetration of the simulated systems. The open square symbols show interpenetration as predicted by self consistent field theory[46] for the same grafting density, chain length, and surface separation. As only the dependence on surface separation was investigated here, the theoretical results were scaled by a common numerical pre-factor for comparison to the simulations results.

Figure 4-7 quantitatively represents interpenetration as the fraction of polymer brush past the mid-plane. As can be seen in Figure 4-7, the interpenetration is insignificant at large separation distances, but under higher confinement interpenetration increases substantially. In fact, interpenetration grows to the point where each brush extends completely through the opposing brush, as is seen in the density profiles in Figure 4-6. In the three most confined systems, each brush passes all the way through the other brush and interacts with the opposing wall. The point at which each polymer layer extends to the other surface also corresponds to the level of confinement where substantial repulsive pressures are observed in Figure 4-3. Another way to describe the density profile at this point is that there is no longer a minimum in the overall density profile in the middle. Essentially, at this level of compression the structure no longer is distinguishable as two separate brushes, but more resembles one very high density brush confined between two surfaces.

Solvent density profiles can also be calculated to examine how the solvent behaves under confinement. Figure 4-8 shows the solvent densities for a low and highly compressed system.

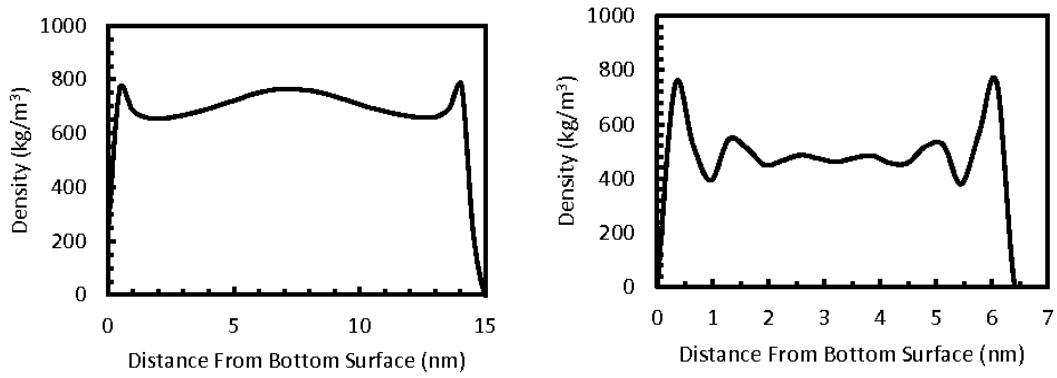

Figure 4-8. Solvent density profiles for 15 nm (left) and 6.75nm (right) separation distances.

As can be seen for both levels of confinement, there is a significant peak in the solvent density profile near the surface. This indicates a polymer depletion layer, which persists even when the system is very highly compressed.

An additional structural feature which can be examined is the chain end distribution. This distribution represents the behavior of the free end of each chain, illustrating if the chains have a tendency to collapse back into the brush or extend far away into the opposing layer. The distribution of each brush layer at both a high and a low level of confinement are shown in Figure 4-9.

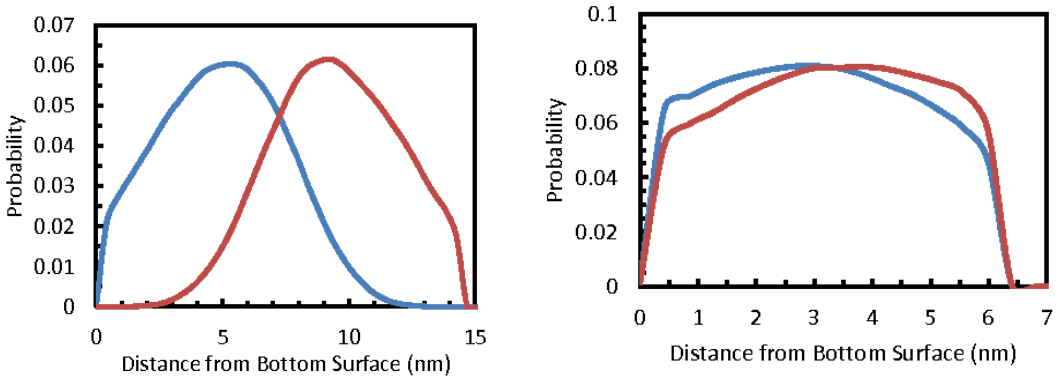

Figure 4-9. Chain end distributions for a low (left) and high (right) level of confinement. Blue and red indicate the bottom and top brush chain ends repectively. The chain end distribution was determined from the density profile of the last monomer of each chain, and normalized to a total probability of 1.

From Figure 4-9 it can be seen that at lower levels of compression the chain end distributions have a definite peak, however upon significant compression, the chain end distriubtions becomes much wider, indicating no significant preference throughout the brush.

4.5 Conclusions

Opposing polymer brushes were simulated and characterized under confinement. A static compression was conducted where all separation distances examined are separate simulations. Using methods previously developed, a realistic confinement was achieved by requiring all simulations at different surface separations to be at the same solvent chemical potential. Both structure, in the form of density profiles, and the interactions between brush layers, represented by normal pressure, were examined for each separation distance. The total density of the system increased substantially with compression, indicating that a model allowing for changing density was indeed necessary.

Interaction forces were calculated in the form of normal pressure versus distance plots. By comparing the normal pressure plot with the density profiles at each separation distance, structural explanations for observed trends in the normal pressure can be developed. The normal pressure experiences a large increase at the same time that interpenetration of the brush layers becomes more significant in the density profiles. When each brush layer extends all the way through to the opposing surface, the normal pressure profile increases sharply. Being able to directly compare structure and forces simultaneously is a major benefit of simulations. While both of these characteristics can be measured experimentally, doing so in the same experiment would not be feasible. Interpenetration was calculated for each system to examine this observation further. It follows a monotonic increase with decreasing separation distance, and follows self consistent field theory predictions qualitatively within a numerical constant.

The main effect of the compression on structure when compared to a single equilibrium brush is that the peak in the density profile becomes larger and the extended tail diminishes for each individual layer of the brush. Further, the chain end distributions have a single clear peak for each brush when interacting at larger separation distances, but this broadens under compression and is distributed across the entire box length. This indicates there is a mixture of chains that collapse back to the surface, extend through the opposing brush, and everything in between.

Future work will involve shearing the brushes at different separation distances to determine the lubrication properties of the brush, and how this changes with load. The systems are already set up at various separation distances at the correct solvent density, so the problem is greatly simplified.

4.6 Acknowledgment

This work was supported by the United States Department of Energy, Office of Basic Energy Science, under grant DE-FG02-06ER46340. I.G.E. additionally thanks the Graduate Assistance in Areas of National Need (GAANN) program of the U.S. Department of Education. Computer time at the National Energy Research Supercomputer Center, which is supported by the Office of Science of the U.S. Department of Energy under contract number DE-AC03-76SF00098, has been used for parts of the simulations.

4.7 References

1. Napper, D. H., *Polymeric Stabilization of Colloidal Dispersions*. Academic Press: London, 1983.

2. Halperin, A.; Tirrell, M.; Lodge, T., Tethered chains in polymer microstructures Macromolecules: Synthesis, Order and Advanced Properties. In Springer Berlin / Heidelberg: 1992; Vol. 100, pp 31-71.

3. Yokoyama, H.; Miyamae, T.; Han, S.; Ishizone, T.; Tanaka, K.; Takahara, A.; Torikai, N. Spontaneously Formed Hydrophilic Surfaces by Segregation of Block Copolymers with Water-Soluble Blocks. *Macromolecules* 2005, 38, (12), 5180-5189.

4. Moro, T.; Takatori, Y.; Ishihara, K.; Konno, T.; Takigawa, Y.; Matsushita, T.; Chung, U.-i.; Nakamura, K.; Kawaguchi, H. Surface grafting of artificial joints with a biocompatible polymer for preventing periprosthetic osteolysis. *Nat Mater* 2004, 3, (11), 829-836.

5. Pelletier, E.; Belder, G.; Hadziioannou, G.; Subbotin, A., Nanorheology of Adsorbed Diblock Copolymer Layers. In HAL - CCSD: 1997.

6. Grest, G. S. Interfacial Sliding of Polymer Brushes: A Molecular Dynamics Simulation. *Phys. Rev. Lett.* 1996, 76, 4979.

7. Grest, G. Normal and Shear Forces Between Polymer Brushes. *Adv. Polym. Sci.* 1999, 138, 149-183.

8. Klein, J.; Kumacheva, E.; Perahia, D.; Mahalu, D.; Warburg, S. Interfacial sliding of polymer-bearing surfaces. *Faraday Discussions* 1994, 98, 173-188.

9. Klein, J.; Kumacheva, E.; Mahalu, D.; Perahia, D.; Fetters, L. J. Reduction of frictional forces between solid surfaces bearing polymer brushes. *Nature* 1994, 370, (6491), 634-636.

10. W. A. Hamilton, G. S. S., N. A. Alcantar, J. Majewski, R. G. Toomey, T. L. Kuhl,. Determining the density profile of confined polymer brushes with neutron reflectivity. *Journal of Polymer Science Part B: Polymer Physics* 2004, 42, (17), 3290-3301.

11. Ell, J. R.; Mulder, D. E.; Faller, R.; Patten, T. E.; Kuhl, T. L. Structural Determination of High Density, ATRP Grown Polystyrene Brushes by Neutron Reflectivity. *Macromolecules* 2009, 42, (24), 9523-9527.

12. Klein, J.; Kamiyama, Y.; Yoshizawa, H.; Israelachvili, J. N.; Fredrickson, G. H.; Pincus, P.; Fetters, L. J. Lubrication forces between surfaces bearing polymer brushes. *Macromolecules* 1993, 26, (21), 5552-5560.

13. Tian, P.; Uhrig, D.; Mays, J. W.; Watanabe, H.; Kilbey, S. M. Role of Branching on the Structure of Polymer Brushes Formed from Comb Copolymers. *Macromolecules* 2005, 38, (6), 2524-2529.

14. Schorr, P. A.; Kwan, T. C. B.; Kilbey, S. M.; Shaqfeh, E. S. G.; Tirrell, M. Shear Forces between Tethered Polymer Chains as a Function of Compression, Sliding Velocity, and Solvent Quality. *Macromolecules* 2002, 36, (2), 389-398.

15. Watanabe, H.; Tirrell, M. Measurement of forces in symmetric and asymmetric interactions between diblock copolymer layers adsorbed on mica. *Macromolecules* 1993, 26, (24), 6455-6466.

16. Liao, W.-P.; Kuhl, T. L. Steric Forces of Tethered Polymer Chains as a Function of Grafting Density: Studies with a Single Diblock Molecular Weight. *Macromolecules* 2012, 45, (14), 5766-5772.

17. Alexander, S. Adsorption of chain molecules with a polar head: a scaling description. *Journal de physique.* 1977, 38, 983-987.

18. de Gennes, P. G. Conformations of Polymers Attached to an Interface. *Macromolecules* 1980, 13, (5), 1069-1075.

19. Milner, S. T.; Witten, T. A.; Cates, M. E. Theory of the grafted polymer brush. *Macromolecules* 1988, 21, (8), 2610-2619.

20. Pastorino, C.; Binder, K.; Müller, M. Coarse-Grained Description of a Brush-Melt Interface in Equilibrium and under Flow. *Macromolecules* 2009, 42, (1), 401-410.

21. Dimitrov, D. I.; Milchev, A.; Binder, K. Polymer brushes in solvents of variable quality: Molecular dynamics simulations using explicit solvent. *J. Chem. Phys.* 2007, 127, (8), 084905.

22. Grest, G. S.; Murat, M. Structure of grafted polymeric brushes in solvents of varying quality: a molecular dynamics study. *Macromolecules* 1993, 26, (12), 3108-3117.

23. Kreer, T.; Müser, M. H.; Binder, K.; Klein, J. Frictional Drag Mechanisms between Polymer-Bearing Surfaces. *Langmuir* 2001, 17, (25), 7804-7813.

24. Neelov, I. M.; Binder, K. Brownian dynamics simulation of grafted polymer brushes. *Macromolecular Theory and Simulations* 1995, 4, (1), 119-136.

25. Neelov, I. M.; Borisov, O. V.; Binder, K. Shear deformation of two interpenetrating polymer brushes: Stochastic dynamics simulation. *J. Chem. Phys.* 1998, 108, (16), 6973-6988.

26. Grest, G. S. Grafted polymer brushes in polymeric matrices. *J. Chem. Phys.* 1996, 105, (13), 5532-5541.

27. Galuschko, A.; Spirin, L.; Kreer, T.; Johner, A.; Pastorino, C.; Wittmer, J.; Baschnagel, J. Frictional Forces between Strongly Compressed, Nonentangled Polymer Brushes: Molecular Dynamics Simulations and Scaling Theory. *Langmuir* 2010, 26, (9), 6418-6429.

28. Spirin, L.; Galuschko, A.; Kreer, T.; Johner, A.; Baschnagel, J.; Binder, K. Polymer-brush lubrication in the limit of strong compression. *Eur. Phys. J. E* 2010, 33, (4), 307-311.

29. Goujon, F.; Malfreyt, P.; Tildesley, D. J. Dissipative Particle Dynamics Simulations in the Grand Canonical Ensemble: Applications to Polymer Brushes. *ChemPhysChem* 2004, 5, (4), 457-464.

30. Goujon, F.; Malfreyt, P.; Tildesley, D. J. Mesoscopic Simulation of Entangled Polymer Brushes under Shear: Compression and Rheological Properties. *Macromolecules* 2009, 42, (12), 4310-4318.

31. Goujon, F.; Malfreyt, P.; Tildesley, D. J. Interactions between polymer brushes and a polymer solution: mesoscale modelling of the structural and frictional properties. *Soft Matter* 2010, 6, (15), 3472-3481.

32. Hess, B.; Kutzner, C.; van der Spoel, D.; Lindahl, E. GROMACS 4: Algorithms for Highly Efficient, Load-Balanced, and Scalable Molecular Simulation. *J. Chem. Theory Comput.* 2008, 4, (3), 435-447.

33. Marrink, S. J.; de Vries, A. H.; Mark, A. E. Coarse Grained Model for Semiquantitative Lipid Simulations. *J. Phys. Chem. B* 2004, 108, (2), 750-760.

34. Hatakeyama, M.; Faller, R. Coarse-grained simulations of ABA amphiphilic triblock copolymer solutions in thin films. *Phys. Chem. Chem. Phys.* 2007, 9, (33), 4662-4672.

35. Elliott, I. G.; Mulder, D. E.; Traskelin, P. T.; Ell, J. R.; Patten, T. E.; Kuhl, T. L.; Faller, R. Confined polymer systems: synergies between simulations and neutron scattering experiments. *Soft Matter* 2009, 5, (23), 4612-4622.

36. Elliott, I. G.; Kuhl, T. L.; Faller, R. Molecular Simulation Study of the Structure of High Density Polymer Brushes in Good Solvent. *Macromolecules* 2010, 43, (21), 9131-9138.

37. Rossi, G.; Elliott, I. G.; Ala-Nissila, T.; Faller, R. Molecular Dynamics Study of a MARTINI Coarse-Grained Polystyrene Brush in Good Solvent: Structure and Dynamics. *Macromolecules* 2012, 45, (1), 563-571.

38. Berendsen, H. J. C.; Postma, J. P. M.; Gunsteren, W. F. v.; DiNola, A.; Haak, J. R. Molecular dynamics with coupling to an external bath. *J. Chem. Phys.* 1984, 81, (8), 3684-3690.

39. Humphrey, W.; Dalke, A.; Schulten, K. VMD: Visual molecular dynamics. *J. Mol. Graphics* 1996, 14, (1), 33-38.

40. Milner, S. T. Polymer Brushes. *Science* 1991, 251, (4996), 905-914.

41. Elliott, I. G.; Kuhl, T. L.; Faller, R. A Molecular Dynamics Technique to Extract Forces in Soft Matter Systems Under Compression With Constant Solvent Chemical Potential. *J. Chem. Theory Comput.* 2012, 8, (3), 1072-1077.

42. Widom, B. Some Topics in the Theory of Fluids. *J. Chem. Phys.* 1963, 39, (11), 2808-2812.

43. Lindahl, E.; Edholm, O. Spatial and energetic-entropic decomposition of surface tension in lipid bilayers from molecular dynamics simulations. *J. Chem. Phys.* 2000, 113, (9), 3882-3893.

44. Ollila, S.; Hyvönen, M. T.; Vattulainen, I. Polyunsaturation in Lipid Membranes: Dynamic Properties and Lateral Pressure Profiles. *J. Phys. Chem. B* 2007, 111, (12), 3139-3150.

45. Ollila, O. H. S.; Risselada, H. J.; Louhivuori, M.; Lindahl, E.; Vattulainen, I.; Marrink, S. J. 3D Pressure Field in Lipid Membranes and Membrane-Protein Complexes. *Phys. Rev. Lett.* 2009, 102, (7), 078101.

46. Whitmore, M. D.; Baranowski, R. End-Anchored Polymers: Compression by Different Mechanisms and Interpenetration of Apposing Layers. *Macromolecular Theory and Simulations* 2005, 14, (2), 75-95.

47. Murat, M.; Grest, G. S. Interaction between grafted polymeric brushes: A molecular-dynamics study. *Phys. Rev. Lett.* 1989, 63, (10), 1074.

Chapter 5

Normal and Shear Interactions between High Grafting Density Polymer Brushes Grown by Atomic Transfer Radical Polymerization

Submitted to Soft Matter, August 21, 2012, under the same title, with authors: Wei-Po Liao, Ian G. Elliott, and Tonya L. Kuhl.

This work was a collaboration with Wei-Po Liao. Ian G. Elliott contributed the synthesis work, while Wei-Po Liao contributed the characterization.

5.1 Chapter Abstract

The normal and shear interactions in toluene of polystyrene polymer brushes with ultra-high surface coverage ranging from 15 to 70 mg/m^2 formed by atom transfer radical polymerization were measured with a surface force apparatus. Significant hysteresis was observed between compression and separation cycles over the experiment time scale for all surface coverages. The magnitude of the hysteresis increased with increasing film thickness. The experimental relaxation time of the thickest brush layer was at least four orders of magnitude longer than that predicted by the Rouse model. Remarkably, the shear performance of the thickest brushes still demonstrated very good lubricity under compressions down to 35% solvent content. These findings are consistent with a reduction in solvent quality with compression leading to a shrinkage or collapse of the brush under high compression, while still maintaining a region of well solvated chains in the overlap region between the brushes. Thus, hysteresis in compression is primarily due to intra-brush entanglements and collapse of the brush layer rather than inter-brush entanglements and brush-brush interpenetration.

5.2 Introduction

Polymer brushes are frequently used to modify interfacial properties where they can act as steric stabilizers, adhesion modifiers, or enhance lubricity.[1-3] A polymer brush is formed when one end of the chain is confined to the interface or surface and the spacing between these anchor points is smaller than the polymer chain's radius of gyration, R_g. As the spacing between neighboring chains decreases, the chains are forced to stretch away normal to the grafting surface to decrease crowding. These structural changes due to osmotic crowding result in very different behaviors from free polymer chains in solution.[4, 5] In typical experiments, the polymer brush layer is formed by a "grafting to" approach in which chains are selectively anchored to the surface through physical adsorption methods that rely on diblock polymer chains and preferential solvation or by functionalizing the chain end leading to strong electrostatic binding or chemical bond formation to the surface. In both cases, the grafting density of the brush is limited by steric hindrance between the surface grafted chains. [6]

Because the brush structure and its physical properties depend intimately on the chain molecular weight, surface coverage, and solvent quality,[7-9] polymer brushes can be used to tailor interfacial properties[1-3]. Motivated by the wide application potential of polymer brush systems, a large number of theoretical,[5, 10-14] experimental[15-19] and simulation[20-25] studies have been carried out in order to characterize and ultimately predict the properties of polymer brushes. In particular, the tribological behavior of polymer-bearing surfaces has drawn significant attention as ultra-low friction coatings.[26-31] For example, Klein et al[26] found that the friction coefficient between mica surfaces grafted with end-functionalized Polystyrene (PS) brushes in good solvent conditions was two orders of

magnitude lower than that of bare mica in toluene. Similarly, Raviv et al.[28] found similar low friction behavior with physically adsorbed poly(ethylene oxide) (PEO) bearing surfaces in good solvent condition under moderate compressions. For high shear rates and high compression, some loss of the polymer brush layer was observed and a transition of the shear interface from polymer/polymer to polymer/substrate was suggested. A detailed comparison of normal and shear behavior in good and theta solvent conditions was carried out by Schorr et al[31] using amphiphilic polystyrene-poly(vinylpyridine) (PS/P2VP) diblocks. The best lubricant performance was found for good solvent conditions and shear-thinning behavior was observed with increasing sliding velocity. Using the same system, Forster et al.[32] found similar behavior where the onset of detectable shear force was found to shift to higher compression ratios as the solvent quality increased. Thus, the compression and interpenetration of opposing brush layers plays an important role in their frictional properties and the extent of interpenetration has been shown to increase with compression ratio and grafting density.[29, 33, 34] At a molecular level, recent molecular dynamic simulations have directly linked better lubrication behavior in good solvent conditions to fewer inter-brush contacts.[35] However, these previous studies were on dilute to semi-dilute brushes and the properties of ultra-high grafting density brushes have not yet been systematically studied.

Intrinsically, steric overlap between neighboring chains limits "grafting-to" polymer brushes to the dilute or semi-dilute grafting density regime. This can constrain the practical application needs of a stable and durable surface, particularly under high load. In contrast, the "grafting from" method where the polymer chain grows monomer by monomer from a surface using living polymerizations[36] can yield much higher grafting

densities. However, only a handful of experiments have studied brush properties in this regime. Ruth et al[37] performed the first comprehensive measurements of the interaction force between "grafting-from" brushes by replacing the chemically inert mica surfaces typically used in the surface force apparatus (SFA) with thin silica films that could be functionalized with a covalently grafted ATRP initiator layer. High molecular weight polystyrene brushes were grown directly on the surfaces, however the high polydispersity of the chains made quantitative comparison to polymer theory challenging.[38] Subsequently, Yamamoto et al.[39, 40] investigated Poly(methyl methacrylate) (PMMA) brushes by AFM. Discrepancies between the experimentally measured force-distance profile and scaling predictions[41] were attributed to the fact that the polymer concentration under this highly grafted condition significantly exceeded the semi-dilute concentration range assumptions used in the scaling theory. The tribology properties of "grafted from" brushes have primarily been investigated macroscopically[42-44] using conventional ball-on-disk type tribometers. Sakata et al.[43] measured PMMA brushes in different solvent conditions including the dry state. As in the microscopic SFA measurements, the lowest dynamic friction coefficient was found in good solvent conditions. In contrast, Kobayashi et al[42] found that the high density brushes of biocompatible polymer 2-methacryloyloxyethyl phosphorylcholine (MPC) had the best lubricant performance when in a high-humidity environment rather than when fully solvated in bulk water. They hypothesized that the dense brushes interpenetrated more in bulk water leading to higher friction compared to brushes in high humidity. Recently, Dunlop et al.[45] demonstrated a means to functionalize mica surfaces with a strongly absorbed poly-initiator film in order to obtain high grafting densities of a surface-grown polyelectrolyte

brushes of poly [2-(Methacryoyloxy)ethyl][29, 46] trimethylammonium chloride (poly(METAC)). A small hysteresis was observed between the polyelectrolyte brushes during compression-decompression which was attributed to attractive bridging interactions. Frictional properties were similar to earlier studies on polyelectrolyte brushes. This approach opens a straightforward means to carryout high resolution SFA experiments on high grafting density polymer layers.

In this work, an SFA was used to measure the normal and shear forces of high density "grafted from" polystyrene chains in toluene, a good solvent for polystyrene. The brushes were grown from silica films electron-beam deposited on mica enabling higher film thicknesses and grafting densities to be studied, while still preserving the high force and distance resolution of the SFA technique. In contrast to previous work on "grafted to" brushes at lower grafting densities that have primarily shown reversible compression forces, significant hysteresis was observed in the high density, "grafted from" system. The hysteresis, however, did not correlate with an increased friction between the brushes during shear force measurements at modest solvation. The work demonstrates that ultra-high density polymer brushes provide a very robust, low friction coating even under conditions where solvent quality is significantly reduced.

5.3 Experimental Section

5.3.1 Surface Functionalization of Mica

To provide an appropriate substrate for ATRP synthesis of the grafted from polymer brush chains, a thin-coating of silica was electron beam (E-beam, AUTO-TECH II, CHA industries) deposited on freshly cleaved sheets of mica. The procedure used followed the methodology described by Vigil et al.[47] In the present work, the silica layer was 1000Å

silica layer. The thickness and the refractive index of the silica layer were further confirmed by ellipsometry (EL2, Rudolph) yielding values of thickness and the refractive index of 1048±12Å and 1.48±0.01, respectively. The peak-to-valley roughness of the deposited silica was 5Å as determined by AFM and is consistent with the number previously reported by Vigil et al. The silica film was found to swell ~4% in bulk water. The thickness and refractive index of the silica film was also characterized in the SFA using multiple beam interferometry prior to ATRP polymer film growth. Freshly cleaved mica with the desired thickness and size was first cut into one or two larger pieces (few cm^2) and one smaller piece (few mm^2). The smaller piece was not coated with silica and used as a reference system to determine the mica substrate thickness. Silica was then deposited on the larger mica piece(s). After silica deposition, the mica pieces were flipped and placed on another mica backing sheet. A ~550Å of silver layer was deposited on the mica side of both the small mica pieces and the silica deposited mica pieces. The coated mica surfaces were then glued, silver side down, onto cylindrically curved glass disks using an optical adhesive (NOA 61, Norland Product Inc.) and cured by exposure to UV light for 5 minutes. Details of the thickness and refractive index determination by multiple beam interferometry are provided later under the heading *Thickness Determination*.

5.3.2 Atom Transfer Radical Polymerization

Materials. Styrene was purchased from Fisher Scientific, Karstedt catalyst was purchased from Gelest, and all other chemicals were from Sigma-Aldrich. Styrene was stirred with CaH_2 overnight to remove any water and vacuum distilled to remove the

inhibitor. The distilled styrene was stored at 4°C under nitrogen. CuBr was stirred over glacial acetic acid overnight, filtered, and washed with large quantities of ethanol.

5.3.3 10-undecenyl 2-bromoisobutyrate Synthesis

10-undecenyl 2-bromoisobutyrate, a precursor required for the initiator synthesis, was synthesized following the work of Matyjaszewski.[48] A stir bar, 5.9 mL 10-undecen-1-ol, 5.3 mL triethylamine, and 50 mL dichloromethane were added to a 100 mL round bottom flask in an ice bath. 3.7 mL 2-bromoisobutyryl bromide were added to the flask dropwise over a period of 5 minutes. The flask was removed from the ice bath and stirred at room temperature for 15 hours. The solution was washed with 65 mL of 0.5 molar HCL, and then washed with 65 mL DI water 3 times. Solvent was removed by rotovap. The solution was run through a column of silica gel with 100 mL of a 25:1 hexane:ethyl acetate solvent solution. The solution was again rotovaped to remove hexane. This procedure yielded approximately 7.5 g of a clear liquid.

5.3.4 Initiator Synthesis

The surface active initiator (11-(2-Bromo-2-methyl)propionyloxy)undecyl trichlorosilane was synthesized following previous work.[49] 4.6 mL of 10-undecenyl 2-bromoisobutyrate and a stir bar were added to a 50 mL schlenk flask. The flask was sealed and purged with nitrogen. Three freeze-pump-thaw cycles followed to ensure no oxygen was in the flask or liquid. 82 μL of Karstedt catalyst (2.1-2.4% Pt in xylene) were added and the flask was transferred to an ice bath. 4.75 mL trichlorosilane was added dropwise to the solution. The flask was allowed to slowly warm to room temperature and stirred for five hours under nitrogen. The product was transferred to a

round bottom flask and vacuum distilled at 30 mtorr. The distillation yielded 2.72 grams of initiator.

5.3.5 Initiator Deposition

The silica surfaces glued on the SFA discs were cleaned prior to initiator deposition by stirring in acetone for 10 minutes, followed by rinsing with isopropyl alcohol, Millipore filtered water, pure ethanol, and then dried with nitrogen. The surfaces were then exposed to UV/ozone for 20 minutes to hydroxilate the surfaces. Afterwards, the substrates were placed in a gently stirred solution of 34 μL (11-(2-Bromo-2-methyl)propionyloxy)undecyl trichlorosilane in 50 mL toluene for one hour. Upon removal of the substrates, partial dewetting of the toluene solution at the edge of the surfaces was evident of the formation of a self-assembled layer of initiator. The surfaces were then immediately rinsed in clean toluene (5-10 minute immersion with gentle stirring), removed and dried with nitrogen. Finally, the dry initiator coated surfaces were annealed at 75ºC to promote cross-polymerization and robust attachment of the initiator layer.

5.3.6 Polymerization

End-grafted polystyrene chains were synthesized from the initiator coated surfaces using established procedures.[49, 50] A custom reaction flask was used which could be taken apart to add or remove the surfaces.[49] After placing the surfaces in the reaction flask, 124 mg CuBr, 10 mg $CuBr_2$, and a stir bar were added. The flask was sealed and evacuated and backfilled with nitrogen three times. In a separate schlenk flask 10 mL styrene, 5 mL toluene, and 189 μL N,N,N',N',N"-Pentamethyldiethylenetriamine (PMDETA) were added and oxygen was removed by performing three Freeze-Pump-

Thaw cycles. Afterwards, 13 μL ethyl 2-bromoisobutyrate were added to the flask, and the solution was immediately transferred to the custom reaction flask at 90°C using a syringe. The reaction was allowed to proceed for a designated time, generally three to eight hours. To quench the reaction at the designated time, the heat was turned off, the solution was exposed to air, and THF was added. Finally, the surfaces were stirred in hot toluene for 20 minutes to remove unreacted monomer and stirred in IPA for 20 minutes to remove copper salts.

5.3.7 Surface Force Apparatus

The surface force apparatus (SFA) technique has been widely used for measuring the interactions between two opposing surfaces as a function of separation and details of the instrument and measurements have been explicitly described elsewhere.[51-55] Briefly, the interaction forces are obtained by determining the deflection of a force measuring spring supporting the lower surface while the distance between two surfaces are measured by monitoring the fringes of equal chromatic order (FECO) using a spectrometer. The polymer coated discs are placed in cross cylinder geometry and the measured radius of surface curvature for each contact position was used to normalize the measured force to enable quantitative comparison between different contact positions and experiments. The Derjaguin approximation[56] gives the relationship between the interaction energy per unit area, *E*, for two flat plates from the measured force-distance, *F (D)*, relationship between two crossed cylinders

$$\mathrm{E(D)} = \frac{\mathrm{F(D)}}{2\pi \mathrm{R}} \tag{5-1}$$

The Derjaguin approximation is valid at small distances where $D << R$. The radius of curvature was measured for two cross sections, at 90º and the geometrical mean was used

in calculations. For these experiments the measured radius of curvature was 1.0 ± 0.15 cm.

In the present work, normal and shear force profiles between the ATRP grown brushes were measured by a Mark II SFA with a shear device (by SurForce). The shear device includes both a receiver where the top surface was mounted and a bimorph slider device where the lower surface was mounted. As in previous designs[57, 58], application of a triangular signal to the bimorph slider enables linear lateral movement of the lower surface relative to the upper surface, here up to 1mm.[58] The top receiver assembly has semi-conductor strain gauges to work as a force sensor.

5.3.8 Thickness Determination

The thickness in air and the refractive index of the layers was determined by the FECO wavelength positions using a multi-matrix method (MMM)[59] and additional details are provided elsewhere.[60] Briefly, a model of the optical cavity is used to generate the FECO wavelength pattern by MMM with input parameters such as thickness and refractive index of each layer. A fitting algorithm determines the set of parameters that minimizes the difference between the experimental measurement and the model. Figure 5-1 provides an example of the contact fringes obtained from the corresponding geometries of the system where subsequent layers are added to demonstrate how the thickness and refractive index of the various layers (silver, mica, silica, polymer) were determined.

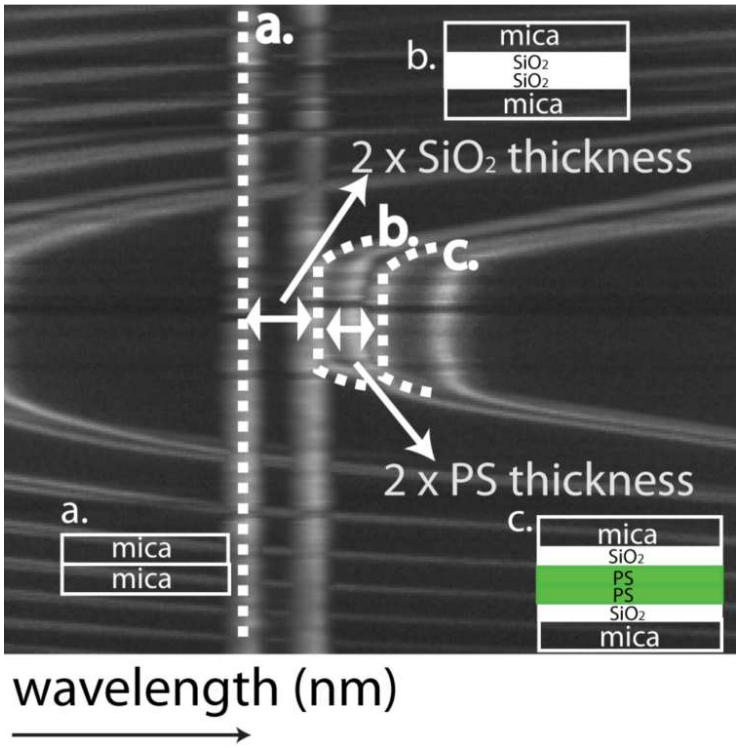

Figure 5-1. An example image of how the fringes of equal chromatic order (FECO) wavelengths shift as the number of layers between the surfaces is increased. The optical cavity between the silver layers is modeled and the data fitted to extract the thicknesses and refractive index of the different layers (silver, mica, silica, and polymer) sequentially. The image itself is an overlay of the contact FECO wavelengths for the three measured geometries used; (a) contact of mica-mica surfaces, (b) contact of silica-silica surfaces, (c) contact of PS-PS surfaces. The dashed lines are guides to distinguish different contact geometries.

First, the bare mica-mica contact (a) was always measured as a control in order to determine the thickness and the refractive index of the silver and mica sheets before adding subsequent layers, e.g. silica and polymer. Next, the contact of silica-silica (b) was measured for identical mica sheets and the thickness and refractive index of the deposited silica film was determined. The accuracy of the fitting program and approach was confirmed by comparing the thickness obtained from ellipsometry to that of multiple experiments with different mica and silica thicknesses. Throughout any given experiment, differences between the control measurements before and after adding

additional optical layers were less than 3% in thickness and 1% in refractive index. After establishing the thicknesses and refractive indexes of the silver, mica, and silica layers, the thickness of the ATRP-grown polystyrene was determined be simply fitting the FECO wavelengths of the entire system (c). At least four different positions on the surfaces of different sets of samples were measured to confirm the uniformity of the film.

5.3.9 Normal and Shear Force Measurements of Polymer Layers

In the normal force setting, after the measurements of the dry PS film thickness, the surfaces were separated a couple of millimeters and the SFA was filled with toluene. The surfaces were brought closer together (≤0.5mm) and the film was left solvating for 24 hours before measuring the force profile. The distance "D" utilized in the force-distance profiles provided in the following sections was defined as the spacing between the opposing silica surfaces which corresponds directly to the thickness or extension of the two PS brushes. Multiple compression-decompression cycles for different positions on the surfaces were measured. At least 10 seconds was elapsed after each displacement before taking a reading of the surface separation and 30 minutes was elapsed between different approach/separation cycles to allow for chain relaxation. As is commonly done, the shear force measurements used a droplet of toluene as the shear attachment cannot be fully immersed in solvent.[16] A small vial of toluene was placed inside the SFA chamber during shear measurements to maintain the vapor pressure and prevent evaporation of the toluene droplet between the surfaces. The lateral, parallel movements of the lower surface mounted in the bimorph device were achieved by applying a triangular signal with a function generator (3325B, Hewlett Packard) while a signal conditioning amplifier (2300, Vishey) was used to magnify the signal obtained from the receiver where the

upper surface was mounted. The magnified response voltage was collected by a XYt chart recorder (BD41, Kipp&Zonen) and converted to the force (N) between the surfaces. An example of the XYt output is shown in Figure 5-2.

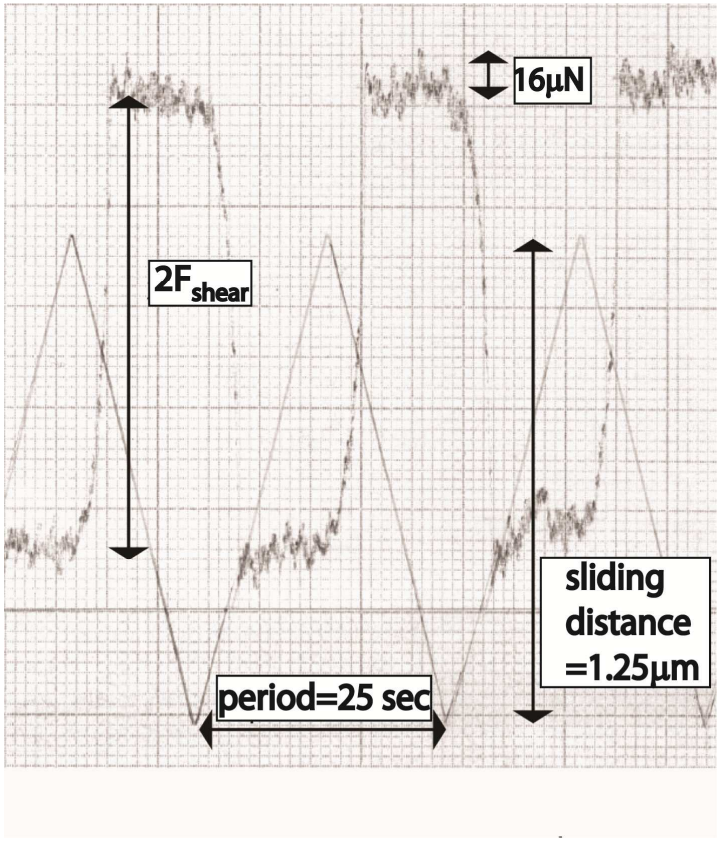

Figure 5-2. Example of a XYt plot used for shear force analysis of ATRP grown PS brushes (D=1767±33Å). The maximum sliding distance was 1.25 μm obtained from the peak-to-peak value of the triangular wave. The shear force between the opposing PS brushes is denoted as F_{shear} and is determined from the plateau height difference.

The applied triangular signal and the detected voltage were monitored simultaneously. The sliding distance and the velocity of the lateral motion from the lower surfaces were controlled by the applied voltage and the frequency of the function generator, respectively. In the present work, the maximum sliding distance was fixed at 1.25μm while the velocity was 100nm/s.

For several measurements, the normal force profile was measured in both the normal and shear force setting to confirm reproducibility, and that the brush layers remained fully solvated in toluene throughout the droplet experiment. The normal force profile and the film thickness were also checked before and after the shear measurements to confirm the stability of the ATRP grown PS brushes. No substantive change in thickness was detected. Both the shear and normal force measurement were performed in a temperature controlled environment at 25±0.2°C.

5.4 Results and Discussions

5.4.1 Brush Properties

In this work, the physical properties of ultra-high density PS brushes formed by the "grafting from" method were studied using an SFA. The dimensionless overlap surface density, $\Sigma = \sigma\pi R_g^2$, is typically used to describe and compare different brushes, where σ is the experimental chain grafting density (chains/Å^2), and R_g is the radius of gyration of a free polymer chain in solution[20]. A clear challenge in using "grafting from" brushes is defining the MW and grafting density of the formed polymer brush layer. Fortunately, it is straightforward to measure the dry film thickness and uniformity of the grown film using SFA measurements. Table 5-1 reports the average measured polymer thickness for three different ATRP grown PS films.

	SFA Measured			GPC Measured	
Sample	PS Dry Thickness (Å)	Measured Brush Extension h_{exp}, (Å)	mg/m^2	MW (kg/mole)	PDI
A	142±13	630±50	15±1.3	23.5	1.088
B	502±36	1950±100	52±3.1	60.5	1.211
C	665±41	2370±125	70±4.5	100.0[Δ]	1.285
D[§]	73±13	525±50	7.6±1.0	57.0	1.080

	Estimated		
Sample	$\sigma \times 10^2$ (chains $Å^{-2}$)	Overlap Surface Density Σ^*	Fully Stretched Length $L^¥$, (Å)
A	0.38	26	588
B	0.52	111	1513
C	0.18	162	2500
D[§]	0.08	15.8	1425

*$Rg=1.86 \times N^{0.595}$, where N=degree of polymerization[61]
[§]Physically adsorbed brush formed from a 50:50 PS-P2VP diblock copolymer
[¥]L=aN where a is the repeating PS monomer size of 2.6Å.[9]
[Δ] Estimated based on the inset of Figure 5-1 measured by GPC.

Table 5-1. Characterizations of the ATRP grown Polystyrene

The error was established by measuring the film thickness at a minimum of 4 different contact positions between the layers. Given the bulk density of PS, $\rho=1.05 g/cm^3$, the mass per unit area of the grown PS film can be easily calculated from the measured dry thickness. To provide information on the MW of the brush layer, free initiator was present in the reaction solution during our polymerizations. It has been previously reported that chains grown free in solution provide a good indication of the MW of chains grown simultaneously from initiator layers from the surface.[49, 62-64] The MW and PDI of the free chains in the polymerization supernatant were determined by GPC. These values verses the measured dry film thickness are reported in Table 5-1 and plotted in the inset of Figure 5-3. Typically, a linear increase in dry film thickness with MW is expected and has been reported in earlier studies. In this work, the two lower MW

polymerizations follow a linear increase in film thickness. However, the thickest film, which also had the highest PDI, clearly deviates significantly from this trend. This deviation at high polymerizations is attributed to termination events in the surface film. Even with this caveat, the supernatant measurements of MW and PDI do provide an estimate of the surface grown polymer film properties and three clearly different conditions were achieved (Table 5-1). The calculated value of Σ~191 for the thickest film is likely a significant overestimation. Based on the measured film thickness, a more modest MW of ~100k yields an Σ~162.

5.4.2 Force Profile Measurements

Next, the interaction force profiles as a function of distance for three different ATRP grown PS films in toluene are described. As will be discussed in the next section, significant hysteresis was observed in the normal force measurements. The data reported in Figure 5-3 were measured after allowing the systems to relax for at least 24 hours before compressing.

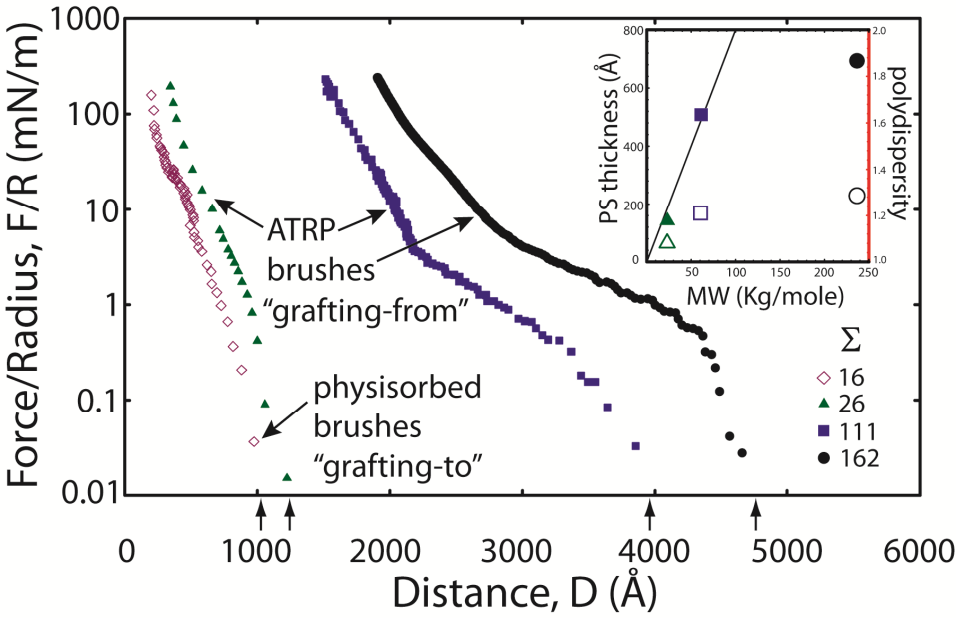

Figure 5-3. Measured force profiles of ATRP grown PS brushes for three different grafting densities (solid symbols). Force profile data for a well-defined brush formed from a 50:50 PS-P2VP diblock copolymer with Σ=16 (diamonds) is also shown for comparison. The inset shows the relationships among dry PS thickness (closed symbols), MW and the polydispersity (opened symbols) determined by GPC.

The extension of the brush in toluene, as depicted by the arrows in Figure 5-3, was defined as the onset of the repulsive force under these equilibrated conditions (Table 5-1). The onset distance increases with the thickness of the dry PS film, consistent with the expected increase in the grafted brush MW with increasing film thickness. With further compression, the repulsive force increased monotonically with decreasing separation. One fact that needs to be noted here is that unlike the grafting-to brushes, the extensions of the ATRP grown PS were very close or even exceeded the fully-stretched length based on the GPC measurements. Although the PDI of the chains can account for this discrepancy, the GPC results from the supernatant chains should only be considered a rough indication of the MW and PDI of the surface grafted chains. The primary characterization of the surface films is obtained by direct measurement of the film thickness and solvated brush extension by SFA.

For comparison, the force to compress a physically adsorbed brush formed from a 50:50 polystyrene-b-poly-(2-vinylpyridine) (PS-P2VP) diblock copolymer with Σ=16 is also shown. The physical properties of this well-defined "grafted to" brush are also provided in Table 5-1. As can be seen, the force profile for this PS-P2VP brush (PS MW = 57k) is very similar to that of the Σ~26 ATRP PS brush ($MW_{estimate}$=23.5k). Moreover, both the ~PDI and dry film thickness are very similar for both of these cases although their MWs may differ by almost a factor of 3. In contrast, the high MW ATRP brushes (Σ~111, 162) have a much softer long-range repulsion due to their higher PDI and MW. This soft repulsion further suggests that the GPC measurements should be considered as a lower bound estimate for the grafted brush PDI. Although the MW of the PS diblock matches the Σ~111 ATRP PS brush ($MW_{estimate}$=60.5k), the brush extension is much longer with the ATRP brush due to the presumably large increase in grafting density. To the best of our knowledge, these are the highest grafting density brushes for which interaction force profiles have been measured.

The measured repulsive force was also compared to the self-consistent mean field theory developed by Milner, Witten and Cates (MWC) for two polymer brushes in good solvent conditions;[18, 38, 65]

$$\frac{F(D)}{R} = 2\pi h_0 \sigma^{4/3} \nu^{2/3} \omega^{1/3} \left(\frac{1}{u} + u^2 - \frac{u^5}{5} - \frac{9}{5}\right) \quad (5\text{-}2)$$

where $u=h/h_0$, h_0 is defined as the unperturbed extension of the monodisperse brush calculated from $h_0=(12/\pi^2)^{1/3} N\sigma^{1/3}\omega^{1/3}\nu^{-1/3}$, ω is the excluded volume parameter, and the effective size parameter ν, which has the dimension of length^{-2}, is found from the statistical segment size, b , using $\nu=3/b^2$. The values of ω and b used were $(3.2Å)^3$ and 7.6Å, respectively, based on the work with a similar ATRP system carried out by Ell et

al.[49] As shown in Figure 5-4 for Σ~26 the MWC prediction matches reasonably well to the measured force after repeated compression and separation cycles.

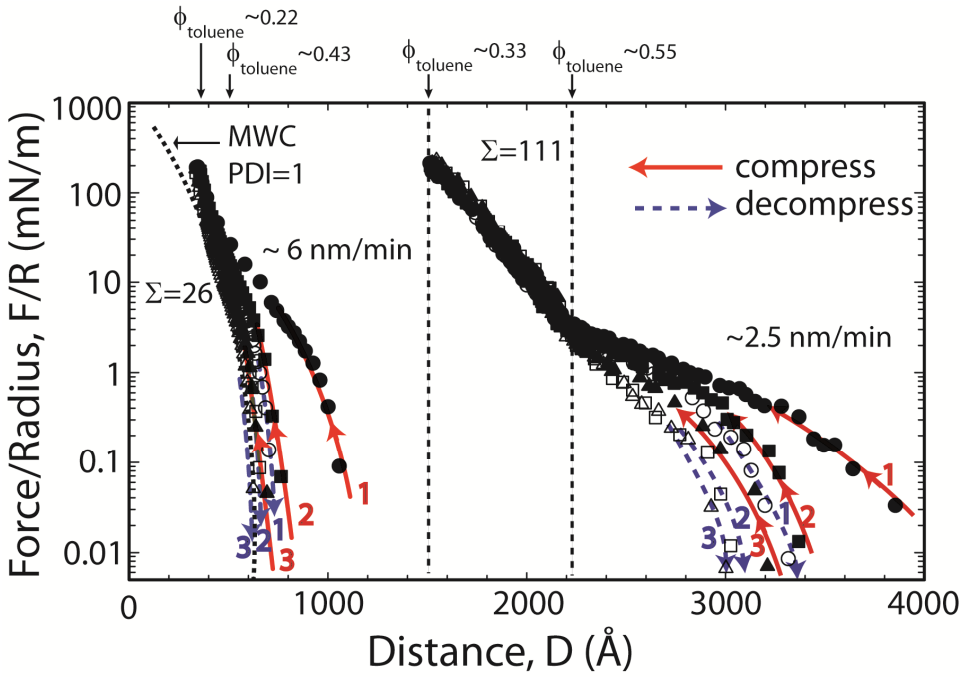

Figure 5-4. Compression/decompression cycles for forces profiles of two opposing ATRP grown PS brushes in toluene with overlap surface density Σ=26 and 111. Solid symbols and empty symbols with corresponding shapes represent a single compression and decompression cycle, respectively. The solid and dashed lines with arrowheads are the guides to the eye. At least 30 minutes between different cycles and 8-12 seconds between each surface displacement were allowed for brush relaxation. The average approach rates for each system are provided. The long-dashed line shows the predictions of mono-disperse MWC theory for Σ=26.

As originally demonstrated by Milner and subsequently others,[37, 66, 67] a small increase in the chain PDI leads to a significant increase in the onset of the measured repulsion between opposing polymer brushes as observed here. It is, however, somewhat surprising that the MWC theory provides a reasonable estimate given that the theory assumes dilute/semi-dilute polymer concentration and simple pairwise interactions. The strong stretching limit is likely more reasonable for these high grafting density brushes than more typical, lower density "grafting-to" brushes.[66] Based on our estimated grafting

density of Σ~26, the average concentration of the polymer was already significantly above the limit of the semi-dilute concentration range.[68] Not surprisingly, at the higher grafting densities, Σ~111 and 162, the agreement was very poor. However, the MW and polydispersity of the grafted brushes may not be well represented by the measured values for free chains in solution during the polymerization. For thicker films, it is more difficult to maintain a constant growth rate and there is a greater chance for chain transfer termination events between neighboring chains.[69]

A more interesting feature of the grafted brushes is the significant hysteresis observed in the force profiles, where the measured interaction force upon separation was much less than that on surface approach. Such behavior has only rarely been reported between end-grafted polymer brushes in good solvent conditions. Indeed, the only examples we are aware of also studied polydisperse, "grafting-from" polymer brushes[37, 45, 70] and "grafting-to" system with high MW and polydispersity.[28, 70] More commonly, hysteresis is observed under poor solvent conditions where the polymer layers are somewhat adhesive; when there is incomplete brush coverage on the surfaces resulting in bridging interactions; or, the polymer film is absorbed and undergoes long-lived structural rearrangements during the measurements. Examples of compression decompression cycles of our ATRP brushes are shown in Figure 5-4 for Σ~26 and Σ~111. The solid and empty symbols represent the compression and decompression processes, respectively, while the solid and dashed lines with arrow heads are provided as a guide to distinguish different approach and separation cycles. The initial compression was carried out on equilibrated brushes that had been allowed to relax for at least 24 hours before compressing. After each surface displacement during the force measurement, the brushes

were allowed to relax for 8-12 seconds before measuring the surface separation. The average approach rate is reported in Figure 5-2. Similar behavior is observed for the three ATRP brush systems where the brush extension becomes less for subsequent compression decompression cycles. The magnitude of the hysteresis increases with the polydispersity and thickness (MW) of the brush layer. With increased cycling, the curves collapse to a master interaction force profile that is similar to that expected for a more monodisperse brush system. In other words, with cycling the force is dominated by the osmotic repulsion rather than the details of the brush structure. These findings suggest that the structure of the diffuse outer layer of the brush is greatly modified by compression and takes a significant time to relax back to a more equilibrium state. Osaki et al.[71] developed an empirical formula to calculate the relaxation time of a polymer in semi-dilute solution by modeling the dynamic modulus using the Rouse model. Using this method, the relaxation time over our polymer MW range is on the order of 10^{-2} seconds - much faster than the experimental time scale of the force profile measurements. Indeed, the experimental time scale is over three orders of magnitude longer, but still not sufficient for the system to equilibrate. The entanglement MW of PS in melt is ~18 kg/mole,[72] and increases with decreasing polymer volume fraction with a -4/3 power.[46, 73] All the studied ATRP brushes are above the entanglement MW. In contrast, most physisorbed brushes formed by grafting-to method are below the entanglement MW once the polymer volume fraction is accounted for. This is consistent with the fact that the highly hysteric behavior was only observed with the ATRP brushes, but no any noticeable hysteresis in the force profile measurements was observed between cycles over similar time scales for the 50:50 PS-P2VP diblock brush (PS MW 57k).

5.4.3 Shear Force Measurements

Lateral shear force measurements were carried out on the thickest ATRP brush layer, Σ~162. In particular, we were very interested in determining the friction behavior as this brush system had the highest hysteresis in the compression cycles. Figure 5-5 plots both the normal and shear force as a function of separation between the brush layers.

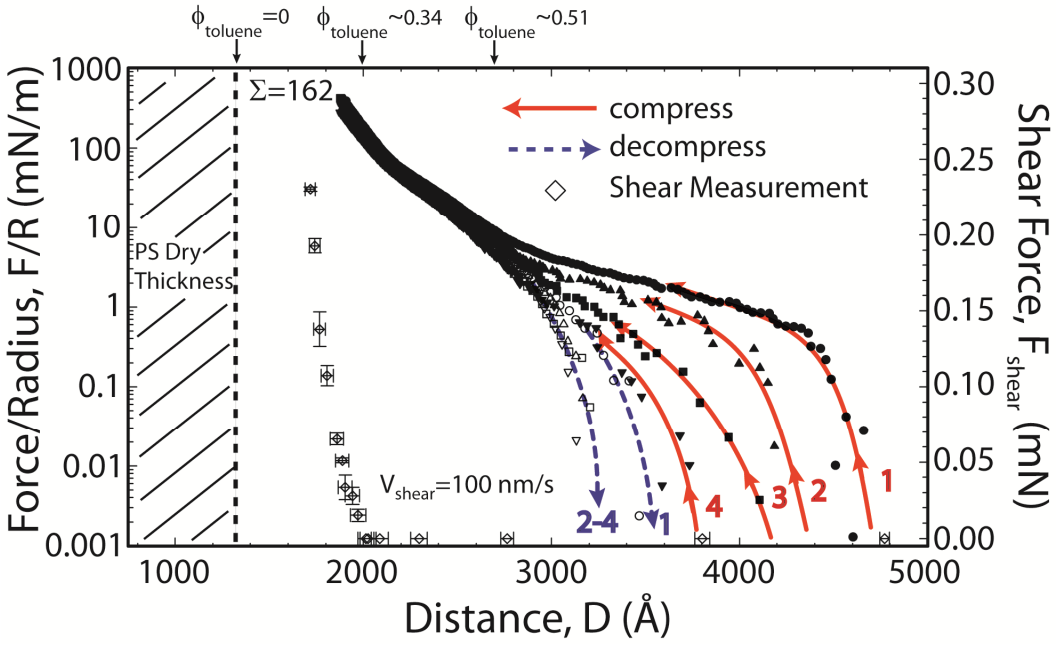

Figure 5-5. Normal and shear forces as a function of separation between two opposing ATRP grown PS brushes with Σ=162 in toluene. Four compression (closed symbols) / decompression (open symbols) cycles are shown. The solid and dashed lines are the guides to the eye for the different compression/decompression cycles. Shear force measurements (2nd Y axis) were carried out with a velocity of 0.1 μm/s and sliding distance of1.25μm.

Again, the high hysteresis in the normal force profiles demonstrate that the experimental time scale is shorter than the relaxation process of the brush layer. Surprisingly, lateral shear force was undetectable within the experimental resolution until the opposing layers were highly-compressed. This demonstrates that these polydisperse brushes provide an excellent lubrication layer. Even at a volume fraction of only 34%

toluene the effective friction coefficient of the layers was less than 0.02. It is commonly suggested that the friction force between polymer brush layers originates from viscous dissipation within the mutual interpenetration region of the opposing polymer brushes.[29, 30] Based on MD simulations, Spirin et al.[74] have suggested that two types of entanglements need to be taken into consideration in polymer brush systems during sliding; intra-brush entanglements inside an individual brush layer and inter-brush entanglements that occur between the opposing brush layers. As no adhesion was observed between the brush layers during force compression measurements, the findings suggest that intra-brush entanglements within each brush layer increase during compression. These intra-brush entanglements are more dominate than inter-brush entanglements between the two brushes which reduces opposing brush interpenetration and enables low friction sliding between the brushes even under high compression. This important intra-brush entanglement behavior is consistent with the observation of Ruths et al.[37]

The low friction sliding of these ultra-high density brushes is even more remarkable given the low solvation of the brushes. The friction force between the brushes only becomes measurable when the volume fraction of toluene drops below 34%. After this point, the friction rapidly increases as the brushes are further compressed. Kobayashi et al.[42] also observed better lubricant performance for high density P(MPC) brushes in reduced solvent conditions. In this case, the friction was significantly lower in a high-humidity environment compared to that when fully hydrated in water. Similar to the argument presented here, Kobayashi et al. suggested that inter-brush contacts and greater interpenetration occurred in bulk water compared to high humidity conditions.

An important consideration for understanding the properties of high density brushes is possible changes in solvent quality with compression. All the brush systems reported here greatly exceed the semi-dilute regime. Thus, as the brushes are compressed and the polymer concentration in the gap between the surfaces increases, the solvent quality can be significantly reduced resulting in more favorable polymer contacts.[75] This is consistent with more intra- and inter-brush contacts. In addition, the reduction in the solvent quality will substantially decrease the extension of the polymer brushes, which may also reduce the interpenetration region.[31, 32] For higher grafting densities (Σ=111 and 162), the observed force profiles can be reasonably divided into two distinct concentration ranges: a highly hysteretic region and a reversible region after multiple compressions. These regions correspond to less dense outer brush layer and more dense or collapsed inner brush layer, respectively. The denser region could be possibly attributed to the entanglement network formed during the process of chain-transfer termination when the polymerization was conducted at higher temperature[69] while other "escaped" chains continue growing linearly and created a less dense outer region. Without sufficient relaxation time, the extension of the brush from the dense region is greatly diminished presumably due to formation of favorable intra-brush contacts under solvent starved conditions. Likewise, inter-brush contacts become more favorable and with high compression (Φ<35%) and the friction increases rapidly. For lower compressions the outer region of the brush layers remain well solvated and provide frictional properties similar to semi-dilute brushes that have been commonly studied in the past.

5.5 Conclusion

Both normal and shear interactions between ultra-high grafted polymer brushes have been examined in the present work. Very long relaxation times are evident from the observed hysteresis with compression separation cycles. The hysteresis increases with increasing brush polydispersity. Remarkably, the friction behavior is found to be very similar to low density brushes in the semi-dilute regime and does not increase appreciably until the solvent volume fraction is less than 35%. The importance of the high density brushes yielding favorable lubrication properties is that a highly durable lubricating layer can be formed. These findings demonstrate that high grafting density brushes with high polydispersity – a real system rather than ideal monodisperse system – have potential as lubricants in more practical applications.

5.6 References

1. Klein, J.; Kamiyama, Y.; Yoshizawa, H.; Israelachvili, J. N.; Fredrickson, G. H.; Pincus, P.; Fetters, L. J. Lubrication forces between surfaces bearing polymer brushes. *Macromolecules* **1993,** 26, (21), 5552-5560.

2. Brochard-Wyart, F.; de Gennes, P. G.; Leger, L.; Marciano, Y.; Raphael, E. Adhesion promoters. *J. Phys. Chem.* **1994,** 98, (38), 9405-9410.

3. Devaux, C.; Chapel, J. P.; Beyou, E.; Chaumont, P. Controlled structure and density of "living" polystyrene brushes on flat silica surfaces. *The European Physical Journal E - Soft Matter* **2002,** 7, (4), 345-352.

4. Milner, S. T. Polymer Brushes. *Science* **1991,** 251, (4996), 905-914.

5. de Gennes, P. G. Conformations of Polymers Attached to an Interface. *Macromolecules* **1980,** 13, (5), 1069-1075.

6. Zhao, B.; Brittain, W. J. Polymer brushes: surface-immobilized macromolecules. *Progress in Polymer Science* **2000,** 25, (5), 677-710.

7. Kent, M. S.; Lee, L. T.; Factor, B. J.; Rondelez, F.; Smith, G. S. Tethered chains in good solvent conditions: An experimental study involving Langmuir diblock copolymer monolayers. *The Journal of Chemical Physics* **1995,** 103, (6), 2320-2342.

8. Goujon, F.; Malfreyt, P.; Tildesley, D. J. The compression of polymer brushes under shear: the friction coefficient as a function of compression, shear rate and the properties of the solvent. *Molecular Physics* **2005,** 103, (19), 2675-2285.

9. Devaux, C.; Cousin, F.; Beyou, E.; Chapel, J. P. Low Swelling Capacity of Highly Stretched Polystyrene Brushes. *Macromolecules* **2005,** 38, (10), 4296-4300.

10. Alexander, S. Adsorption of Chain Molecules with a Polar Head a-Scaling Description. *J Phys-Paris* **1977,** 38, (8), 983-987.

11. Alexander, S. Polymer adsorption on small spheres: A scaling approach. *Journal de physique.* **1977,** 38, (8), 977-982.

12. De Gennes, P. G. Polymer solutions near an interface. Adsorption and depletion layers. *Macromolecules* **1981,** 14, (6), 1637-1644.

13. Milner, S. T.; Witten, T. A.; Cates, M. E. A Parabolic Density Profile for Grafted Polymers. *EPL (Europhysics Letters)* **1988,** 5, (5), 413-418.

14. Milner, S. T.; Witten, T. A.; Cates, M. E. Theory of the grafted polymer brush. *Macromolecules* **1988,** 21, (8), 2610-2619.

15. Taunton, H. J.; Toprakcioglu, C.; Fetters, L. J.; Klein, J. Interactions between surfaces bearing end-adsorbed chains in a good solvent. *Macromolecules* **1990,** 23, (2), 571-580.

16. Kilbey, S. M.; Bates, F. S.; Tirrell, M.; Yoshizawa, H.; Hill, R.; Israelachvili, J. Direct Force and Friction Measurements Reflecting Structural Changes in Confined Diblock Copolymer Liquids. *Macromolecules* **1995,** 28, (16), 5626-5631.

17. Kilbey, S. M.; Watanabe, H.; Tirrell, M. Structure and Scaling of Polymer Brushes near the theta Condition. *Macromolecules* **2001,** 34, (15), 5249-5259.

18. Alonzo, J.; Mays, J. W.; Kilbey Ii, S. M. Forces of interaction between surfaces bearing looped polymer brushes in good solvent. *Soft Matter* **2009,** 5, (9), 1897-1904.

19. Kent, M. S.; Lee, L. T.; Farnoux, B.; Rondelez, F. Characterization of diblock copolymer monolayers at the liquid-air interface by neutron reflectivity and surface tension measurements. *Macromolecules* **1992,** 25, (23), 6240-6247.

20. Baranowski, R.; Whitmore, M. D. Numerical self-consistent field study of tethered chains in Theta solvent. *J. Chem. Phys.* **1998,** 108, (23), 9885-9892.

21. Baranowski, R.; Whitmore, M. D. Theory of the structure of adsorbed block copolymers: Detailed comparison with experiment. *J. Chem. Phys.* **1995,** 103, (6), 2343-2353.

22. Grest, G. S. Grafted polymer brushes in polymeric matrices. *The Journal of Chemical Physics* **1996,** 105, (13), 5532-5541.

23. Grest, G. S. Grafted polymer brushes: a constant surface pressure molecular dynamics simulation. *Macromolecules* **1994,** 27, (2), 418-426.

24. Pastorino, C.; Blinder, K.; Kreer, T.; Müller, M. Static and dynamic properties of the interface between a polymer brush and a melt of identical chains. *J. Chem. Phys.* **2006,** 124, (6), 064902.

25. Elliott, I. G.; Kuhl, T. L.; Faller, R. Molecular Simulation Study of the Structure of High Density Polymer Brushes in Good Solvent. *Macromolecules* **2010,** 43, (21), 9131-9138.

26. Klein, J.; Kumacheva, E.; Mahalu, D.; Perahia, D.; Fetters, L. J. Reduction of frictional forces between solid surfaces bearing polymer brushes. *Nature* **1994,** 370, (6491), 634-636.

27. Klein, J.; Perahia, D.; Warburg, S. Forces between polymer-bearing surfaces undergoing shear. *Nature* **1991,** 352, (6331), 143-145.

28. Raviv, U.; Tadmor, R.; Klein, J. Shear and Frictional Interactions between Adsorbed Polymer Layers in a Good Solvent. *The Journal of Physical Chemistry B* **2001,** 105, (34), 8125-8134.

29. Klein, J.; Kumacheva, E.; Perahia, D.; Fetters, L. J. Shear forces between sliding surfaces coated with polymer brushes: The high friction regime. *Acta Polymerica* **1998,** 49, (10-11), 617-625.

30. Tadmor, R.; Janik, J.; Klein, J.; Fetters, L. J. Sliding Friction with Polymer Brushes. *Physical Review Letters* **2003,** 91, (11), 115503.

31. Schorr, P. A.; Kwan, T. C. B.; Kilbey, S. M.; Shaqfeh, E. S. G.; Tirrell, M. Shear Forces between Tethered Polymer Chains as a Function of Compression, Sliding Velocity, and Solvent Quality. *Macromolecules* **2003,** 36, (2), 389-398.

32. Forster, A. M.; Mays, J. W.; Kilbey, S. M. Effect of temperature on the frictional forces between polystyrene brushes. *Journal of Polymer Science Part B: Polymer Physics* **2006,** 44, (4), 649-655.

33. Grest, G. S. Interfacial Sliding of Polymer Brushes: A Molecular Dynamics Simulation. *Physical Review Letters* **1996,** 76, (26), 4979-4982.

34. Witten, T. A.; Leibler, L.; Pincus, P. A. Stress relaxation in the lamellar copolymer mesophase. *Macromolecules* **1990,** 23, (3), 824-829.

35. Kreer, T.; Müser, M. H.; Binder, K.; Klein, J. Frictional Drag Mechanisms between Polymer-Bearing Surfaces. *Langmuir* **2001,** 17, (25), 7804-7813.

36. Ejaz, M.; Yamamoto, S.; Ohno, K.; Tsujii, Y.; Fukuda, T. Controlled Graft Polymerization of Methyl Methacrylate on Silicon Substrate by the Combined Use of the Langmuir−Blodgett and Atom Transfer Radical Polymerization Techniques. *Macromolecules* **1998,** 31, (17), 5934-5936.

37. Ruths, M.; Johannsmann, D.; Ruhe, J.; Knoll, W. Repulsive Forces and Relaxation on Compression of Entangled, Polydisperse Polystyrene Brushes. *Macromolecules* **2000,** 33, (10), 3860-3870.

38. Milner, S. T.; Witten, T. A.; Cates, M. E. Effects of polydispersity in the end-grafted polymer brush. *Macromolecules* **1989,** 22, (2), 853-861.

39. Yamamoto, S.; Ejaz, M.; Tsujii, Y.; Matsumoto, M.; Fukuda, T. Surface Interaction Forces of Well-Defined, High-Density Polymer Brushes Studied by Atomic Force Microscopy. 1. Effect of Chain Length. *Macromolecules* **2000,** 33, (15), 5602-5607.

40. Yamamoto, S.; Ejaz, M.; Tsujii, Y.; Fukuda, T. Surface Interaction Forces of Well-Defined, High-Density Polymer Brushes Studied by Atomic Force Microscopy. 2. Effect of Graft Density. *Macromolecules* **2000,** 33, (15), 5608-5612.

41. de Gennes, P. G. Polymers at an interface; a simplified view. *Advances in Colloid and Interface Science* **1987,** 27, (3-4), 189-209.

42. Kobayashi, M.; Terayama, Y.; Hosaka, N.; Kaido, M.; Suzuki, A.; Yamada, N.; Torikai, N.; Ishihara, K.; Takahara, A. Friction behavior of high-density poly(2-methacryloyloxyethyl phosphorylcholine) brush in aqueous media. *Soft Matter* **2007,** 3, (6), 740-746.

43. Sakata, Y.; Kobayashi, M.; Otsuka, H.; Takahara, A. Tribological Properties of Poly(methyl methacrylate) Brushes Prepared by Surface-Initiated Atom Transfer Radical Polymerization *Polym. J.* **2005,** 37, (10).

44. Kobayashi, M.; Takahara, A. Synthesis and Frictional Properties of Poly(2,3-dihydroxypropyl methacrylate) Brush Prepared by Surface-initiated Atom Transfer Radical Polymerization. *Chemistry Letters* **2005,** 34, (12), 1582.

45. Dunlop, I. E.; Briscoe, W. H.; Titmuss, S.; Jacobs, R. M. J.; Osborne, V. L.; Edmondson, S.; Huck, W. T. S.; Klein, J. Direct Measurement of Normal and Shear Forces between Surface-Grown Polyelectrolyte Layers†. *The Journal of Physical Chemistry B* **2009,** 113, (12), 3947-3956.

46. Colby, R. H.; Rubinstein, M.; Viovy, J. L. Chain entanglement in polymer melts and solutions. *Macromolecules* **1992,** 25, (2), 996-998.

47. Vigil, G.; Xu, Z.; Steinberg, S.; Israelachvili, J. Interactions of Silica Surfaces. *Journal of Colloid and Interface Science* **1994,** 165, (2), 367-385.

48. Matyjaszewski, K.; Miller, P. J.; Shukla, N.; Immaraporn, B.; Gelman, A.; Luokala, B. B.; Siclovan, T. M.; Kickelbick, G.; Vallant, T.; Hoffmann, H.; Pakula, T. Polymers at Interfaces: Using Atom Transfer Radical Polymerization in the Controlled Growth of Homopolymers and Block Copolymers from Silicon Surfaces in the Absence of Untethered Sacrificial Initiator. *Macromolecules* **1999,** 32, (26), 8716-8724.

49. Ell, J. R.; Mulder, D. E.; Faller, R.; Patten, T. E.; Kuhl, T. L. Structural Determination of High Density, ATRP Grown Polystyrene Brushes by Neutron Reflectivity. *Macromolecules* **2009,** 42, (24), 9523-9527.

50. Xia, J.; Matyjaszewski, K. Controlled/"Living" Radical Polymerization. Atom Transfer Radical Polymerization Using Multidentate Amine Ligands. *Macromolecules* **1997,** 30, (25), 7697-7700.

51. Israelachvili, J. N. Thin film studies using multiple-beam interferometry. *Journal of Colloid and Interface Science* **1973,** 44, (2), 259-272.

52. Israelachvili, J. N.; Adams, G. E. Direct measurement of long range forces between two mica surfaces in aqueous KNO3 solutions. *Nature* **1976,** 262, (5571), 774-776.

53. Israelachvili, J. N.; Adams, G. E. Measurement of forces between two mica surfaces in aqueous electrolyte solutions in the range 0–100 nm. *J. Chem. Soc., Faraday Trans.* **1978,** 1, (74), 975 - 1001.

54. Israelachvili, J. N.; McGuiggan, M. Adhesion and short-range forces between surfaces. Part I: New apparatus for surface force measurements. *J. Mater. Res.* **1990,** 5.

55. Parker, J. L.; Christenson, H. K.; Ninham, B. W. Device for measuring the force and separation between two surfaces down to molecular separations. *Review of Scientific Instruments* **1989,** 60, (10), 3135-3138.

56. Derjaguin, B. V. *Kolloid Zeits* **1934,** 69, 155-164.

57. Israelachvili, J. direct measurement of forces between surfaces in liquids at the molecular level. *Proc. Natl. Acad. Sci. USA* **1987,** 84, 4722-4724.

58. Luengo, G.; Schmitt, F. J.; Hill, R.; Israelachvili, J. Thin Film Rheology and Tribology of Confined Polymer Melts: Contrasts with Bulk Properties. *Macromolecules* **1997,** 30, (8), 2482-2494.

59. Clarkson, M. T. Multiple-beam interferometry with thin metal films and unsymmetrical systems. *Journal of Physics D: Applied Physics* **1989,** 22, (4), 475.

60. Orozco-Alcaraz, R.; Kuhl, T. Interaction forces between DPPC bilayers on glass. *Manuscript to be submitted for publication*.

61. Higo, Y.; Ueno, N.; Noda, I. osmotic pressure of semidilute solutions of branched polymers. *polymer journal* **1983,** 15, (5), 367-375.

62. Biesalski, M.; Rühe, J. Scaling Laws for the Swelling of Neutral and Charged Polymer Brushes in Good Solvents. *Macromolecules* **2001,** 35, (2), 499-507.

63. Biesalski, M.; Rühe, J. Preparation and Characterization of a Polyelectrolyte Monolayer Covalently Attached to a Planar Solid Surface. *Macromolecules* **1999,** 32, (7), 2309-2316.

64. Wu, T.; Gong, P.; Szleifer, I.; Vlček, P.; Šubr, V.; Genzer, J. Behavior of Surface-Anchored Poly(acrylic acid) Brushes with Grafting Density Gradients on Solid Substrates: 1. Experiment. *Macromolecules* **2007,** 40, (24), 8756-8764.

65. Milner, S. T. Compressing polymer brushes—a quantitative comparison of theory and experiment. *Europhysics Letters* **1988,** 7, 695-699.

66. Kim, J. U.; Matsen, M. W. Compression of Polymer Brushes: Quantitative Comparison of Self-Consistent Field Theory with Experiment. *Macromolecules* **2009,** 42, (9), 3430-3432.

67. Liao, W.-P.; Kuhl, T. L. Steric Forces of Tethered Polymer Chains as a Function of Grafting Density: Studies with a Single Diblock Molecular Weight. *Macromolecules* **2012**.

68. Noda, I.; Higo, Y.; Ueno, N.; Fujimoto, T. Semidilute region for linear polymers in good solvents. *Macromolecules* **1984,** 17, (5), 1055-1059.

69. Samadi, A.; Husson, S. M.; Liu, Y.; Luzinov, I.; Michael Kilbey, S. Low-Temperature Growth of Thick Polystyrene Brushes via ATRP. *Macromolecular Rapid Communications* **2005,** 26, (23), 1829-1834.

70. Israelachvili, J. N.; Tandon, R. K.; White, L. R. Measurement of forces between two mica surfaces in aqueous polyethylene oxide solution. *Journal of Colloid and Interface Science* **1980,** 78, (2), 430-443.

71. Osaki, K.; Inoue, T.; Uematsu, T.; Yamashita, Y. Evaluation methods of the longest Rouse relaxation time of an entangled polymer in a semidilute solution. *Journal of Polymer Science Part B: Polymer Physics* **2001,** 39, (14), 1704-1712.

72. Onogi, S.; Masuda, T.; Kitagawa, K. Rheological Properties of Anionic Polystyrenes. I. Dynamic Viscoelasticity of Narrow-Distribution Polystyrenes. *Macromolecules* **1970,** 3, (2), 109-116.

73. Tao, H.; Huang, C.-i.; Lodge, T. P. Correlation Length and Entanglement Spacing in Concentrated Hydrogenated Polybutadiene Solutions. *Macromolecules* **1999,** 32, (4), 1212-1217.

74. Spirin, L.; Galuschko, A.; Kreer, T.; Johner, A.; Baschnagel, J.; Binder, K. Polymer-brush lubrication in the limit of strong compression. *Eur. Phys. J. E* **2010,** 33, (4), 307-311.

75. Zhou, Z. W.; Daivis, P. J. Molecular dynamics study of polymer conformation as a function of concentration and solvent quality. *Journal of Chemical Physics* **2009,** 130, (22), 224904-1~224904-10.

Chapter 6

Conclusion and Outlook

Polymer brushes have been characterized using both experimental and computational methods. The overall purpose was to understand how polymer brushes react to confinement, so as to be able to effectively design surfaces which can be modified to address a number of needs. Additionally, new methods for studying polymer brushes have been developed as a result of the work in this dissertation. Both experiments and simulations focused on very high grafting density brushes, examining more durable layers which could find use in artificial joints as lubricants and potentially extend the lifetime of the device.

Molecular dynamics simulations were used to characterize both a single brush in equilibrium conditions and an opposing brush system under confinement. The single brush studies served two purposes. First, the brush system was characterized by calculating and analyzing density profiles, radial distribution functions, chain end distributions, chain orientation, and average brush height for the same grafting density and chain length that would be used later for the compression simulation. This allowed for the unperturbed brush system to be well defined, so that responses to confinement could be easily interpreted. The brush was also characterized at different grafting densities and chain lengths to fully understand the effect of these variables. Second, this initial single brush study ensured that the MARTINI model was suitable for polymer brush systems. Results of this study compared favorably to theoretical predictions, and

these comparisons served to validate the model for use with polymer brushes. These results were presented in detail in Chapter 2.

Following the single brush study, a method was developed to realistically confine polymer brushes, or any soft matter, using molecular dynamics. This method allowed for an explicit solvent and NVT simulations to be used to simulate a compression, with minimal alterations to the standard Gromacs code. When volume is fixed, the amount of solvent to use in a simulation is not clear. Especially when normal forces are to be investigated, performing a simulating at the incorrect density will make the interaction results useless. The principle idea behind this confinement method was to determine what solvent density, or simply what number of solvent particles, should be used for a given separation distance prior to conducting a production run simulation. The solvent chemical potential of each confined system was calculated, and then compared to that of a reference system. If the values were not equal, the confined system's solvent density was changed until the chemical potentials were the same. From there, all confined systems could be run NVT as normal, and the results are physically meaningful. The details of developing and implementing this method were presented in Chapter 3.

This method could be particularly useful if the production run simulation is going to be very long. In that case, the costs associated with setting up the systems at the correct density would be small compared to the length of the simulation. Simulating the system at the correct solvent density from the start could be far more efficient for long runs than performing chemical potential calculations and altering the solvent density during the simulation, which is the idea behind grand canonical ensemble simulations. Additionally, many researchers would prefer to employ only one simulation method for a project if

possible. This allows only molecular dynamics to be used, with no need to implement grand canonical or Monte Carlo simulations.

The confinement method was used to simulate a static compression of polymer brushes. The system was characterized at several separation distances. Both structure and interaction pressures were analyzed, and observations in the pressure-distance profiles were explained by corresponding density profile features. At high levels of compression, the brush layers interpenetrated each other to the point where each brush would reach the opposing surface. This was the same level of compression where the pressure-distance profile increased sharply, suggesting that the significant interpenetration was linked to large increases in normal forces.

The density profiles of the individual brush layers change in shape considerably at higher levels of confinement. With increasing compression, the elongated tail diminishes and the density profile becomes more parabolic, approaching zero much more sharply than when unconfined. Even at very high confinement, there is still a polymer depletion layer near the surface, as was observed in the single brush studies. This is confirmed with peaks in the solvent density just above either surface. During the compression, the chain end distribution broadens out, changing from a well defined peak to an almost even distribution going across the simulation box. The compression results were provided in Chapter 4.

Chapter 5 covered experimental studies of polymer brushes, which were focused on high grafting density brushes created from atomic transfer radical polymerization reactions. These can reach a higher grafting density than “grafted to” techniques due to the decrease in steric hindrance by growing the polymers monomer by monomer from the

surface, rather than adsorbing fully grown chains to the surface. To allow for the initiator to chemically bond to the surface, new surfaces had to be created that were reactive, but were still smooth and thin enough to be used in the surface force apparatus. Mica with SiO_2 deposited on it was used as the surface that could accommodate these requirements.

High grafting density, durable polystyrene polymer brushes were synthesized and tested in the SFA. The results showed that friction was insignificant until there was a very high normal load applied. This indicates that even though they were made at a very high density, the brushes were still acting as good lubricants.

Future work on this project should include simulations shearing the systems that were studied in the static compression. The same system and model could easily be used by examining shear effects at surface separation distances that were used for the normal force calculations. These systems are already set up at the correct density, and as such should be much quicker to get results. Shear can be implemented in Gromacs using oscillating cosine acceleration and defining which groups in the index file it will be applied to. A shear simulation could take place by two different methods. First, the surface and grafted monomers could be the groups accelerated, which would provide conditions similar to a shear experiment in the SFA where one surface is moved relative to the other. A second option which may be more easily implemented is to use the solvent as the accelerated group. This mimics conditions of a solvent flowing through the surfaces. Accelerating the solvent molecules would be easier computationally because the surface and grafted monomers in the simulation are frozen groups. Accelerating a frozen group in one dimension while keeping it frozen in the other

dimensions is not as straightforward as accelerating a group with no restrictions placed on it.

Further studies could involve different methods of compression. Instead of two opposing brushes, a brush could be compressed by a bare surface to demonstrate the effect of compression by a hard and soft surface. This would illustrate the impact interpenetration has on the structure and interactions of the brush.

Additional work will be published shortly involving the same characterization conducted in Chapter 4, but investigating different grafting densities and chain lengths. Two systems were selected which will provide the same overlap grafting density by different means. One will have the same grafting density as the system in Chapter 4, but with longer chains. The other will have the same chain length that was already studied, but a higher grafting density. By placing both chain length and grafting density into one term, the assumption is that they affect brush structure similarly. As the choice of these two variables led to the same overlap grafting density value, characterizing these systems under compression will demonstrate whether systems of the same overlap grafting density can be reasonably compared when the value of overlap grafting density is arrived at by two very different means. This work is already well underway, but will not be finished in time to be described in this dissertation.

Future experiments should focus on polymer layers that are biocompatible. While polystyrene is a good starting point for any polymer study, working with a material that could feasibly be used for artificial joints would be a significant next step in developing a high grafting density durable lubricant for joint replacements.

Additional experiments with the system used for this work could involve characterizing the brushes at different grafting densities, by using different surface active initiators. This would provide a more thorough characterization of the brush by examining both grafting density and molecular weight, which are two variables that greatly influence brush structure.

Chapter 7

Appendix

This appendix will cover some technical details concerning simulation methods which may be used as a reference for future researchers conducting similar work. The idea is to make some of the less common information available so work conducted in this dissertation can be easily replicated or continued. This will consist of some instructions for using Gromacs tools necessary for chemical potential calculations, along with an explanation of how to alter the source code to omit surfaces. The text in this section assumes a working knowledge of Gromacs and molecular dynamics.

7.1 Gromacs Source Code Modifications

Gromacs has a tpi option for calculating chemical potential, but it must be modified to work properly when frozen surfaces are involved, such as with polymer brush systems. The code needs to be altered to prevent any insertions from occurring inside the surfaces, and this process will be described here. Specifically for this work Gromacs 4.5.2 was used for all test particle insertion calculations, so will be the version referenced when code modification is described in examples. The procedure should be similar for other versions as well, however versions before 4.5 had a bug in this part of the code, so Gromacs 4.5 or newer should be used.

A new source code was used for each separation distance by reinstalling Gromacs with the alterations to the code in a local directory that could be referenced later. Therefore, the file gromacs-4.5.2.tar.gz (or whatever install of Gromacs is to be used)

will need to be copied and expanded in a local directory. From there, the specific file that needs to be changed is tpi.c, and can be found at gromacs-4.5.2/src/mdlib/

The program works by generating a random number for each *x*, *y*, and *z* dimensions to choose a coordinate for each particle insertion. As the surface is in the *x*-*y* plane, the code must bias the *z* coordinate to avoid the surface. This can be done at line 440 in the tpi.c program (for version 4.5.2). The line that must be changed is shown in Equation 7-1.

```
x_init[ZZ] = gmx_rng_uniform_real(tpi_rand)*state->box[ZZ][ZZ];
```
(7-1)

As an example, a system with a surface separation of 25 nm is used. The system had a box of height 25.94 nm and three surface layers: one at the bottom (z = 0 nm), and two at the top (z = 25 and 25.47 nm). All particle sizes in this case are 0.47 nm. It is desired that the inserted particles never overlap with the surface, so must be inserted one full particle diameter away from the surface. To bias it away from the bottom surface, the random number generator will have a particle diameter added to it, so the lowest possible value obtained is 0.47 nm. Next, the old random number will be divided by the box height, which was the total range where the particle could be inserted in the standard code, and multiplied by the new range. The top value for particle insertion should be one diameter below the surface at 25 nm. Given that the new lowest value is 0.47 nm, and the new highest value is 24.53 nm, the new range will be the difference between them, 24.06 nm. That said, the altered code for this example will now appear as in Equation 7-2.

x_init[ZZ] =

0.47 + (24.06/25.94)*gmx_rng_uniform_real(tpi_rand)*state->box[ZZ][ZZ]; (7-2)

As can be seen, the only differences from Equation 7-1 are the three numbers immediately to the right of the equal sign, and all the rest remains unchanged. Once this change is made, create a new directory for the altered source code to be installed in. Change directory to Gromacs-4.5.2, and type the following commands.

```
module load fftw/3.2.1
module load openmpi/1.4.2
./configure --enable-shared --enable-mpi --prefix=full path of new directory
make
make install
```

Programs from this new modified version of Gromacs can be called in a script by using the path to the directory. For this example, mdrun can be called as:

/share/home6/igelliott/sourcecode/gromacs_25nmthicksurfz0/bin/mdrun

with the rest of the options for mdrun following as normal. For each separation distance or different system height, a new version of Gromacs will have to be installed following these steps.

7.2 Using the Gromacs Features with the Modified Code

Once the modifications to the code have been made, performing the test particles insertion method can be completed in Gromacs using the tpi option of mdrun. A configuration, topology, index, and mdp file must also be supplied to grompp ahead of time like normal. However, the configuration, topology, and index files need to have one particle added to them, and the extra particle is the one Gromacs uses to theoretically insert in the trajectory. For the work in Chapters 3 and 4, the extra particle in each file

was therefore a solvent particle. As described in chapters 3 and 4, only selected frames of the total trajectory are used, so a script was written to produce one frame of the trajectory every 0.1, 0.5 or 1 ns depending on the system size and desired accuracy. Each frame will have a number of theoretical insertions performed equal to the nsteps value in the grompp.mdp file. The trajectory is rerun with mdrun to perform the insertions. For this example the overall procedure using the modified code and the tpi options are shown below.

```
/share/home6/igelliott/sourcecode/gromacs_25nmthicksurfz0/bin/mdrun –rerun traj.xtc –s topol.tpr –tpi tpi.xvg –tpid tpid.xvg
```

In this case tpi.xvg is the file which contains the ensemble average value, and tpid.xvg will show a distribution.

After being analyzed with the test particles insertion, the output file (tpi.xvg) will contain 10 columns of data. The fourth column is the value for the ensemble average $\langle \exp(-\Delta U_{tpi}/kT) \rangle$ which is used to determine the excess portion of the solvent chemical potential, as described in detail in Chapter 3.